A STUDY OF FULLY DEVELOPED TURBULENT FLOW BETWEEN PARALLEL PLATES BY A STATISTICAL METHOD

A THESIS

Presented to

The Faculty of the Division of Graduate Studies

By

Ramanujam Srinivasan

In Partial Fulfillment

of the Requirements for the Degree

Doctor of Philosophy

in the School of Aerospace Engineering

Georgia Institute of Technology

June, 1977

A STUDY OF FULLY DEVELOPED TURBULENT FLOW

BETWEEN PARALLEL PLATES BY A STATISTICAL METHOD

Approved:

Dr. D. P. Giddens, Chairman

Dr. L. H. Bangert

Dr. J. C. Wu

Date approved by Chairman: 11 May '77

ACKNOWLEDGEMENTS

I would like to express my deep gratitude to my advisor, Dr. D. P. Giddens, for his guidance and encouragement during this research effort and for his constant willingness to discuss various aspects of this endeavor. I am indebted to him for many enlightening discussions and suggestions which significantly contributed to my research work. I am extremely grateful to my thesis advisors, Dr. L. H. Bangert and Dr. J. C. Wu for their valuable advice, criticisms and encouragement throughout this work. Dr. P. G. Mayer and Dr. R. G. Roper, who served as members of the reading committee are gratefully thanked for their valuable comments.

I owe my thanks to many of my friends for the numberous discussions which have been very helpful to this research effort.

My appreciation goes to Ms. Claudine Taylor for an excellent job done in typing this thesis.

My parents and other members of my family made many sacrifices during my academic career. Without their help, moral support and understanding, higher education may not have been possible for me.

The financial support of the Georgia Institute of Technology and the services of the Rich Electronic Computing Center are gratefully acknowledged.

TABLE OF CONTENTS

TABLE OF CONTENTS (Continued)

LIST OF ILLUSTRATIONS

LIST OF ILLUSTRATIONS (Continued)

LIST OF ILLUSTRATIONS (CONTINUED)

NOMENCLATURE

a	Constant of proportionality in $\varepsilon/3U^2 \sim 1/y$.
$\vec{c}$	Turbulence velocity vector.
c_1	Constant used in the equation for dissipation rate (1.45).
c_2	Constant used in the equation for dissipation rate (1.92).
c_f	Skin-friction coefficient ($2\ u_*^2/u_w^2$).
$\overline{c_x c_y}$	Reynolds shear stress per unit mass; defined in Equation (9c).
$\overline{c_x^2}$	Mean square of the x-component of turbulence velocity; defined in Equation (9e).
$\overline{c_y^2}$	Mean square of the y-component of turbulence velocity; defined in Equation (9d).
$\overline{c_z^2}$	Mean square of the z-component of turbulence velocity; defined in Equation (9e).
$2d$	Distance between the parallel plates.
D_1, D_2, D_3	Coefficients of Lagrange interpolation polynomial used to approximate the derivatives with respect to velocities; defined in Apprendix B.
E_k	Turbulence kinetic energy; defined in Equation (9b).

f Distribution function of velocities of fluid elements.

F Gaussian (equilibrium) distribution function; defined in Equation (2).

g First reduced distribution function; defined in Equation (7a).

G Equilibrium form of the first reduced distribution function.

h Third reduced distribution function; defined in Equation (7c).

H Equilibrium form of the third reduced distribution function.

j Second reduced distribution function; defined in Equation (7b).

j_v Fourth reduced distribution function; defined in Equation (7d).

J_v Equilibrium form of the fourth reduced distribution function.

K Constant of proportionality in the expression for relaxation time; defined in Equation (4).

K_u Kurtosis or flatness factor of the g distribution function; defined in Equation (9h).

$\bar{p}$ Mean pressure.

P_x Non-dimensionalized pressure gradient in the x-direction $\frac{d}{\rho u_*^2} \frac{\partial \bar{p}}{\partial \bar{x}}$.

P_y Non-dimensionalized pressure gradient in the y-direction $(\frac{d}{\rho u_*^2} \frac{\partial \bar{p}}{\partial \bar{y}})$.

P_{xy} Turbulent shear stress, defined in Equation (9c).

$(P_{xy})_w$ Wall shear stress.

Q_y Flux of turbulence kinetic energy in the y direction; defined in Equation (9f).

$\vec{r}$ Position vector.

Re Reynolds number based on plate velocity in Couette flow, $(u_w\, d/\nu)$, and on the centerline velocity in channel flow $(u_0 d/\nu)$.

Re_* Reynolds number based on friction velocity $(u_* d/\nu)$.

S Skewness factor of the g distribution function; defined in Equation (9g).

$\vec{u}$ Time averaged flow velocity vector.

u_* Friction velocity $[(P_{xy})_w/\rho]^{1/2}$.

u_w Plate velocity in the Couette flow.

u_0 Centerline velocity in channel flow.

u_x Mean velocity in the x direction; defined in Equation (9a).

u Non-dimensionalized mean velocity in the x direction.

U Non-dimensionalized turbulence intensity; defined in Eq. (9b).

$\langle v'^2 \rangle$ Non-dimensionalized mean square of y component velocity fluatuations; defined in Equation (9d).

$\langle u'^2+w'^2 \rangle$ Non-dimensionalized sum of the mean square of x and z component velocity fluctuations; defined in Equation (9e).

w_1 Defined in Equation (A-12) in Appendix A.

w_2 Defined in Equation (A-13) in Appendix A.

x Cartesian coordinate parallel to the primary flow direction.

$\bar{y}$ Cartesian coordinate perpendicular to the primary flow direction.

y Non-dimensionalized y coordinate (y/d).

y_* Local Reynolds number ($u_* y/\nu$).

z Cartesian coordinate perpendicular to the plane containing x and y coordinates.

α Approximate profile for the dissipation rate, defined in Appendix C.

ϵ Viscous dissipation rate per unit mass.

θ Correction about approximate profile for the dissipation rate.

κ Von Karman constant (0.41).

ν Kinematic viscosity.

$\bar{\nu}_T$ Turbulent or eddy viscosity [$-Re_* P_{xy}/(du/dy)$].

ν_T Non-dimensionalized turbulent viscosity (ν_T/ν).

ρ Fluid density.

σ_ε Constant used in the equation for dissipation rate (about 1.3).

$\bar{\tau}$ Relaxation time; defined in Equation (4).

τ Non-dimensionalized relaxation time ($u_* \bar{\tau}/d$).

Superscripts

$\bar{(\ )}$ Time averaged, and dimensional quantities.

$+$ Indicates outgoing stream or in the positive c_y direction.

$-$ Indicates incoming stream or in the negative c_y direction.

Subscripts

b Quantities denoting boundary condition.

i Evaluated at the i^{th} physical node.

x Component in the x direction.

y Component in the y direction.

z Component in the z direction.

σ Evaluated at the discrete velocity point c_σ.

SUMMARY

Turbulent flow between parallel plates is studied utilizing a model equation, similar to the Boltzmann equation of kinetic theory, which was developed by Lundgren for the velocity distribution of fluid elements. This equation is applied to the plane Couette flow problem with zero pressure gradient and the two-dimensional Channel flow problem. Solutions to the governing equation are obtained numerically, employing the discrete ordinate method and finite differences. Two types of boundary conditions on the distribution function are considered for each of the flow problems. They are the Chapman-Enskog boundary condition and the gradient boundary condition. For the Couette flow problem, the latter reduces to zero-gradient boundary condition. The results of the calculations using these conditions are compared with available experimental data.

The computed results for mean velocity in plane Couette flow agree well with experimental data. The skin-friction coefficients obtained in this study compare very well with the empirical curve fit. The Channel flow results are obtained with the assumption that the cross-stream pressure gradients are zero. Due to this assumption, the computed mean flow properties are slightly different from the experimental data even though they are in good qualitative agreement.

This study establishes that Lundgren's model equation provides a very good description of turbulence for the flow problems considered. For problems involving pressure gradients, if an independent equation is

available for computing cross-stream pressure gradients, this model equation can be used as a good analytical tool for further studies. In addition, the discrete ordinate method is shown to be an effective method for direct solution for the probability distribution, thus avoiding recourse to assuming, a priori, approximate forms for this function.

CHAPTER I

INTRODUCTION

Background and Review of Related Works

Turbulence is one of the most complex phenomena in fluid mechanics. It represents a mechanical system with a large number of degrees of freedom, and is consequently very difficult to treat, either experimentally or theoretically. From the point of view of engineering predictions, most successes have been achieved with phenomenological theories based on Reynolds equations. Since the Reynolds equations have more unknowns than the number of equations, there is a problem of closure of the system. To circumvent this difficulty, phenomenological theories resort to semi-empirical relations among the unknowns. Different relations have led to varying degrees of success. The phenomenological theories, however, are not sufficiently general to allow treatment of various correlation terms. The lack of generality arises because the closure of the system of equations is achieved by representing the higher order correlations terms as a function of lower order correlations.

Similarities between the statistical behavior of molecules in a gas and the velocity fluctuations of fluid elements in a turbulent flow suggest the possibility of describing both phenomena in terms of a velocity distribution function from which mean properties may be computed by forming appropriate moments. Since the length scales of

turbulence are many times larger than the molecular mean free path, continum equations are adequate for the description of turbulent flows. In addition to the uniqueness in treating various correlation terms, the use of velocity distribution functions can potentially provide more details of turbulence structure than the phenomenological approaches. It has been shown by Batchelor [1] that the velocity distribution function in grid-generated turbulence is nearly Gaussian. However, for inhomogeneous turbulent flows, the velocity distribution function is no longer Gaussian. The departures from this state are important features of most turbulence processes.

One of the earliest formulations utilizing probability density or characteristic functional is due to Hopf [2]. Other related works are based on moment formulations and their clorues. A hierachy of equations for probability distribution functions was derived by Monin [3], using a similar but more generalized approach than that of Hopf. In this respect, Hopf's equation parallels the Liouville equations of statistical mechanics from which the Bogoliubov-Born-Green-Kirkwood-Yvon (BBGKY) equations [4] are derived. All these works have been confined to closure hypotheses.

A hierarchy of equations for multi-point probability distribution functions, similar to that of Monin, has been developed by Lundgren [5] starting from the Navier-Stokes equations. This hierarchy resembles the BBGKY equations and has the familiar closure problem. To close the set of equations, various models have been explored. Fox [6, 7] has used cluster expansions, analogous to that used with BBGKY equations in kinetic theory, for the case of homogeneous

turbulence. In another work, Lundgren [8] was able to find the kolmogorov spectrum in the inertial range by using Gaussian closure at the third level. Lundgren [9] has also attempted to close the system at the one-point level by employing a relaxation model identical in form to the Bhatnagar-Gross-Krook (BGK) model [10] of kinetic theory. However, this model is not, within itself, sufficient to define a turbulent flow. An additional equation is required to relate the turbulence dissipation rate to other flow properties. This implies that an ad hoc assumption must be made regarding the relaxation rate in this model. None of the above closure models have been applied to wall-bounded flows.

A different approach using probability distribution functions has been developed by Chung [11, 12] in which similarities between turbulence and Brownian motion have been employed. Chung has obtained a closed Fokker-Planck equation for the probability distribution functions based on the Langevin equation for generalized Brownian motion. He has used this Fokker-Planck equation to obtain solutions for the plane Couette flow problem employing moment methods [13] familiar in kinetic theory. In these methods, specific functional forms are assumed for the distribution function and unknown coefficients are determined from a set of moment equations. Chung [14] has also extended his approach to chemically reacting flows.

In the present work, Lundgren's model equation with a BGK type relaxation term is employed to study fully developed turbulent flow between parallel plates. The solutions are obtained by applying an extension of the discrete ordinate method [15, 16] as developed for

problems in rarefied gas dynamics. This method differs from moment methods in that no a priori assumption about the form of the distribution function is required. Instead, the numerical solution is obtained directly from the governing differential equation rather than from moment equations. This difference is analogous to that obtained in solutions to boundary layer equations using integral versus finite difference methods. In the former, assumptions are made a priori on the shapes of velocity profiles and undetermined coefficients are evaluated. Finite difference methods, on the other hand, are used to solve the partial differential equations themselves and thus afford a finer detail of the flow structure than can be achieved with integral methods.

Purpose of the Research

Due to the general nature in treating various correlation terms and the potential in revealing finer details of turbulence, there has been increasing interest in obtaining probability distribution functions. Lundgren's model equation will be employed in this work to study fully developed turbulent flows between parallel plates. One of the major difficulties in solving this equation lies in the prescription of appropriate boundary conditions. Unlike cases in the kinetic theory of gases and moment methods, there are no obvious forms for the distribution function that can be specified on the boundaries of the flow field. Besides, the validity of the model equation very near the wall is questionable and so boundary conditions are applied at a location slightly away from the wall.

Thus, the purpose of this research is two-fold: first, to postulate appropriate boundary conditions for the distribution function near the solid boundaries; and second, to obtain accurate numerical solutions of the governing differential equation using discrete ordinate method. The results of this study will be compared with available experimental data.

CHAPTER II

GOVERNING EQUATIONS

The differential equation governing the lowest order probability distribution function is [9]

$$\frac{\partial \bar{f}}{\partial t} + \vec{v} \cdot \frac{\partial \bar{f}}{\partial \vec{r}} + -\left\{\frac{1}{\rho}\frac{\partial \bar{p}}{\partial \vec{r}} + \nu \cdot \frac{\partial}{\partial \vec{r}} \cdot \frac{\partial}{\partial \vec{r}} \vec{u}\right\} \cdot \frac{\partial \bar{f}}{\partial \vec{v}} \tag{1}$$

$$= \frac{1}{\bar{\tau}}(\bar{F}-\bar{f}) + \frac{1}{3}\frac{\bar{\varepsilon}}{\bar{U}^2}\frac{\partial}{\partial \vec{v}} \cdot (\vec{v} \cdot \vec{u})\ \bar{f}$$

Where $\bar{f}(\vec{r}, \vec{v}, t)\, dv$ is the probability that the instantaneous velocity at $\vec{r}$ in physical space is within the range $\vec{v}$ to $\vec{v} + d\vec{v}$ in velocity space. The mean pressure, density and kinematic viscosity are represented by $\bar{p}$, ρ and ν, respectively. The relaxation time is represented by $\bar{\tau}$ which is related to the characteristic turbulence diffusion time. $\bar{F}$ is a Gaussian (equilibrium) distribution given by

$$\bar{F} = (2\pi\bar{U}^2)^{-3/2} \quad \exp[-(\vec{v}-\vec{u})^2/2\bar{U}^2] \tag{2}$$

The mean flow velocity vector is $\vec{u}$ and $3\bar{U}^2$ is the mean square of the velocity fluctuations. These are obtained from the distribution function by the relations

$$\vec{u} = \int \vec{v}\ \bar{f}\ d\vec{v} \tag{3a}$$

$$3\bar{U}^2 = \int (\vec{v}-\vec{u})^2\ \bar{f}\ d\vec{v} \tag{3b}$$

where the integrations are taken over the entire velocity space ($-\infty$ to $+\infty$ for each component). The first term on the right-hand side of Equation (1) represents the rate of change of the probability distribution function due to turbulence diffusion and the last term depicts the effect of turbulence dissipation rate.

Lundgren [9] modeled the relaxation time, the characteristic time for decay of anisotropy, by the equation

$$\frac{1}{\bar{\tau}} = \frac{K(\bar{\varepsilon} + \frac{3}{2} D\bar{U}^2/Dt)}{\bar{U}^2} \tag{4}$$

Here, $\bar{\varepsilon}$ is the turbulence dissipation rate and K is a constant of proportionality.

To make the analysis simpler, it is desirable to introduce the turbulence velocity $\vec{c} = \vec{v} - \vec{u}$ as an independent variable. Making this change of variable and simplifying the physical coordinates to the case of one dimension, the governing equation, Eq. (1), becomes

$$\bar{c}_y \frac{\partial \bar{f}}{\partial \bar{y}} - \left(\bar{c}_y \frac{d\bar{u}_x}{d\bar{y}} + \frac{1}{\rho} \frac{\partial \bar{p}}{\partial \bar{x}} - \nu \frac{d^2 \bar{u}_x}{d\bar{y}^2} \right) \frac{\partial \bar{f}}{\partial \bar{c}_x} - \frac{1}{\rho} \frac{\partial \bar{p}}{\partial \bar{y}} \frac{\partial \bar{f}}{\partial \bar{c}_y} \tag{5}$$

$$= \frac{1}{\bar{\tau}} (\bar{F} - \bar{f}) + \frac{\bar{\varepsilon}}{3\bar{U}^2} \left(3\bar{f} + \bar{c}_x \frac{\partial \bar{f}}{\partial \bar{c}_x} + \bar{c}_y \frac{\partial \bar{f}}{\partial \bar{c}_y} + \bar{c}_z \frac{\partial \bar{f}}{\partial \bar{c}_z} \right)$$

Here, $\bar{y}$ is the direction normal to the mean flow and $\bar{c}_x$, $\bar{c}_y$ and $\bar{c}_z$ are the turbulence velocity components. The distribution function should satisfy the constraints

$$\int_{-\infty}^{\infty} \int\int \bar{f} \, d\bar{c}_x \, d\bar{c}_y \, d\bar{c}_z = 1 \tag{6a}$$

$$\int\int\int_{-\infty}^{\infty} \bar{c}_i \, \bar{f} \, d\bar{c}_x \, d\bar{c}_y \, d\bar{c}_z = \bar{c}_i = 0 \tag{6b}$$

where the subscript i represents a component of $\vec{c}$. Equation (6a) states that the probability of finding a fluid element somewhere in $\vec{r}$, $\vec{v}$ space is unity, while equation (6b) requires that the mean of the fluctuating velocity components be zero.

Reduced Distribution Functions

A reduction in computer storage requirements is secured by defining the reduced distribution functions as follows:

$$\bar{g}(\bar{y},\bar{c}_y) = \int\int_{-\infty}^{\infty} \bar{f}(\bar{y},\bar{c}_x,\bar{c}_y,\bar{c}_z) d\bar{c}_x \, d\bar{c}_z \tag{7a}$$

$$\bar{j}(\bar{y},\bar{c}_y) = \int\int_{-\infty}^{\infty} \bar{c}_x \, \bar{f}(\bar{y},\bar{c}_x,\bar{c}_y,\bar{c}_z) \, d\bar{c}_x \, d\bar{c}_z \tag{7b}$$

$$\bar{h}(\bar{y},\bar{c}_y) = \int\int_{-\infty}^{\infty} (\bar{c}_x^2 + \bar{c}_z^2)\bar{f}(\bar{y},\bar{c}_x,\bar{c}_y,\bar{c}_z) d\bar{c}_x d\bar{c}_z \tag{7c}$$

Also, let

$$\bar{j}_v(\bar{y},\bar{v}_y) = \int\int_{-\infty}^{\infty} (\bar{c}_x + \bar{u}_x)\bar{f}(\bar{y},\bar{c}_x,\bar{c}_y,\bar{c}_z) \, d\bar{c}_x d\bar{c}_z, \tag{7d}$$

and $\bar{G}$, $\bar{H}$ and $\bar{J}_v$ be the reduced Gaussian (equilibrium) distributions. Equation (5) is transformed into a set of equations in terms of the reduced distribution functions which are easier to treat numerically. These are

$$\bar{c}_y \frac{\partial \bar{g}}{\partial \bar{y}} = \frac{1}{\bar{\tau}} (\bar{G} - \bar{g}) + \frac{\bar{\varepsilon}}{3\bar{U}^2} \left(\bar{g} + \bar{c}_y \frac{\partial \bar{g}}{\partial \bar{c}_y} \right) + \frac{1}{\rho} \frac{\partial \bar{p}}{\partial \bar{y}} \frac{\partial \bar{g}}{\partial \bar{c}_y} \tag{8a}$$

$$\bar{c}_y \frac{\partial \bar{j}}{\partial \bar{y}} = \frac{-\bar{j}}{\bar{\tau}} + \left(\nu \frac{d^2 \bar{u}_x}{d\bar{y}^2} - \frac{1}{\rho} \frac{\partial \bar{p}}{\partial \bar{x}} - \bar{c}_y \frac{d\bar{u}_x}{d\bar{y}} \right) g + \left(\frac{\bar{\varepsilon}}{3\bar{U}^2} \bar{c}_y + \frac{1}{\rho} \frac{\partial \bar{p}}{\partial \bar{y}} \right) \frac{\partial \bar{j}}{\partial \bar{c}_y} \tag{8b}$$

$$\bar{c}_y \frac{\partial \bar{h}}{\partial \bar{y}} = \frac{1}{\bar{\tau}} (\bar{H} - \bar{h}) + 2 \left(\nu \frac{d^2 \bar{u}_x}{d\bar{y}^2} - \frac{1}{\rho} \frac{\partial \bar{p}}{\partial \bar{x}} - \bar{c}_y \frac{d\bar{u}_x}{d\bar{y}} \right) \bar{j} \tag{8c}$$

$$+ \frac{\bar{\varepsilon}}{3\bar{U}^2} \left(-\bar{h} + \bar{c}_y \frac{\partial \bar{h}}{\partial \bar{c}_y} \right) + \frac{1}{\rho} \frac{\partial \bar{p}}{\partial \bar{y}} \frac{\partial \bar{h}}{\partial \bar{c}_y} \tag{8c}$$

and

$$\bar{v}_y \frac{\partial \bar{j}_v}{\partial \bar{y}} = \frac{1}{\bar{\tau}} (\bar{J}_v - \bar{j}_v) + \left(\nu \frac{d^2 \bar{u}_x}{d\bar{y}^2} - \frac{1}{\rho} \frac{\partial \bar{p}}{\partial \bar{x}} + \frac{\bar{\varepsilon}}{3\bar{U}^2} \bar{u}_x \right) \bar{g}$$

$$+ \left(\frac{\bar{\varepsilon}}{3\bar{U}^2} \bar{v}_y + \frac{1}{\rho} \frac{\partial \bar{p}}{\partial \bar{y}} \right) \frac{\partial \bar{j}_v}{\partial \bar{v}_y} \tag{8d}$$

where

$$\frac{1}{\bar{\tau}} = K \frac{\bar{\varepsilon}}{\bar{U}^2} ,$$

$$\bar{G} = (2\pi \bar{U}^2)^{-\frac{1}{2}} \exp(-\bar{c}_y^2 / 2\bar{U}^2)$$

$$\bar{H} = 2\bar{U}^2 \bar{G}$$

and $$\bar{J}_v = \bar{u}_x \bar{G}.$$

Moments of Interest

Once equations (8) are solved, the moments of the distribution functions can be computed. Some of the moments of interest are

$$\bar{u}_x = \int_{-\infty}^{\infty} \bar{j}_v \, d\bar{v}_y \tag{9a}$$

$$E_k = \frac{3}{2}\bar{U}^2 = \frac{1}{2}\int_{-\infty}^{\infty} \bar{h}\, d\bar{c}_y + \frac{1}{2}\int_{-\infty}^{\infty} \bar{c}_y^2\, \bar{g}\, d\, \bar{c}_y \tag{9b}$$

$$\bar{P}_{xy} = \overline{c_x c_y} = \int_{-\infty}^{\infty} \bar{c}_y\, \bar{j}\, d\bar{c}_y \tag{9c}$$

$$\overline{c_y^2} = \int_{-\infty}^{\infty} \bar{c}_y^2\, \bar{g}\, d\bar{c}_y \tag{9d}$$

$$\overline{c_x^2 + c_z^2} = \int_{-\infty}^{\infty} \bar{h}\, d\bar{c}_y \tag{9e}$$

$$Q_y = \frac{1}{2}\int_{-\infty}^{\infty} \bar{c}_y\, \bar{h}\, d\bar{c}_y + \frac{1}{2}\int_{-\infty}^{\infty} \bar{c}_y^3\, \bar{g}\, d\bar{c}_y \tag{9f}$$

$$S = \frac{1}{\bar{U}^3}\int_{-\infty}^{\infty} \bar{c}_y^3\, \bar{g}\, d\bar{c}_y \tag{9g}$$

$$K_u = \frac{1}{\bar{U}^4}\int_{-\infty}^{\infty} \bar{c}_y^4\, \bar{g}\, d\bar{c}_y \tag{9h}$$

These are the mean velocity, turbulence kinetic energy, Reynolds stress, mean square of the y-component velocity fluctuations, mean square of x and z-component velocity fluctuations, kinetic energy flux, skewness and flatness factor, respectively.

Final Reduced Equations

It is convenient to define the following non-dimensional variables:

$$c_y = \frac{\bar{c}_y}{u_*}\ ;\ v_y = \frac{\bar{v}_y}{u_*}\ ;\ U = \frac{\bar{U}}{u_*}\ ;\ u = \frac{\bar{u}_x}{u_*}\ ;\ \tau = \frac{u_*\bar{\tau}}{d}\ ;\ \overline{u'v'} = P_{xy} = \frac{\bar{P}_{xy}}{u_*^2}\ ;$$

$$\langle v'^2 \rangle = \frac{c_y^2}{u_*^2}\ ;\ \langle u'^2 + w'^2 \rangle = \frac{(\overline{c_x^2}+\overline{c_z^2})}{u_*^2}\ ;\ f = u_*^3\, \bar{f}\ ;\ g = u_*\, \bar{g};\ h = \frac{\bar{h}}{u_*}\ ;\ j = \bar{j};$$

$$j_v = \bar{j}_v \; ; \; Q_y = \frac{\bar{Q}_y}{u_*^3} \; ; \; \varepsilon = \frac{\bar{\varepsilon} d}{u_*^3} \; ; \; x = \frac{\bar{x}}{d} \; ; \; y = \frac{\bar{y}}{d} \; ; \; \nu_T = \frac{\bar{\nu}_T}{\nu} \; ; \; Re_* = \frac{u_* d}{\nu} \; ;$$

$$P_x = \frac{d}{\rho u_*^2} \frac{\partial \bar{p}}{\partial \bar{x}} \; ; \; P_y = \frac{d}{\rho u_*^2} \frac{\partial \bar{p}}{\partial \bar{y}} \; ;$$

where 2d is the distance between the parallel plates, $u_* = [(P_{xy})_w/\rho]^{\frac{1}{2}}$, is the usual friction velocity, $(P_{xy})_w$ is the wall shear stress and ν_T is the turbulence viscosity.

Using these quantities, the governing equations become,

$$c_y \frac{\partial g}{\partial y} = \frac{1}{\tau}(G-g) + \frac{\varepsilon}{3U^2}\left(g + c_y \frac{\partial g}{\partial c_y}\right) + P_y \frac{\partial g}{\partial c_y} \qquad (10a)$$

$$c_y \frac{\partial j}{\partial y} = \frac{-j}{\tau} + \left(\frac{1}{Re_*} \frac{d^2u}{dy^2} - P_x - c_y \frac{du}{dy}\right) g \qquad (10b)$$

$$+ \left(\frac{\varepsilon}{3U^2} c_y + P_y\right) \frac{\partial j}{\partial c_y}$$

$$c_y \frac{\partial h}{\partial y} = \frac{1}{\tau}(H-h) + 2\left(\frac{1}{Re_*} \frac{d^2u}{dy^2} - P_x - c_y \frac{du}{dy}\right) j \qquad (10c)$$

$$+ \frac{\varepsilon}{3U^2}\left(-h + c_y \frac{\partial h}{\partial c_y}\right) + P_y \frac{\partial h}{\partial c_y}$$

and

$$v_y \frac{\partial j_v}{\partial y} = \frac{1}{\tau}(J_v - j_v) + \left(\frac{\varepsilon}{3U^2} u + \frac{1}{Re_*} \frac{d^2u}{dy^2} - P_x\right) g \qquad (10d)$$

$$+ \left(\frac{\varepsilon}{3U^2} v_y + P_y\right) \frac{\partial j_v}{\partial v_y} \; .$$

This set of equations is to be solved by the discrete ordinate method, subject to boundary conditions to be discussed in Chapter III.

Examination of this system of equations reveals that it is not yet completely self-contained. The dissipation rate ε is not given as a moment of the distribution function. Therefore, a separate equation for ε is required to close the set. Among the possibilities for such an equation is the differential equation for ε developed by Jones and Launder [17] based upon a semi-empirical approach. For one-dimensional flow, the non-dimensionalized equation is

$$\frac{\nu_T}{\sigma_\varepsilon}\frac{d^2\varepsilon}{dy^2} + \frac{1}{\sigma_\varepsilon}\left(\frac{d\nu_T}{dy}\right)\left(\frac{d\varepsilon}{dy}\right) + \frac{2}{3}c_1\frac{\nu_T}{U^2}\left(\frac{du}{dy}\right)^2\varepsilon \qquad (11a)$$

$$- \frac{2}{3}c_2\,Re_*\frac{\varepsilon^2}{U^2} = 0$$

Here, σ_ε, c_1 and c_2 are constants and $\nu_T = -Re_*\,\overline{u'v'}/(du/dy)$.

For the case of Couette flow, there is another possible expression for ε resulting from equating the rate of production of turbulence kinetic energy to the rate of dissipation. Using the assumption $E_k \approx$ constant, this equation becomes

$$\varepsilon = a\frac{U^3}{y} \qquad (11b)$$

where $a \approx 0.8$.

CHAPTER III

BOUNDARY CONDITIONS

One of the difficult aspects of this study is specification of the appropriate boundary conditions. This difficulty arises as a result of two factors. First, there is no obvious form to assume for the distribution function at a solid boundary. This is in contrast to the situation which arises in establishing boundary conditions for moments of the distribution function. Since the mean flow velocity is a moment of the distribution function, information from continuum flow only gives the no-slip condition that

$$\vec{u} = \int \vec{v}\, f\, d\vec{v} = 0.$$

Because many functions for f could be specified which satisfy this integral constraint, there is lack of uniqueness in prescribing f.

Second, the validity of the turbulence model equation is questionable very near the wall, particularly in the region corresponding to the viscous sublayer. Thus, there is hesitation in applying the analysis in this zone.

With these considerations in mind, the two fundamental factors to be addressed are the functional form for the boundary conditions on the distribution function and the location where it should be applied.

The present study therefore contains, in addition to the development of a capability of obtaining convergent, stable numerical solutions

to the model equation, a detailed examination of two different boundary conditions in light of comparison with experimental data [18, 19, 20, 21]. This division of the problem virtually parallels the situation arising in calculations of rarefied flows from the Boltzmann equation. In this field the study of gas-surface interactions, which are used for boundary conditions in solution of the governing equation, has become almost a separate field of endeavor within itself. Such could well be the case with the statistical approach to turbulent flows.

Matching to the Law of the Wall

The course taken in the present work is to confine the application of the turbulent model equation to regions outside the viscous sublayer. The boundary conditions for the governing equation are applied at points where $y_* = \bar{y}u_*/\nu$ lie between 50 to 150. The usual functional forms for law of the wall were assumed to relate the boundary point to wall conditions. This necessitates that certain matching of the numerical solutions to law of wall variation at this interface be performed. The specific conditions applied are dependent upon the form selected for the distribution at the boundary and will be discussed in more detail in Chapter IV.

Gradient Boundary Condition

In the region where the law of the wall is valid, it is known that the mean velocity profile is logarithmic and the turbulence kinetic energy, or $\bar{U}^2/u_*^2$, is approximately constant [22]. Also in this logarithmic region, the turbulence dissipation rate is approximately equal to the rate of production of turbulence kinetic energy, $-P_{xy}\, du/dy$. Using

the logarithmic mean velocity profile, the dissipation rate is inversely proportional to the distance from the wall. Assuming the pressure gradient, P_y, to be zero, under these requirements, the governing equation itself may be used to develop an appropriate form for the distribution function. The detailed derivation of such a distribution function is shown in Appendix A.

For the simpler case of Couette flow with zero pressure gradient, the momentum equation requires that the total shear stress is constant between the plates. If attention is confined to the region well outside the viscous sublayer, then the viscous stresses are negligible and therefore the Reynolds stress is constant. Assuming that the apparent viscosity coefficient is linear in y, then gives the familiar logarithmic mean velocity profile. Further, in this region, the turbulence kinetic energy is approximately constant. In terms of moments described earlier, these conditions give

$$\iiint_{-\infty}^{\infty} (c_x^2 + c_y^2 + c_z^2) f \, dc_x \, dc_y \, dc_z = 3U^2 = \text{const.}$$

$$\iiint_{-\infty}^{\infty} c_x c_y \, f \, dc_x \, dc_y \, dc_z = P_{xy} = \text{const.}$$

Therefore, under the assumption of linear variation of ν_T for the Couette flow problem, it should be possible to construct a boundary condition for the distribution function such that the governing statistical equation yields a logarithmic mean velocity profile between the plates. A sufficient condition for this is to require $\partial f/\partial y = 0$ at the boundary point, and to require it to match with the law of the wall. In terms

of the reduced distribution functions, this condition implies $\partial g/\partial y = \partial j/\partial y = \partial h/\partial y = 0$ at the boundary point.

The governing equations themselves may be used to develop appropriate forms for the distribution functions by setting $\partial g/\partial y = \partial j/\partial y = \frac{\partial h}{\partial y} = 0$ in Equations (10). If one assumes $du/dy = 1/\kappa y$, $U = U_b$, $\varepsilon = 1/\kappa y$ and $\frac{1}{\tau} = K\varepsilon/U^2$, then, for the case of Couette flow with zero pressure gradient, Equations (10) reduce to

$$3K(G_b - g_b) + g_b + c_y \frac{dg_b}{dc_y} = 0 \tag{12a}$$

$$-3Kj_b + c_y \frac{dj_b}{dc_y} = 3g_b c_y U_b^2 \tag{12b}$$

$$3K(H_b - h_b) - h_b + c_y \frac{dh_b}{dc_y} = 6j_b c_y U_b^2 \ . \tag{12c}$$

The subscript b is used to indicate that the quantities are to be used only as boundary conditions in solving Equations (10). It should be noted that $\partial j_v/\partial y \neq 0$ since the mean velocity is not a constant, but logarithmic. However, j_v can be related to g and j by

$$j_v = \int_{-\infty}^{\infty}\int (c_x + u)\ f\ dc_x dc_y = j + u\ g \tag{13}$$

Hence, at the boundary

$$j_{v_b} = j_b + u_b\ g_b$$

where u_b is the mean velocity at the boundary point. The boundary point is selected such that $y_* = u_* y_b/\nu$ is approximately 100 to ensure that

viscous stresses are negligible there.

The solution to the set of Equations (12) must be obtained numerically. Since the distributions function and all their derivatives with respect to velocity must approach zero as $|c_y| \to \infty$, this is used as a boundary condition in velocity space. The integration proceeds from a large absolute value of c_y toward zero. A second-order finite difference scheme is utilized for the integration. The result of the integration is a set of numerical values for the distribution functions which are then employed as boundary conditions in the solution of the model equation. A similar procedure is employed for a more complicated case like the channel flow, for which the conditions shown in Appendix A are appropriate.

Chapman-Enskog Distribution Function

Flow fields involving pressure gradients do not have constant shear stress profiles. For such problems, the assumption $\partial f/\partial y = 0$ is not valid and the conditions given in Appendix A are more appropriate. However, these conditions are only sufficient conditions and in reality they may not be true. Therefore, it is desirable to seek a boundary condition for the distribution functions which would circumvent this difficulty. Upon first inspection it would seem possible to impose a Gaussian distribution as boundary condition in a manner analogous to the use of Maxwellian re-emission of molecules from a surface in the kinetic theory of gases. However, since a Gaussian distribution function gives zero Reynolds' stress, this is inappropriate for application within a turbulent zone.

An organized manner of obtaining proper boundary conditions is the Chapman-Enskog procedure [23]. By this method one can obtain approximate solutions to Equation (1) using a Series expansion. The Zeroth order

solution gives an equilibrium Gaussian distribution, which, as mentioned earlier, results in zero Reynolds' stress. The first-order solution is commonly termed the Chapman-Enskog distribution, and accommodates a non-zero Reynolds' stress.

The first-order Chapman-Enskog expansion for a one-dimensional flow gives

$$f^{(1)} = F\left\{1 - \frac{\nu_T}{Re_* U^2}\left[\left(\frac{c^2}{2U^2} - \frac{5}{2}\right)\frac{c_y}{U^2}\frac{dU^2}{dy} + \frac{c_x c_y}{U^2}\frac{du}{dy}\right]\right\} \tag{14}$$

where

$$F = \left(\frac{1}{2\pi U^2}\right)^{3/2} \exp[-(c_x^2 + c_y^2 + c_z^2)/2U^2]$$

is the Guassian distribution. The corresponding non-dimensionalized forms for the reduced distribution functions are

$$g^{(1)} = G - \frac{\nu_T}{Re_* U^3}\frac{dU}{dy} c_y\left[\frac{1}{U^2}(H + c_y^2 G) - 5G\right] \tag{15a}$$

$$j^{(1)} = -\frac{\nu_T}{Re_*}\frac{c_y}{U^2}\frac{du}{dy} G \tag{15b}$$

$$h^{(1)} = H - \frac{\nu_T}{Re_* U^3}\frac{dU}{dy} c_y\left[\frac{c_y^2}{U^2} H + 8U^2 G - 5H\right] \tag{15c}$$

$$j_v^{(1)} = j^{(1)} + u\, g^{(1)} \tag{15d}$$

These forms may then be applied as boundary conditions for the governing equation. Details of the application will be discussed in Chapter IV.

Two-Stream Nature of Boundary Conditions

Even though boundary conditions for the distribution functions are established, their implementation is not straightforward. If one examines the physics of the flow problem between parallel plates, it is clear that both plates contribute to the establishment of the flow; and, therefore, boundary conditions should be applied at a y_* value near each plate, giving two boundary conditions. (The symmetric condition at the centerline may be used to reduce the problem to a half-space in y, but still this requires two boundary conditions on f). Yet, if one examines the one-dimensional governing equation, Eq. (5), it is observed that only first-order derivative of f with respect to y is present. It would thus appear that imposition of two boundary conditions would result in overspecifying the problem.

Experience in solving the Boltzmann equation in rarefied gas dynamics gives insight to resolving this paradox. In the molecular approach to rarefied flows, one can specify the velocity distribution function of molecules leaving a surface. The distribution function for those striking the surface is determined as a consequence of the solution. Thus, the boundary conditions possess a "two stream" nature. The interaction of the incoming and outgoing streams is controlled through the collision or relaxation term in the model equation and through integral constraints such as the requirement that the incoming mass flux equal that for the outgoing stream.

If this concept is applied to the problem of turbulent flow between parallel plates, one requires that at the boundary point near the lower plate the distribution function be specified only for positive values of

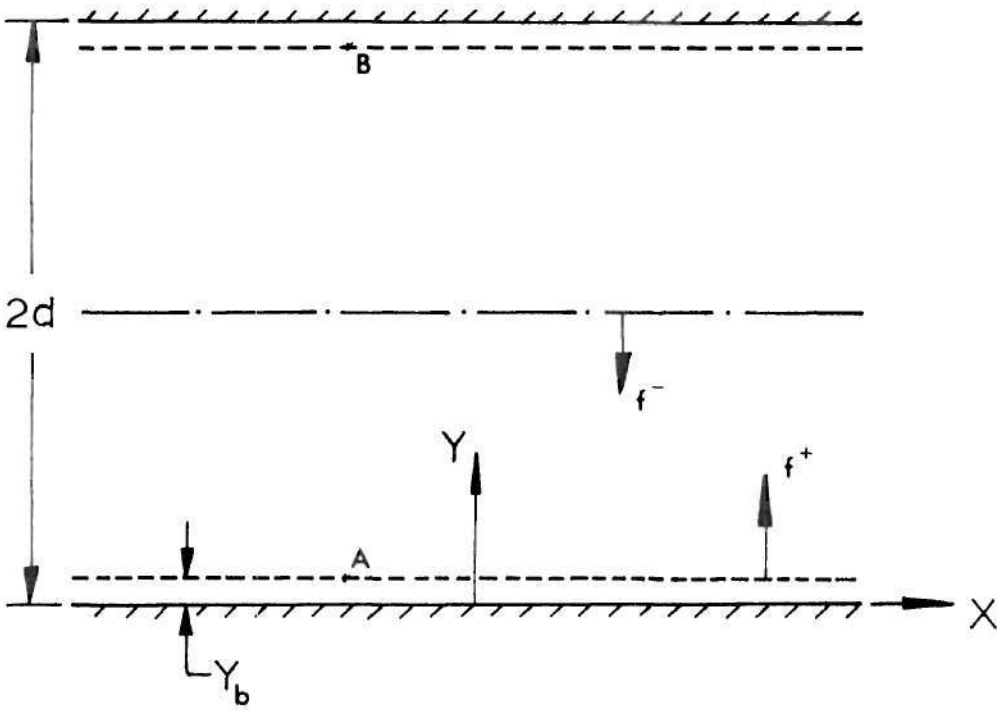

$$y_* = u_* y_b / \nu \simeq 100$$

Figure 1. Two-stream Boundary Conditions.

c_y while for the corresponding point near the upper plate it is specified only for negative value of c_y. This is illustrated in Figure 1. Insofar as the function f is concerned, this is equivalent to imposing a single constraint for all c_y domain values while it allows the effects of each plate to be introduced into the problem. This is mathematically consistent with the first order nature of the y derivative in the governing equation. Further, it seems plausible that such a two-stream approach is justified on a physical basis, since the turbulence motions leaving and approaching the wall region will be affected differently by the presence of the wall.

CHAPTER IV

NUMERICAL APPROACH

Discrete Ordinate Method

The discrete ordinate method is a numerical technique of replacing a continuous independent variable in a system of equations by a set of discrete values and then treating these as parameters in the remaining solutions. Although not restricted to integro-differential equations, the method has proven quite useful in attacking this type of problem. Two examples of this application in physics are radiative transfer [24] and rarefied gas dynamics [15, 16]. The latter field is closely related to the present study since the fundamental equation in rarefied gas dynamics is the Boltzmann equation for the velocity distribution function of molecules. If the BGK model [10] is substituted for the collision integral of the equation, the one-dimensional form of the Boltzmann equation becomes

$$c_y \frac{\partial f}{\partial y} = \frac{1}{\tau}(F - f)$$

in the absence of external forces. This possesses the form similar to Equation (5). However, the latter equation is more difficult to treat since it includes terms containing $\partial f/\partial \vec{c}$. Thus, one of the important extensions of the discrete ordinate method as applied to the present problem has been the treatment of derivatives in velocity space. The presence of external force terms in the Boltzmann equation would introduce derivatives with respect to velocity, and thus the technique devised in the present

numerical solutions for turbulence can be transferred back to rarefied gas dynamics.

Since the flow properties of interest are obtained as integrals over velocity space (as seen from Equations (9)), it is preferable to discretize the velocity variable. The set of discrete velocity points is denoted by $\{c_\sigma\}$, and a continuous function, say, $g(y,c_y)$ is replaced by a set of functions $g_\sigma(y)$, $\sigma = 1,2,\ldots,s$. The same procedure is applied to each of the dependent variables. The integration over c_y to form moments may then be accomplished by numerical quadrature employing appropriate weighting functions,

$$\int_{-\infty}^{\infty} \phi(c_y)\, g(y,c_y)\, dc_y \approx \sum_{\sigma=1}^{s} \phi(c_\sigma)\, g_\sigma(y) W_\sigma \tag{16}$$

where ϕ is a function of c_y, and W_σ are the weighting coefficients in the quadrature. The choice of discrete velocity points, c_σ, depends upon the quadrature formula employed. For functions that are not too far from a Gaussian distribution, open-type quadrature formulae such as the modified Gauss-Hermite quadrature [25] are likely to be quite accurate. However, in anticipation of the discontinuities in velocity space when the Chapman-Enskog distribution functions are used, it is preferable to employ a closed-type quadrature. In the present study, an eleven-point Newton-Cotes formula [26] is used to approximate the integrals over velocity space.

Finite Difference Methods

Since the governing equations, Eqs. (10), contain only first order derivatives with respect to y and c_y, the initial approach taken in

forming finite difference equations from the differential equation was to use simple forward and backward differences, depending upon the direction of integration. However, when this first-order scheme was employed in the Couette flow problem, it resulted in some numerical error in the region near the wall. This is illustrated in Figure 2 for the solutions obtained for Reynolds' stress with the zero-gradient and the Chapman-Enskog boundary conditions. It is expected that the Reynolds stress for Couette flow should remain constant in the turbulent zone. As seen in Figure 2, the deviation from a constant value, when the zero-gradient boundary condition is used, is approximately one per cent. Although this is quite accurate in most cases, the non-constancy of the Reynolds stress, as opposed to the absolute error, is of some concern. The results for the Chapman-Enskog boundary condition, as seen from Figure 2 shows about fifteen per cent variation across the turbulent zone. Some of this variation is due to the model assumed for the boundary condition. However, it is desirable to reduce possible numerical errors so that the effects due to physical modelling can be delineated.

To reduce numerical errors, a more accurate finite difference form for the derivatives is employed. If a function $f(y,c_y)$ is expanded in a Taylor Series about a point (y_i,c_σ), then

$$f_{i-1} = f_{i,\sigma} - \left(\frac{\partial f}{\partial y}\right)_{i,\sigma} \cdot \Delta y + \frac{1}{2}\left(\frac{\partial^2 f}{\partial y^2}\right)_{i,\sigma} (\Delta y)^2$$

$$- \frac{1}{6}\left(\frac{\partial^3 f}{\partial y^3}\right)_{i,\sigma} (\Delta y)^3 + ... \qquad (17a)$$

and

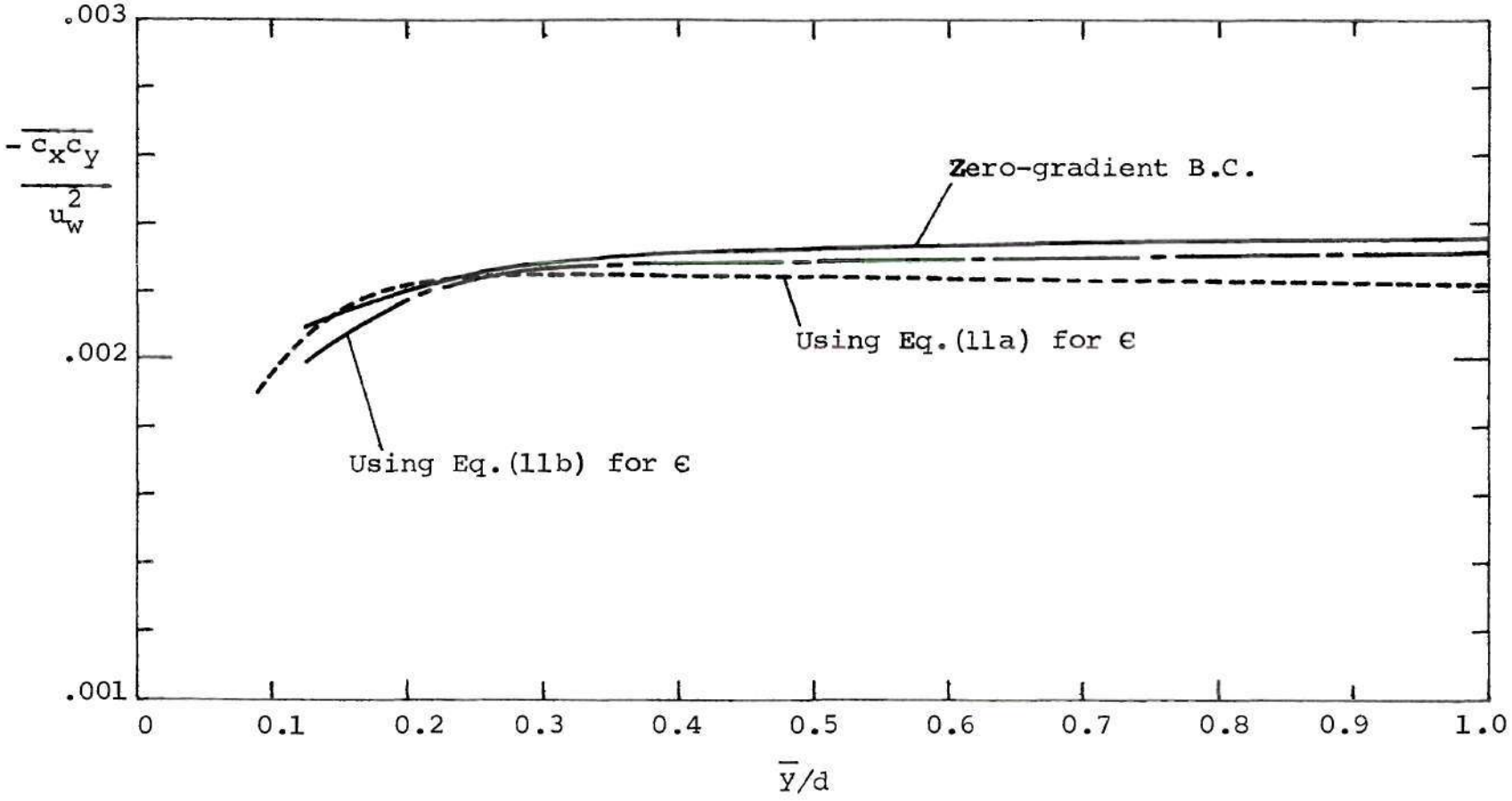

Figure 2. First-order Difference Solutions for the Couette Flow.

$$f_{i-2,\sigma} = f_{i,\sigma} - 2\left(\frac{\partial f}{\partial y}\right)_{i,\sigma} \Delta y + 2\left(\frac{\partial^2 f}{\partial y^2}\right)_{i,\sigma} (\Delta y)^2$$

$$- \frac{4}{3}\left(\frac{\partial^3 f}{\partial y^3}\right)_{i,\sigma} (\Delta y)^3 + \ldots . \qquad (17b)$$

for a constant spacing Δy. Eliminating the second derivative terms from Equations (17a) and (17b), results in the relation

$$4 f_{i-1,\sigma} - f_{i-2,\sigma} = 3 f_{i,\sigma} - 2\left(\frac{\partial f}{\partial y}\right)_{i,\sigma} (\Delta y) + \ldots$$

Solving for the first derivative gives

$$\left(\frac{\partial f}{\partial y}\right)_{i,\sigma} = \frac{3f_{i,\sigma} - 4f_{i-1,\sigma} + f_{i-2,\sigma}}{2(\Delta y)} + O[(\Delta y)^2] \qquad (18a)$$

Thus, this backward difference scheme has a truncation error of order $(\Delta y)^2$ as compared to order Δy for the simple backward difference. A similar form for a second order forward difference scheme can be developed yielding

$$\left(\frac{\partial f}{\partial y}\right)_{i,\sigma} = \frac{4f_{i+1,\sigma} - f_{i+2,\sigma} - 3f_{i,\sigma}}{2(\Delta y)} + O[(\Delta y)^2] \qquad (18b)$$

In the finite difference scheme employed, the distribution function and its derivatives with respect to y are evaluated at the same grid point. Consequently, in the light of the two-stream nature of boundary conditions, the finite difference formulae, Equations (18) are more appropriate than the usual central difference scheme.

A similar approach can be employed for deriving expressions for $(\partial f/\partial c_y)_{i,\sigma}$. However, since the range of integration for calculating macroscopic properties is infinite in the velocity domain, the spacing of discrete velocity points is necessarily variable so that efficient use of the quadrature can be achieved. Therefore, it is preferable to obtain a second order finite difference expression from Lagrange Interpolation formula [26]. This results in the following forms for the derivatives:

Backward difference:

$$\left(\frac{\partial f}{\partial c_y}\right)_{i,\sigma} = \frac{(c_\sigma - c_{\sigma-1})}{(c_{\sigma-2} - c_{\sigma-1})(c_{\sigma-2} - c_\sigma)} f_{i,\sigma-2}$$

$$+ \frac{(c_\sigma - c_{\sigma-2})}{(c_{\sigma-1} - c_{\sigma-2})(c_{\sigma-1} - c_\sigma)} f_{i,\sigma-1}$$

$$+ \frac{(2c_\sigma - c_{\sigma-1} - c_{\sigma-2})}{(c_\sigma - c_{\sigma-1})(c_\sigma - c_{\sigma-2})} f_{i,\sigma} + O[(\Delta c_\sigma)^2] \qquad (19a)$$

Forward difference:

$$\left(\frac{\partial f}{\partial c_y}\right)_{i,\sigma} = \frac{(2c_\sigma - c_{\sigma+1} - c_{\sigma+2})}{(c_\sigma - c_{\sigma+1})(c_\sigma - c_{\sigma+2})} f_{i,\sigma}$$

$$+ \frac{(c_\sigma - c_{\sigma+2})}{(c_{\sigma+1} - c_\sigma)(c_{\sigma+1} - c_{\sigma+2})} f_{i,\sigma+1}$$

$$+ \frac{(c_\sigma - c_{\sigma+1})}{(c_{\sigma+2} - c_\sigma)(c_{\sigma+2} - c_{\sigma+1})} f_{i,\sigma+2} + O[(\Delta c_\sigma)^2] \qquad (19b)$$

As a consequence of the two-stream nature of the distribution functions, the choice of the direction for the difference scheme (either forward or backward) is readily prescribed. For the "positive" stream ($c_\sigma > 0$), the computations should proceed from $+\infty$ (where boundary conditions with respect to velocity space are known) to zero in velocity space, and from the lower boundary point, point A in Figure 1 (where conditions with respect to physical space are known) to the upper boundary point B. Thus, the forward difference in velocity space and the backward difference in physical space are employed. For the "negative" stream ($c_\sigma < 0$) the reverse is true. There, the integration proceeds from $-\infty$ to 0 in c_y and from upper boundary to lower boundary in y. Thus, the backward difference in velocity space and the forward difference in physical space are utilized. When these forms are substituted for the derivative terms in Equation (10), a set of difference equations for the reduced distribution functions is obtained. These equations are given in detail in Appendix B. The results obtained using second order difference schemes show a substantial improvement over the first order results and these solutions are discussed in Chapter V.

Iterative Scheme

The resulting equations are solved by an iteration process since the equations contain terms which depend upon the macroscopic properties. Therefore, initial guesses are made for u, U and ε. The equations for positive stream are then solved from the near wall boundary point up to the centerline, symmetry or antisymmetry conditions are applied, depending upon the geometry, and the negative stream is then computed from centerline to the boundary point. This completes one iteration and yields an

approximate solution for the reduced distribution functions. From these, new profiles for the macroscopic quantities are evaluated and stored for use in the second iteration. If integral constraints are required at the boundary point, these are imposed before the second iteration is started. The required integral constraints for each problem are discussed in Chapter V and Chapter VI. The iterative process continues until satisfactory convergence is obtained for the mean flow quantities.

Constraints at Boundaries

As pointed out in Chapter III, since boundary conditions are applied at a point away from the wall where the law of the wall is applicable, certain matching of the numerical solution to the law of the wall is necessary. The form of the distribution function at the boundary point dictates the constraints which must be applied. Besides, depending upon the geometry of the problem, the conditions to be imposed at the centerline are different. The constraints for Couette flow are described in Chapter V and those required for Channel flow are discussed in Chapter VI.

CHAPTER V

COUETTE FLOW WITH ZERO PRESSURE GRADIENT

Geometry and Boundary Conditions

The configuration of Couette flow problem with zero pressure gradient is shown in Figure 3. The boundary conditions employed for this problem are the zero-gradient and the Chapman-Enskog boundary conditions. The constraints imposed at the centerline are the same regardless of the near wall boundary condition. For Couette flow with zero-pressure gradient, the turbulence quantities U, P_{xy} and $\langle v'^2 \rangle$ should have no gradients in y at the centerline. In other words, these quantities are approximately constant near the centerline. In terms of the distribution function, the condition that $\partial f/\partial y = 0$ seems very appropriate there. Since boundary conditions at centerline are required only for the negative stream, the properties of this condition can be exploited to relate the distribution functions for the negative stream to those of the positive stream. It can be seen from Eqs. (12) that the reduced distribution functions g and h are symmetric in c_y and the function j is anti-symmetric in c_y. If these properties are applied at the centerline, then

$$g^-(y=1, -c_\sigma) = g^+(y=1, c_\sigma) \tag{20a}$$

$$j^-(y=1, -c_\sigma) = -j^+(y=1, c_\sigma) \tag{20b}$$

$$h^-(y=1, -c_\sigma) = h^+(y=1, c_\sigma) \tag{20c}$$

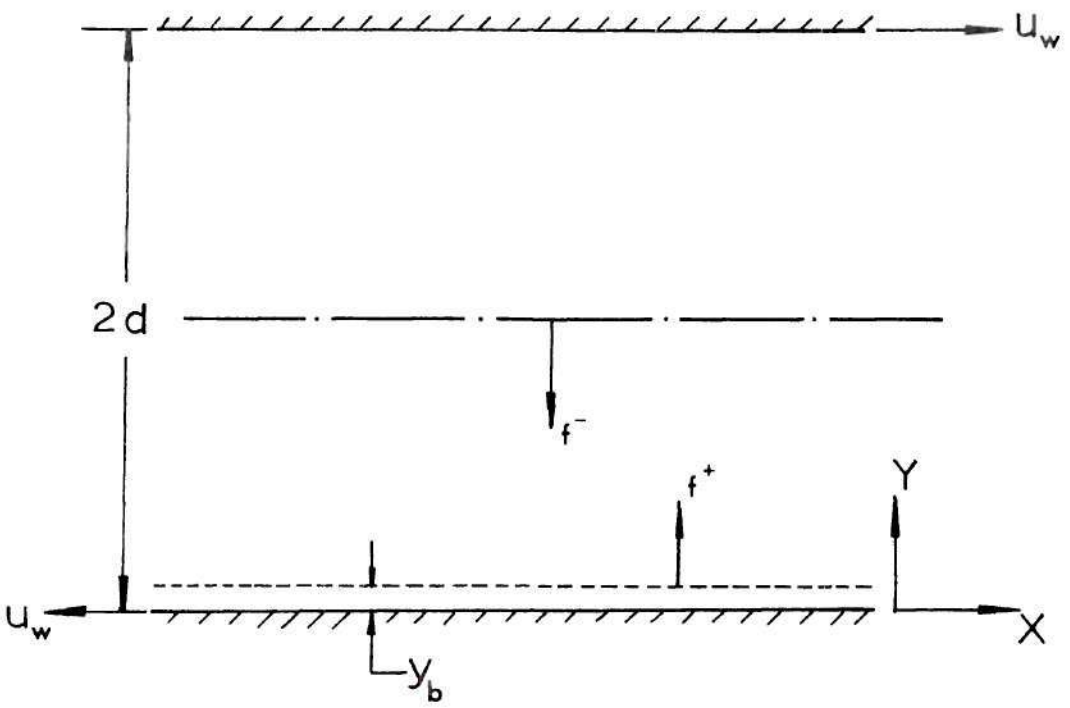

$$y_* = u_* y_b / \nu \simeq 100 \quad ; \qquad Re = u_w d / \nu$$

Figure 3. Geometry of the Couette Flow.

Equation (20a) implies that the probability that the turbulence velocity at the centerline is in the neighborhood of $-c_\sigma$ is the same as it is near $+ c_\sigma$. Equation (20b) states that the contribution of the negative stream to the momentum is opposite of that due to the positive stream, while Equation (20c) states that the contribution of the two streams to turbulence kinetic energy are the same. From the geometry of the Couette flow problem, it is seen that the mean velocity at the centerline is zero. This condition enables j_v to be determined. From Equation (13), it is seen that at the centerline,

$$j_v^- (y=1, -v_\sigma) = j^-(y=1, -c_\sigma).$$

Using Equation (20b), this yields,

$$j_v^- (y=1, -v_\sigma) = j_v^+(y=1, v_\sigma) \qquad (20d)$$

Thus, Equations (20) are used as boundary conditions for the negative stream. The constraints imposed at the near wall boundary, however, depend upon the form of the distribution functions.

Zero Gradient Boundary Condition

In employing the zero-gradient boundary condition, it is necessary to specify U and u_* (hence, the value of the wall shear stress). From the geometry of the problem, then, $Re_* = u_* d/\nu$ can be computed. Thus, if this boundary condition is employed, Re_* must be specified a priori. However, for the zero-gradient condition, the mean velocity should be logarithmic between the plates and be zero at the centerline. This can be satisfied if u_*/u_w has a particular value, given by the relation,

$$\frac{u_w}{u_*} = \frac{1}{\kappa} \ln (Re_*) + 5 \tag{21}$$

Since Re_* is given, Re can immediately be computed from $Re = Re_* \left(\frac{u_w}{u_*}\right)$. The condition for mean velocity at the boundary is given by

$$u_b = \frac{1}{\kappa} \ln(Re_* y_b) + 5 - u_w/u_* \tag{22a}$$

The values of U at $y = y_b$ is obtained from the empirical formula [22]

$$U_b^2 = \frac{2}{3\sqrt{c_D}} \text{ , with } c_D = 0.1 \tag{22b}$$

Equations (12) are then solved subject to these constraints to give boundary conditions on g, j. h, and j_v. These conditions are fixed for all iterations.

Chapman-Enskog Boundary Conditions

When the Chapman-Enskog form is used as a boundary condition for the positive stream, it is possible to deduce the u_* value from the solution, if the value of Re is specified. This is achieved by applying appropriate integral constraints upon the outgoing and incoming streams at the boundary point. Using Equations (15) as conditions on the outgoing or positive stream, the first iteration is started once the initial guesses are made. Then, upon marching back from the centerline of symmetry, certain quantities must be re-evaluated before the second iteration can proceed. These are U, $\frac{\nu_T}{Re_* U^3} \frac{dU}{dy}$, u and $\frac{\nu_T}{Re_*} \frac{du}{dy}$. In this study, the following constraints have been used.

$$\overline{u'v'} = - \frac{\nu_T}{Re_*} \frac{du}{dy} = -1.0 \tag{23a}$$

$$\overline{c_y} = \int_{-\infty}^{\infty} c_y\, g\, dcy = \int_{-\infty}^{0} c_y\, g^{-}\, dc + \int_{0}^{\infty} c_y\, g^{+} dc_y = 0 \qquad (23b)$$

$$\int_{-\infty}^{\infty} g\, dc_y = \int_{-\infty}^{0} g^{-}\, dc_y + \int_{0}^{\infty} g^{(1)}\, dc_y = 1.0 \qquad (23c)$$

$$u = u_b = \frac{1}{\kappa} \ell n \left(Re \frac{u_*}{u_w} y_b\right) + 5.0 - \frac{u_w}{u_*} \qquad (23d)$$

Equation (23a) states that the Reynolds stress at the boundary point is equal to the wall shear stress. (The viscous stresses could be included in this equation and, in fact, several calculations have been performed over the course of this study in which this has been done.) Equation (23b) requires that the time average of the fluctuating vertical velocity component be zero. Equation (23c) states that the probability of finding a fluid element with velocity between $-\infty$ and $+\infty$ is unity, and Equation (23d) is the law of the wall for mean velocity. If the Chapman-Enskog forms of Eqs. (15) are substituted into Eqs. (23), there results,

$$U = -\sqrt{2\pi}\, c_1$$

$$\frac{\nu_T}{Re_* U^2} \frac{dU}{dy} = \sqrt{2\pi}\, (0.5 - c_2) \qquad (24b)$$

where,

$$c_1 = \int_{-\infty}^{0} c_y\, g^{-}\, dc_y \qquad (24c)$$

and

$$c_2 = \int_{-\infty}^{0} g^{-}\, dc_y \qquad (24d)$$

The constants c_1 and c_2 are computed numerically at the conclusion of each iteration, based upon the current value of the g^{-} (or incoming stream) distribution. Thus, the parameters in the outgoing stream may

be readjusted at each iteration to conform with the imposed constraints. The value of u_*, and hence the wall shear stress is obtained from Equation (23d) with the computed value for u_b at the end of each iteration.

During the course of this study it was found that a slight modification to this scheme was appropriate. When these constraints are used on the Couette flow problem with zero pressure gradient, the solutions for mean velocity are found to depend upon Reynolds number, if the profiles are plotted in a velocity defect graph. These results are shown in Figure 4. The velocity defect plot should, in reality, be independent of Reynolds number. It is recalled that the boundary conditions are applied in a two-stream manner. One of the consequences of this is that it can introduce a "slip velocity" at the boundary point; that is, the calculated velocity differs slightly from that of the logarithmic law. This slip velocity depends on the plate velocity and consequently the velocity defect profiles in Figure 4 depend on the Reynolds number.

One way to eliminate such a slip velocity is to require, through an integral constraint, that the mean velocity obtained from both outgoing and incoming streams conform with the law of the wall. Since the law of the wall requires the mean velocity to be logarithmic, it is more appropriate to apply this constraint on the total moment instead of requiring only one of the two streams to follow the law. This can be achieved by treating the quantity u in Equation (15d) as a parameter that is adjusted to match the mean velocity with the law of the wall. In terms of the distribution function, this becomes

$$\int_{-\infty}^{\infty} j_v \, dv_y = \int_{-\infty}^{0} j_v \, dv_y + \int_{0}^{\infty} j_v^{(1)} dv_y = u_b \tag{25}$$

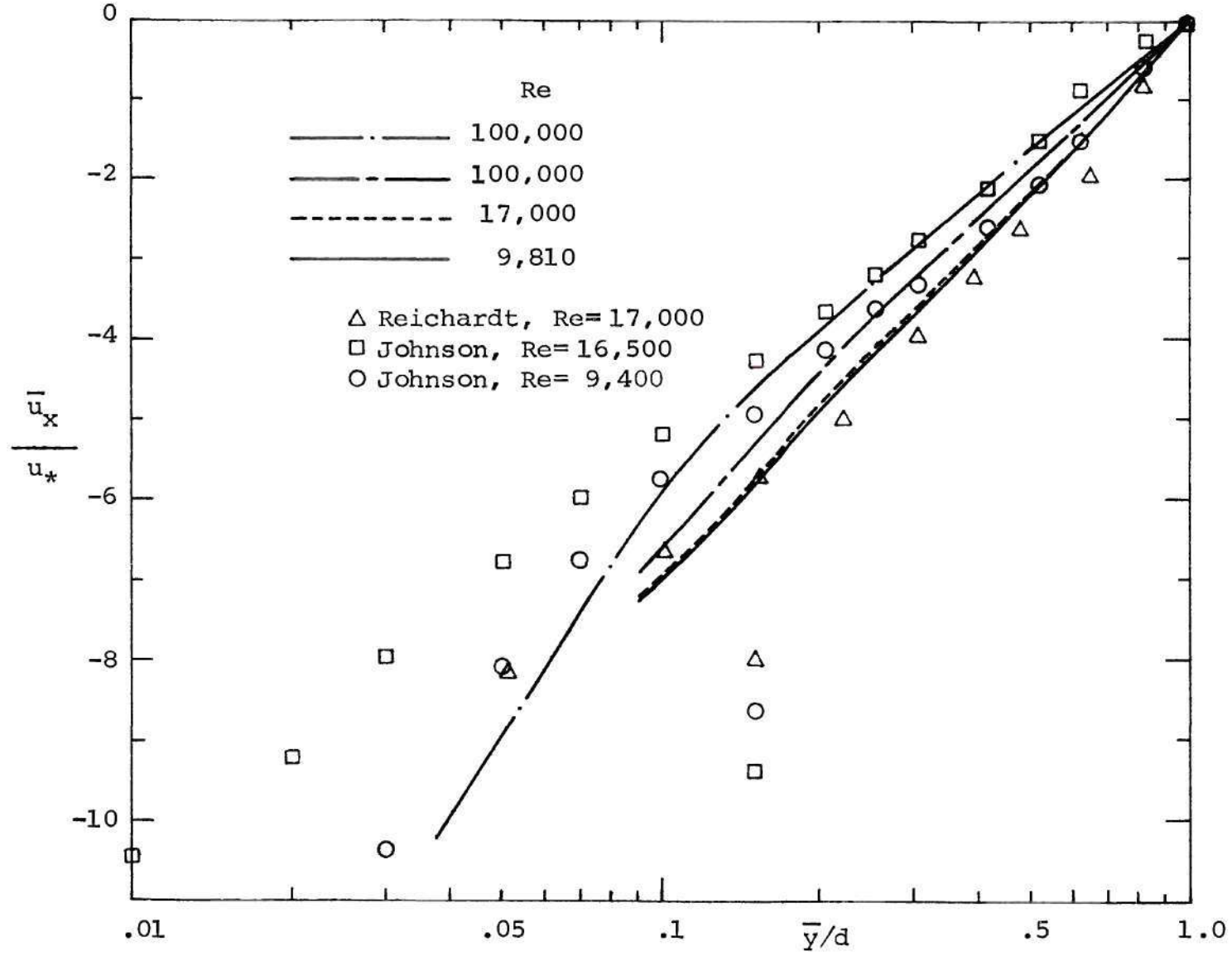

Figure 4. Velocity-defect Plot, Using Equation (23).

where $$u_b = \frac{1}{\kappa} \ln \left(Re \frac{u_*}{u_w} y_b\right) + 5.0 - \frac{u_w}{u_*} .$$

When this constraint is used in the calculations, the resulting mean velocity profiles are independent of Reynolds number. These results are illustrated in the next section. In addition to Equation (25), it is also found desirable to use the empirical relation for U given in Equation (22b). Substitution of Equations (15) into Equation (25) yields

$$u = \left[u_b - c_3 - \frac{\overline{u'v'}}{\sqrt{2\pi}\, U}\right] / (1.0 - c_2) \tag{26a}$$

where $$c_3 = \int_{-\infty}^{0} \bar{j}_v \, dv_y \tag{26b}$$

and c_2 is defined in Equation (24d). It is emphasized that this is the only point, under this Chapman-Enskog scheme for boundary conditions, at which the law of the wall is assumed to hold. This is employed only to avoid using the statistical model for turbulence within the region where viscous stresses are comparable to or larger than the Reynolds stresses.

Once the mean flow quantities are obtained as moments of the distribution functions at the end of each iteration, the dissipation rate, ε, can be obtained from Eqs. (11). The differential equation for ε, Eq. (11a), is a difficult equation to treat since it is non-linear. This equation requires two boundary conditions as it is a second order equation. The boundary condition at the centerline is

$$\frac{d\varepsilon}{dy} = 0 \qquad \text{at } y = 1 \tag{27a}$$

The near wall boundary condition for ε is obtained by assuming that

production and dissipation of turbulence kinetic energy are equal in that region. Since the law of wall is applicable there, for Couette flow, this becomes,

$$\varepsilon_b = \frac{1}{\kappa y_b} \qquad \text{at } y = y_b \tag{27b}$$

Using these boundary conditions, Equation (11a) is solved by employing the methods described in Appendix C. For Couette flow, Equation (11a) is linearized by adopting the method of differential variations [28]. The resulting linearized equations are solved by the Runge-Kutta technique [29]. These procedures are described in detail in Appendix C.

Results

The results obtained for this problem are subject to the assumption that $\partial\bar{p}/\partial\bar{y} = 0$ everywhere. From the y-momentum equation, it is seen that

$$P_y = -\frac{d}{dy}\langle v'^2 \rangle$$

For Couette flow with zero pressure gradient, it is known that $\langle v'^2 \rangle$ is constant throughout the turbulent zone. Thus, the assumption $P_y = 0$ is valid for this case. The computed results for both the zero-gradient and the Chapman-Enskog boundary conditions are discussed in the following sections.

Zero-gradient Boundary Condition

The motivation for deriving this boundary condition and applying it to the Couette flow problem is two-fold. First, it is important to determine whether, under appropriate assumptions, the statistical model

equation can reproduce a turbulent flow within which the mean velocity profile is logarithmic and the Reynolds stress remains constant. Since it is known from experiments that such a region exists near the wall for many turbulent flows, the capability of the model equation to recover this result is a logical test of its validity. Second, it is possible that such a boundary condition is potentially useful in more general situations with non-zero pressure gradient ($\partial p/\partial x \neq 0$) due to the existence of a logarithmic region near the wall for many boundary layer flows.

To obtain a logarithmic region from the model, the expression for the dissipation rate, ε, in the statistical equation must be consistent with the law of the wall. Consequently, Equation (11b) is used to solve for ε.

The zero-gradient conditions obtained from the numerical solution to Equations (12) and (11b) were applied to the equations for Couette flow, Equations (10) with $P_y = 0$. A second-order finite difference was employed in the computational procedure. Using an initial guess for u, U and ε, the iterative procedure was carried out. The value for the constant, κ, used in the logarithmic velocity profile was taken to be 0.41 [27]. The iteration procedure was terminated when changes in U between successive iterations were less than 10^{-6}. When the zero-gradient conditions were used, the solution converged after 45 iterations. As pointed out in Chapter IV, if the mean velocity profile is to be logarithmic in the entire flow field, then, there is only one value for u_*/u_w for a given Reynolds number, $Re = u_w\, d/\nu$. For Re = 17,000, this value is 0.046952.

The result for mean velocity using the zero-gradient boundary

condition is shown in Figure 5. The mean velocity profile remains within 0.05 per cent of the logarithmic profile, and the two curves are hardly discernible in the figure. Reichardt's data [19] for mean velocity is also shown in Figure 5 for comparison. It should be pointed out that by selecting appropriate values for the constants in the law of the wall, it is possible to improve the agreement between Reichardt's data and the logarithmic profile. However, the main purpose of this study is to compare the results for different boundary conditions under the same set of constants; and thus, other values for the constants were not attempted.

Figure 6 shows the results for the Reynolds stress and turbulence intensity. The computed turbulence intensity remains constant within 0.2 per cent of the correct value (U = 1.452). Similarly, the non-dimensional Reynolds stress profile remains constant within 0.8 per cent of the correct value ($\overline{u'v'} = -1.0$). As a check on the uniqueness of the solution, several different initial profiles were assumed and the iteration procedure was repeated until convergence was obtained. The resulting solutions always agreed with the corresponding profiles shown in Figures 5 and 6.

Solutions found by using the zero-gradient boundary conditions clearly illustrate that Lundgren's model equation is a reasonable one, and that realistic results may be obtained from such a statistical approach. Further, these results have demonstrated the numerical accuracy of the discrete ordinate and finite difference schemes presently employed.

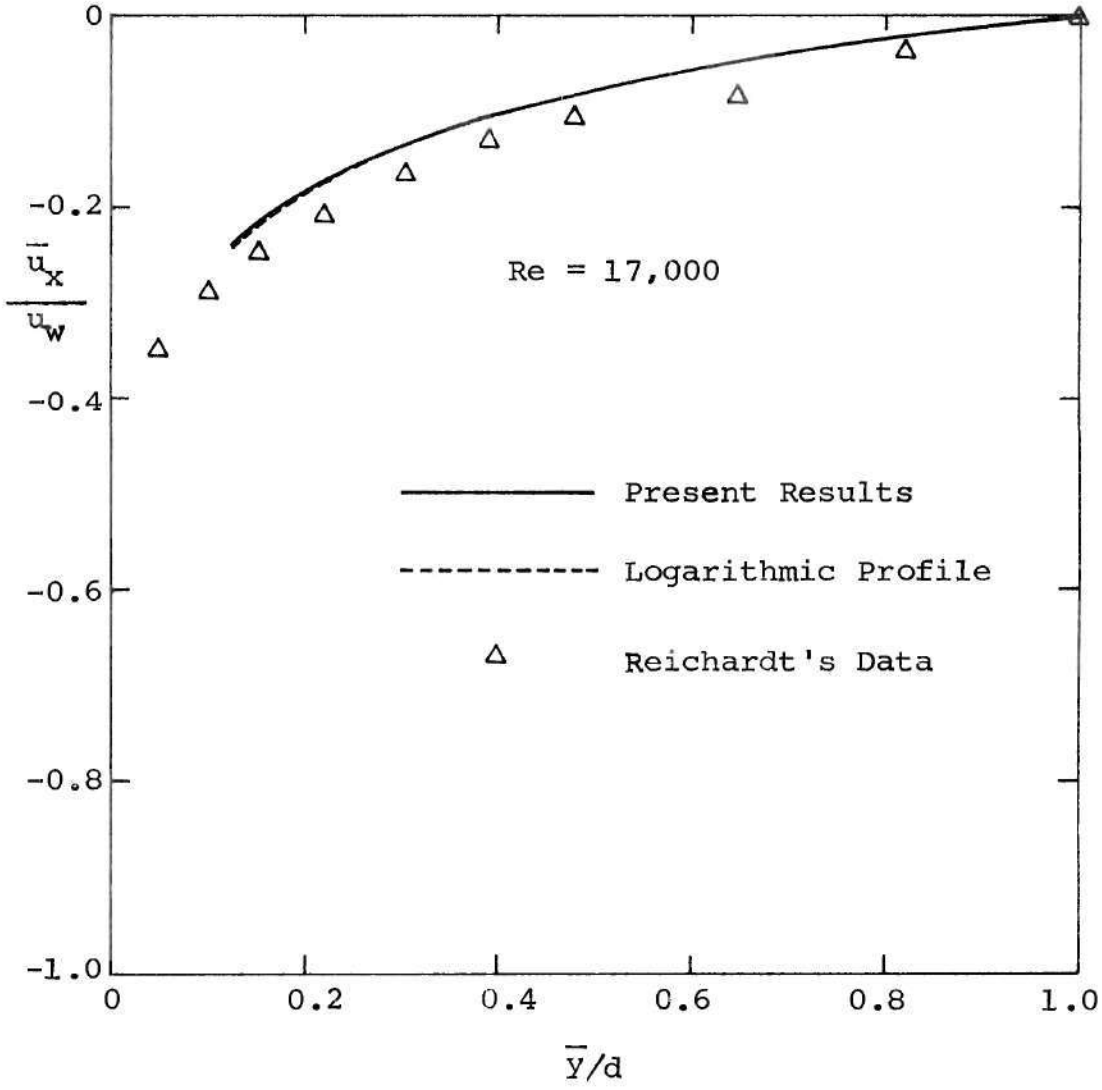

Figure 5. Mean Velocity Profile for Zero-gradient Boundary Conditions.

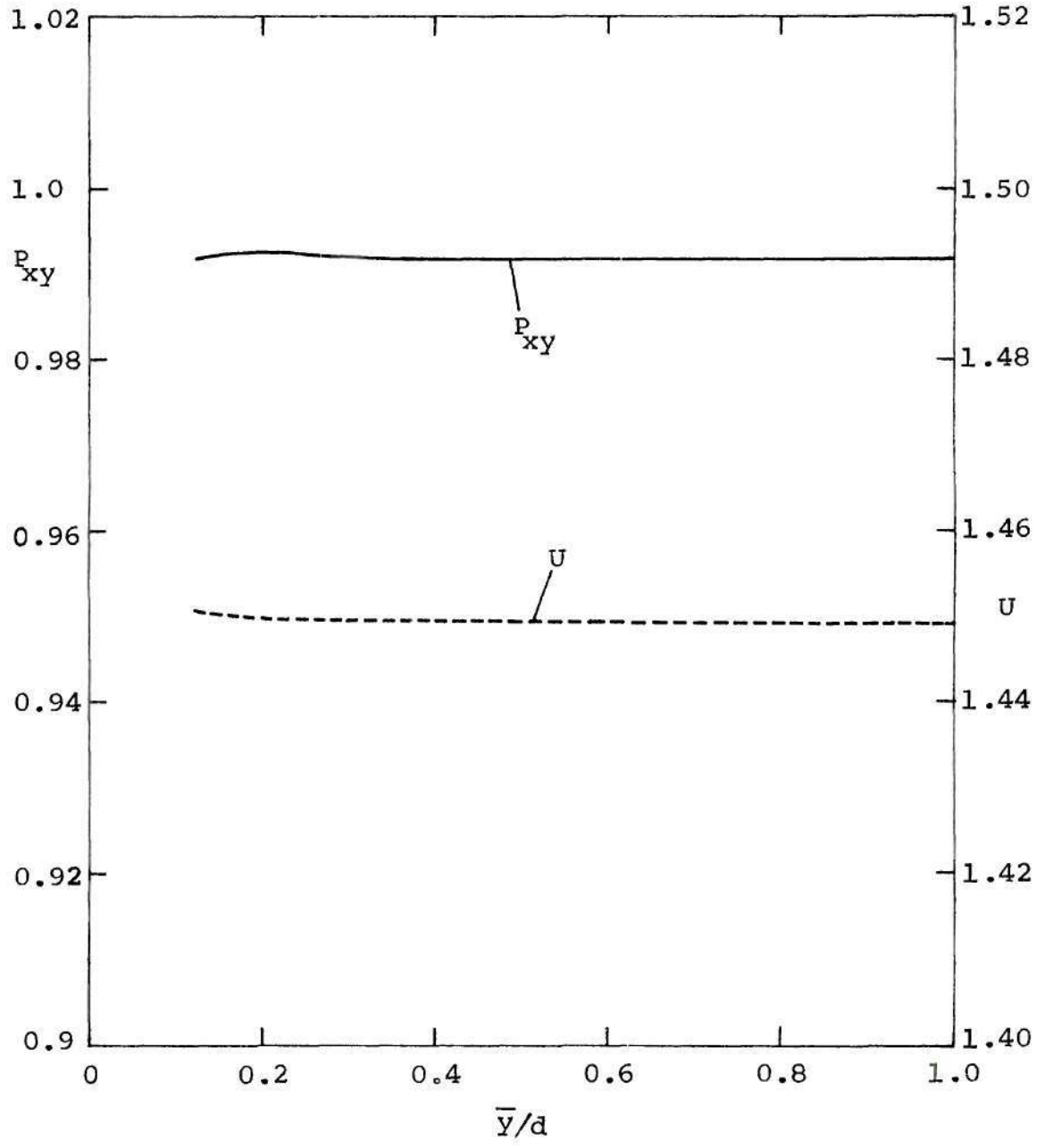

Figure 6. Reynolds Stress and Turbulence Intensity Profiles for Zero-gradient Boundary Conditions.

Chapman-Enskog Boundary Conditions

Although it is established that a logarithmic region exists near the wall for many boundary layer flows, this does not imply that such a region will extend across the entire field for the Couette flow case. Even if the mean velocity profile may apparently be logarithmic, the assumption that the length scale is proportional to the distance from the wall is not valid for the entire flow field. Hence, it is desirable to consider other forms of boundary conditions that may be useful in more general situations. In an effort to achieve this, the Chapman-Enskog form of the distribution function for the outgoing stream was employed in a series of calculations. Numerical solutions have been obtained using both the algebraic (Equation (11b)) and differential (Equation (11a)) equations for ε at a Reynolds number of 17,000. These results for mean velocity are shown in Figure 7. Reichardt's data for Re = 17,000 are also shown for comparison. Both of the solutions using the statistical model equation agree very well with the experimental data. Although differences can be observed between the two solutions, they are relatively minor. In these calculations, the integral constraints given in Equations (24) are used. A similar agreement between the two solutions has been found in the Reynolds stress profiles. These calculations show that Equation (11b) is quite reasonable for Couette flow.

Because of the two-stream manner in which the boundary conditions are employed, the solutions shown in Figure 7 have a slight slip velocity at the boundary point. This slip velocity can be eliminated by using the constraints given in Equations (26). Numerical solutions have been obtained in this study employing Equations (26) and (11a) for three

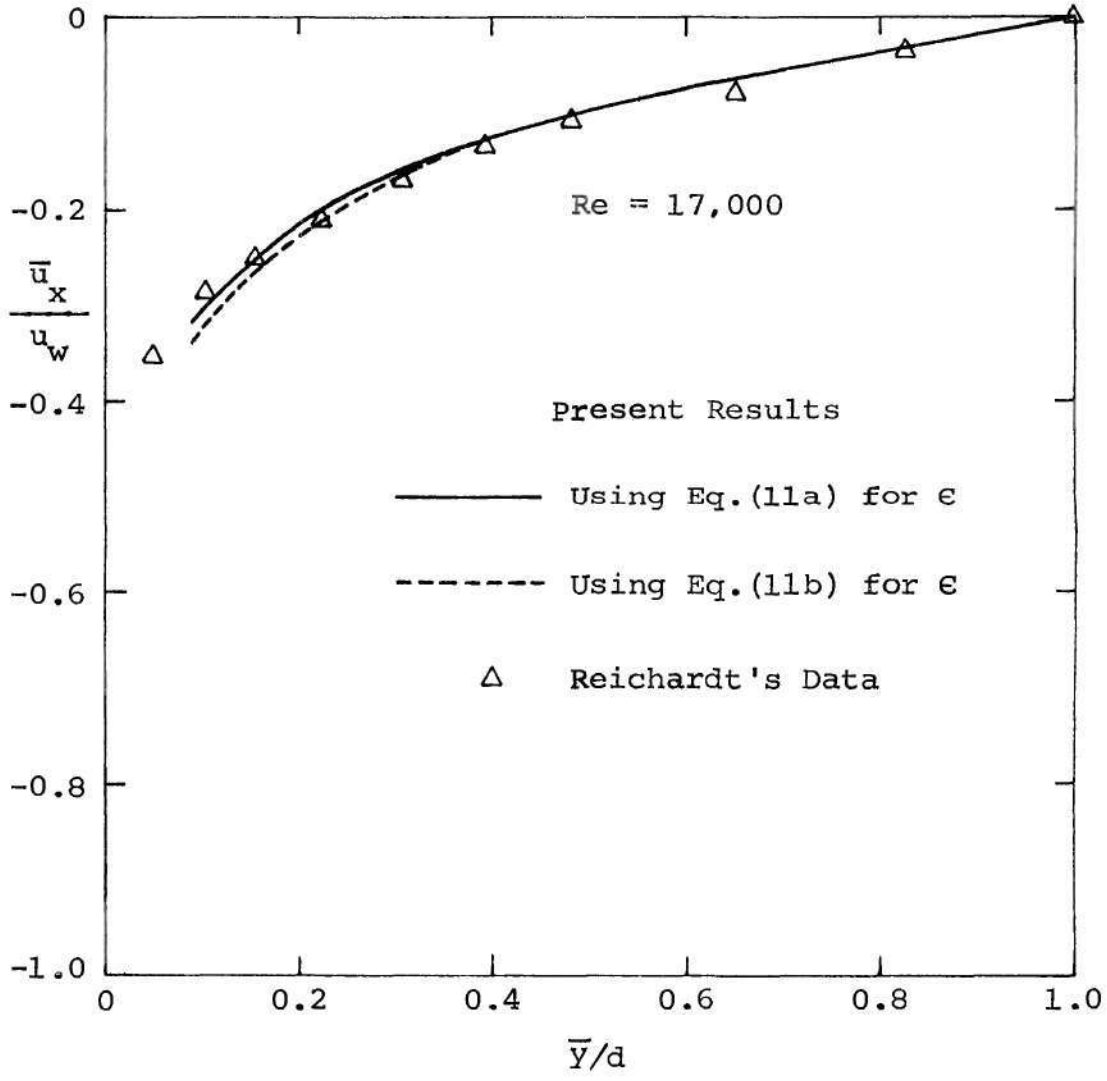

Figure 7. Mean Velocity Profiles for Chapman-Enskog Boundary Conditions; Re=17,000.

different values of Reynolds number, $Re = u_w d/\nu$. Figure 8 shows the calculated mean velocity profiles for these cases, which span a fairly wide range ($9{,}810 \leq Re \leq 100{,}000$). These results illustrate the trend toward fuller profiles as Re increases. Reichardt's data [19] at Re = 17,000 and Johnson's measurements [20] at Re = 9,400 and Re = 16,500 are shown in this figure for comparison. Even though there are differences between the experimental measurements, the general agreement between these data and the present calculations are quite good. This is particularly so with Reichardt's data. Chung's solutions [12] for Re = 9,810 and Re = 86,600 are also plotted in this figure. Those computations give smaller velocity gradients near the wall than in the present case, and his velocity profiles are not as full.

Figure 9 illustrates the computed velocity defect profiles for Reynolds numbers 9,810, 17,000, and 100,000. The experimental data of Reichardt and Johnson are shown for comparison. There are two curves plotted in Figure 9. For one of these, the boundary conditions are applied at $\bar{y}/d = 0.09$ and the Reynolds numbers correspond to 9,810, 17,000, and 100,000. The results for these cases are the same to the limits of graphical comparison, indicating an independence of the flow from Reynolds number when plotted in velocity defect coordinates. The characteristic length scales of the flow are the same for all values of Reynolds number. Since u_*/u_w is the only parameter that is different for different Reynolds numbers, the mean velocity profile should be independent of Re when plotted as a velocity defect.

The second curve in Figure 9 demonstrates an important point. This curve represents the results for Re = 100,000 but with the boundary

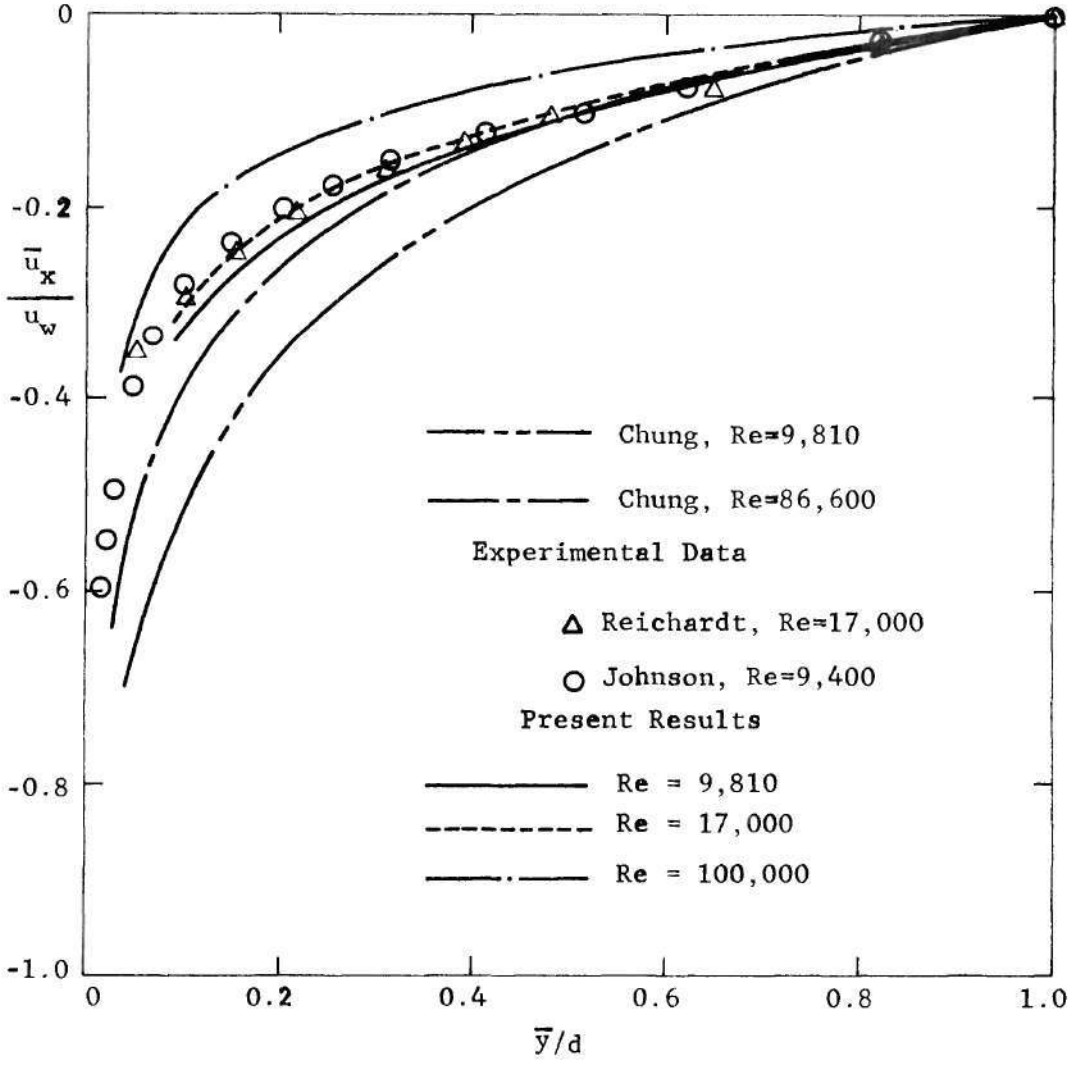

Figure 8. Mean Velocity Profiles in the Couette Flow.

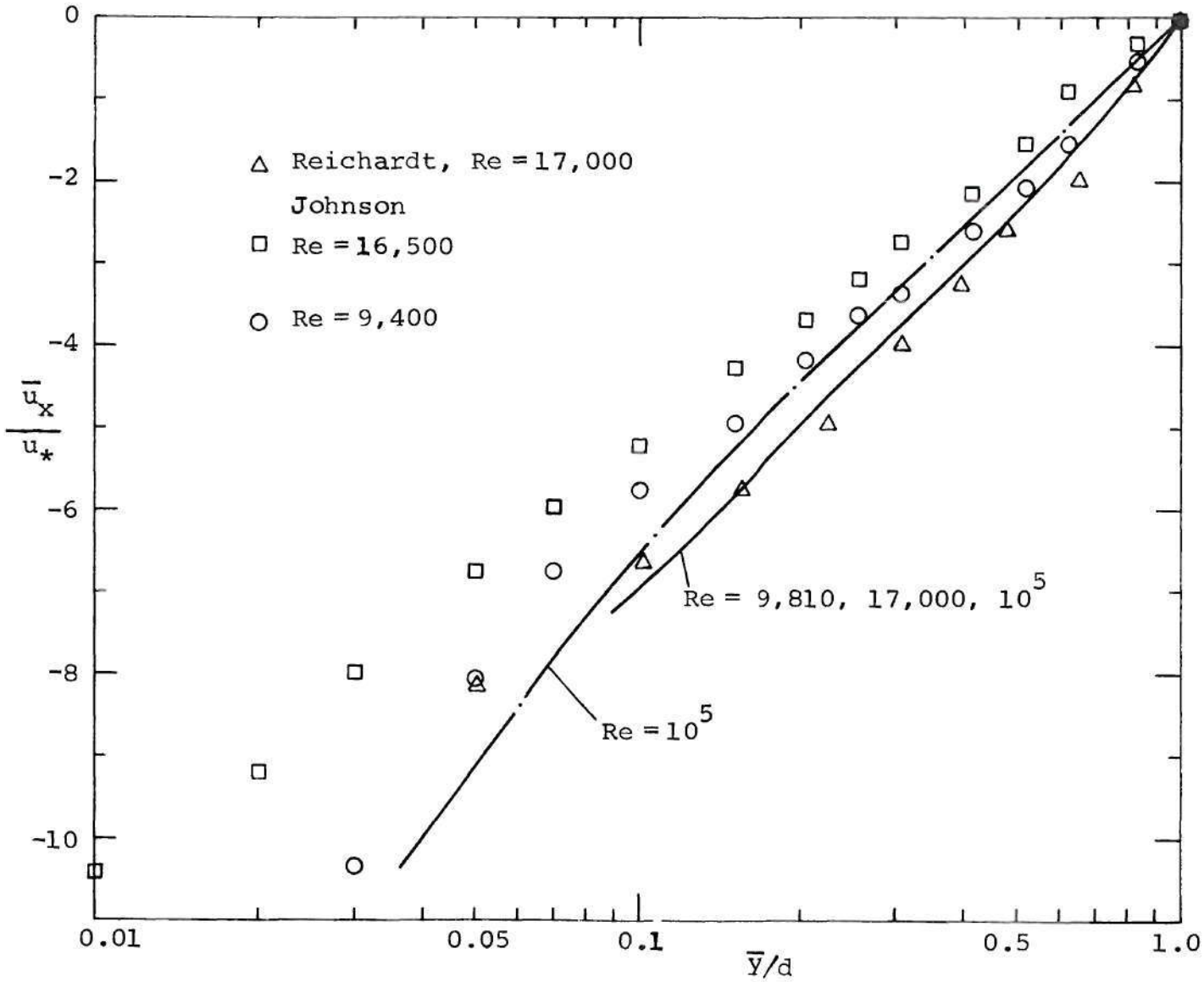

Figure 9. Velocity-defect Profiles in the Couette Flow.

conditions applied at $\bar{y}/d = 0.0375$, or $y_* = u_*\bar{y}/\nu = 137.5$. It is seen that the velocity defect profile is slightly different when the boundary condition is applied at a different station. Although these deviations are somewhat exaggerated by the logarithmic coordinates used, this figure indicates that there is an inadequacy in the representation of the boundary condition. It should be recalled that the Chapman-Enskog distribution function is obtained by perturbing the governing equation, Equation (1), about the Gaussian distribution and neglecting terms higher than first order. It can be seen, by direct substitution, that the Gaussian distribution does not satisfy the governing differential equation. Therefore, when this function is used as a boundary condition, the terms that were previously neglected are now present in the full equation, giving rise to slight gradients which do not follow the law of the wall. Thus, when the velocity profile is matched with the logarithmic law, the velocity gradient does not automatically match and the resulting velocity profile has a sensitivity to the location at which the boundary condition is applied.

Results for Reynolds stress are shown in Figure 10. The calculated values show a variable Reynolds stress near the wall boundary. This variation is not a consequence of increasing viscous stress as the wall is approached, but rather due to the gradients in the distribution functions introduced by the Chapman-Enskog boundary conditions. Chung's results [12] for Reynolds stress are also plotted in Figure 10. These results give somewhat smaller values for the Reynolds stress than the present data. The computed values of u_*/u_w are 0.04692, 0.04441 and 0.03669 for Reynolds numbers 9,810, 17,000 and 100,000, respectively. Chung's calculated

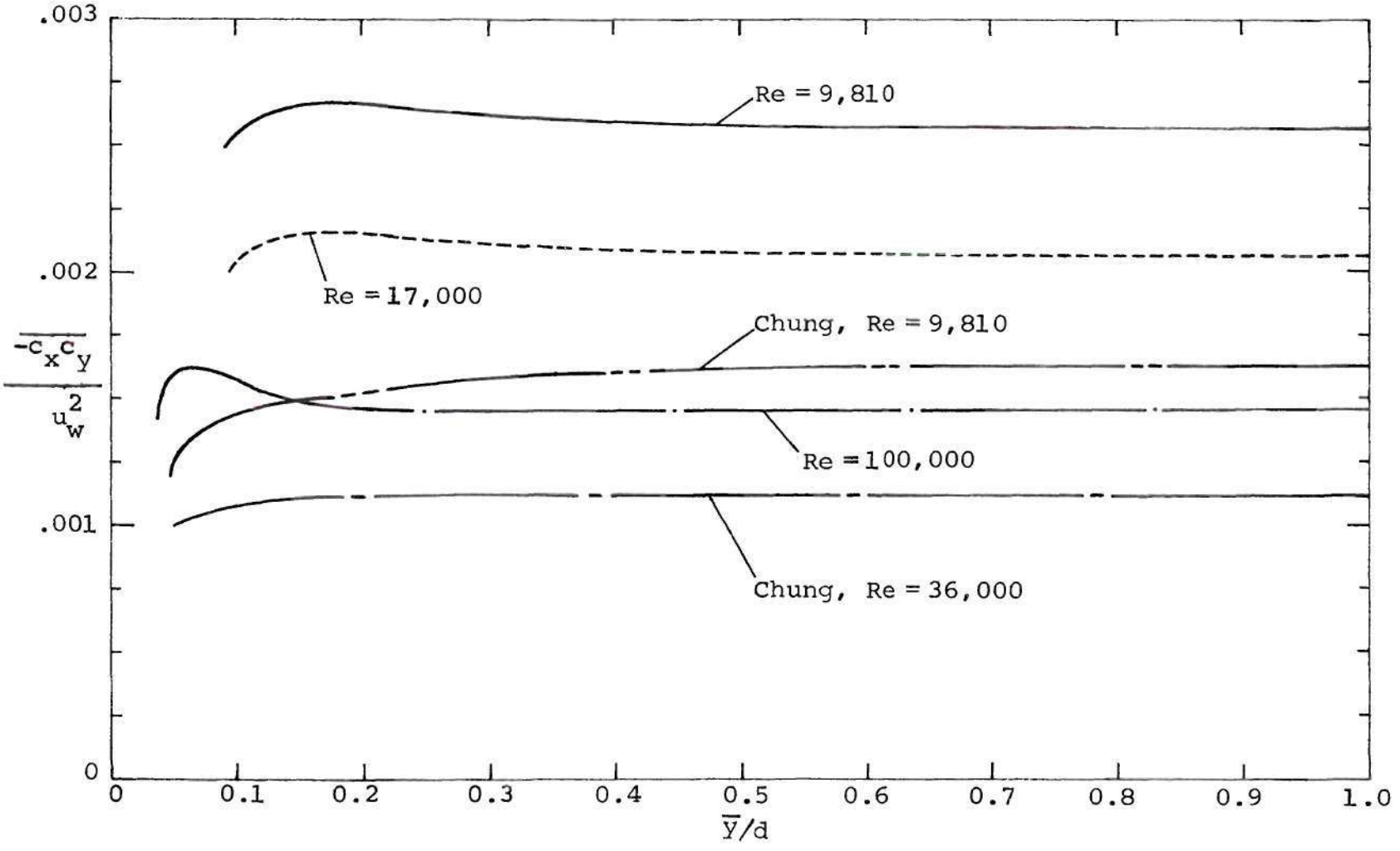

Figure 10. Reynolds Stress Profiles in the Couette Flow.

values for u_*/u_w are reported to be 0.0404 for Re = 9,810 and 0.03284 for Re = 36,000. The value of u_*/u_w obtained by Reichardt for Re = 17,000 is 0.0425, and those found by Johnson are 0.0466 for Re = 16,500 and 0.048 for Re = 9,400.

Figure 11 illustrates the computed variations of eddy viscosity. The solid line represents the results for Reynolds numbers 9,810, 17,000 and 100,000 when boundary conditions are applied at $\bar{y}/d = 0.09$. The broken line is the result obtained for Re = 100,000 when the boundary conditions are applied at $\bar{y}/d = 0.0375$. It is recalled that the eddy viscosity is computed as a ratio of Reynolds stress and mean velocity gradient. The differences in the computed non-dimensional Reynolds stress is less than 3 per cent. Hence, the differences in the eddy viscosity shown in Figure 11 is essentially due to the disagreement in the mean velocity gradients depending upon the location at which boundary conditions are apolied. Near the centerline, there is nearly 30 per cent deviation between the two curves for eddy viscosity and the profiles are not linear.

The results for turbulence intensity, U/u_w, are shown in Figure 12. These results exhibit a behavior quite similar to the Reynolds stress profiles. The variation in the profiles near the wall is again due to the Chapman-Enskog boundary conditions. Chung's results [12] give about 60 per cent of the present solution.

Figure 13 illustrates the results for non-dimensionalized dissipation rate. There are two curves in this plot. Both of these curves are the solutions of the differential equation for ε, Equation (11a). For the curve shown in solid line, the boundary condition is applied at

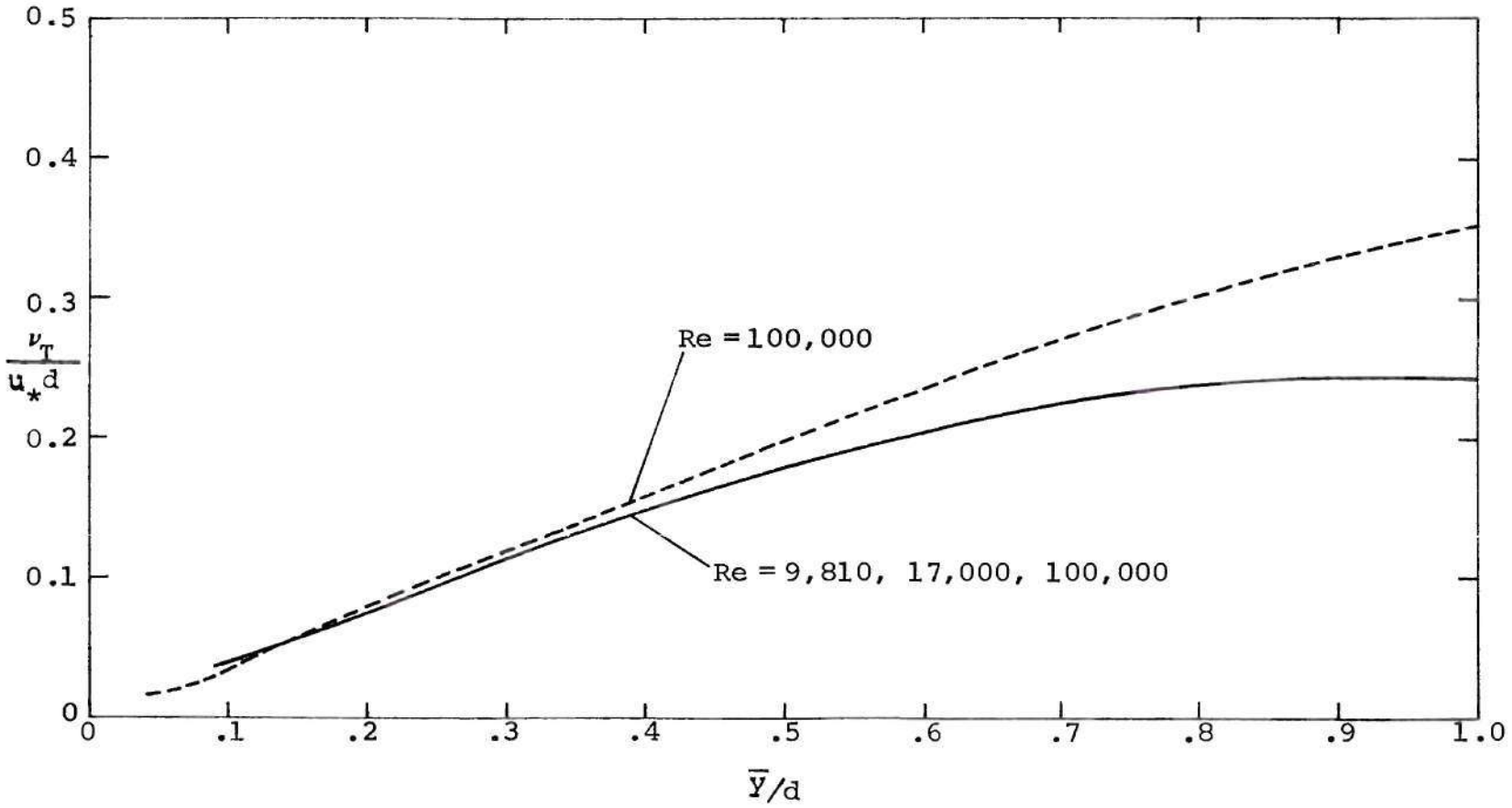

Figure 11. Variation of Eddy Viscosity in the Couette Flow.

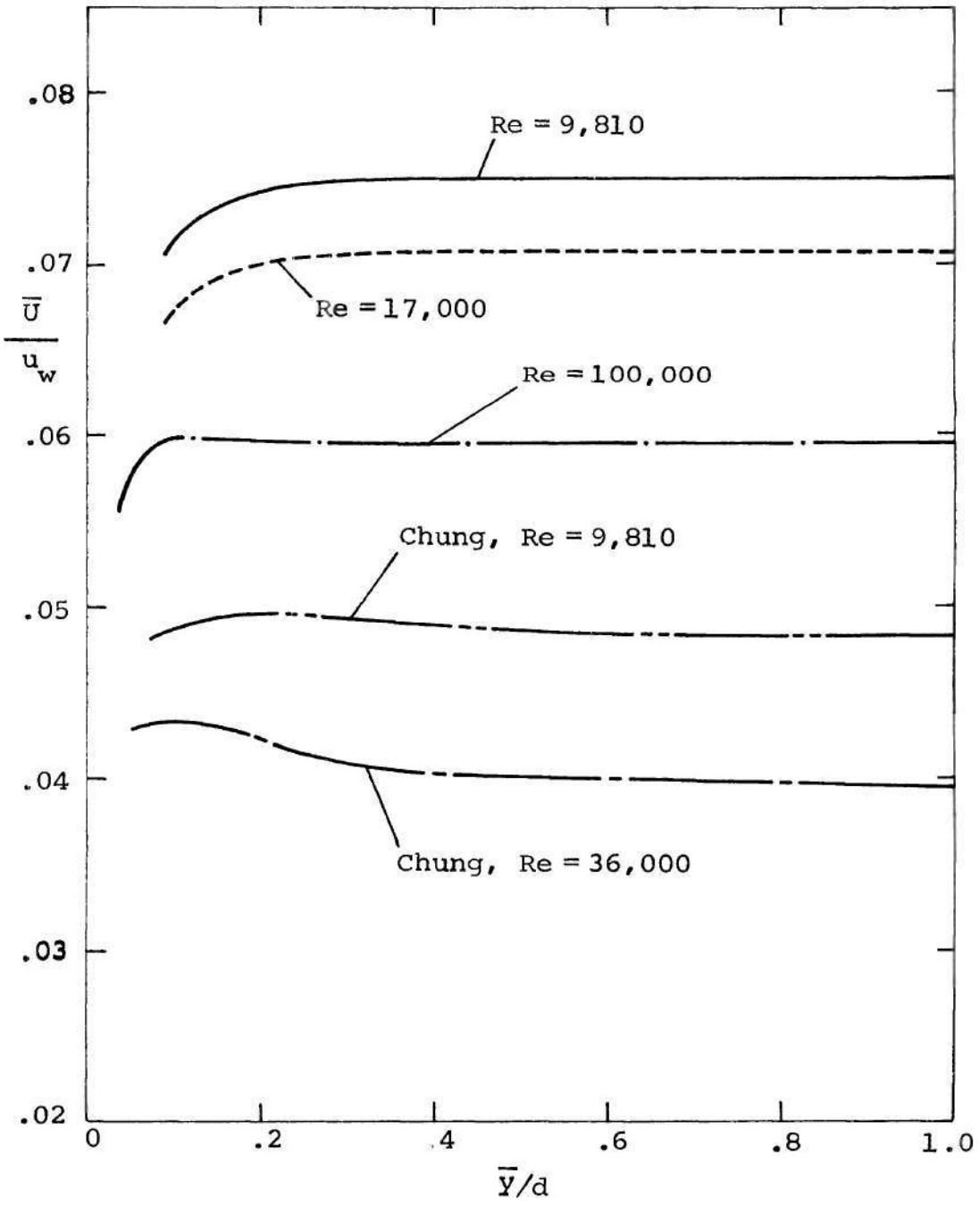

Figure 12. Turbulence Intensities in the Couette Flow.

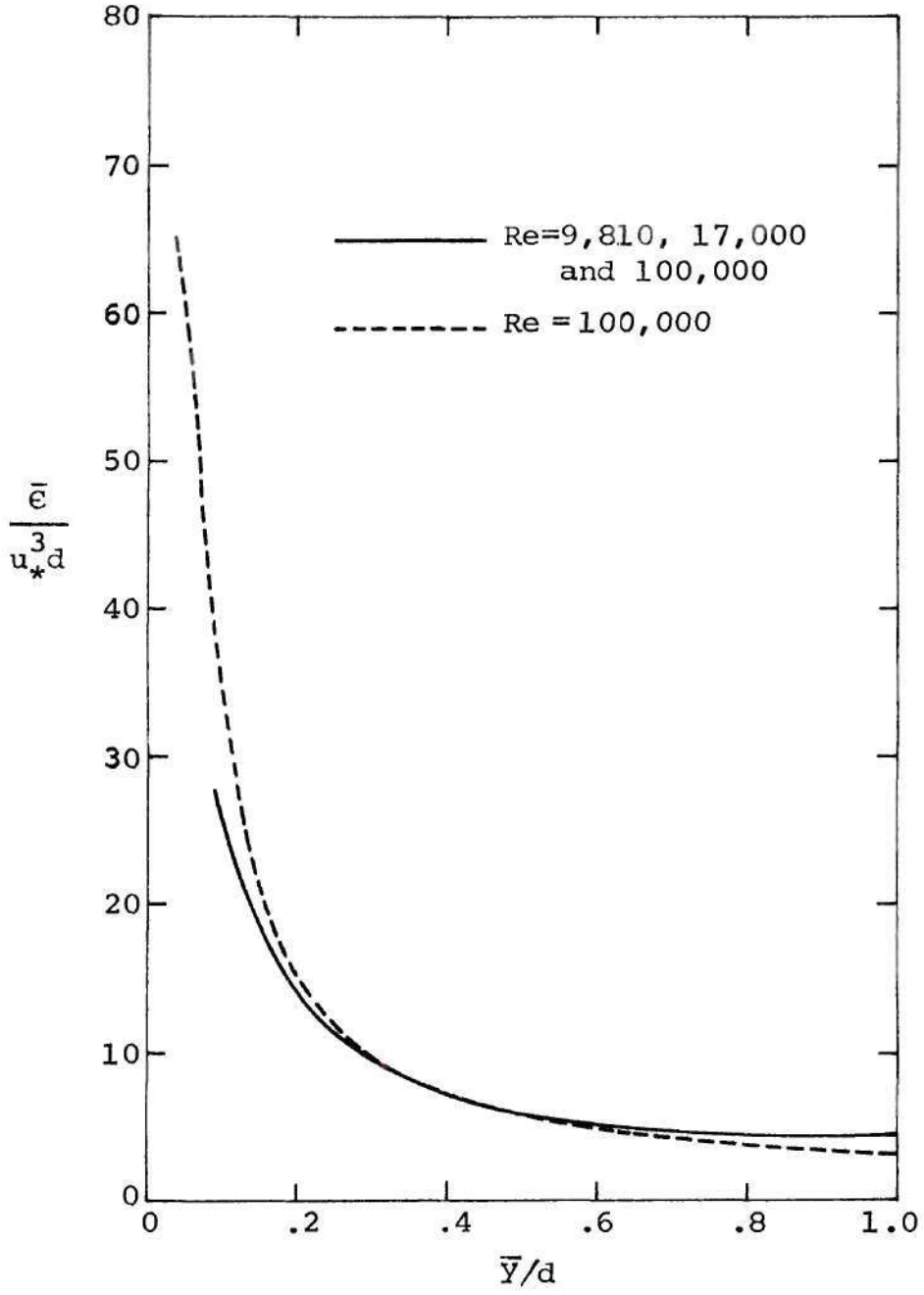

Figure 13. Dissipation Rates in the Couette Flow.

$\bar{y}/d = 0.09$ and the Reynolds numbers are 9,810, 17,000 and 100,000. Results for these different Reynolds numbers have converged to the same solution within the limits of graphical comparison. The curve shown by a broken line represents the solution for Re = 100,000 when the boundary conditions are applied at $\bar{y}/d = 0.0375$. This sensitivity to the location of boundary point is essentially due to the variation of mean velocity gradient, which appears in Equation (11a). The non-dimensionalized kinetic energy profiles for all these cases are the same within a bandwidth of 2 per cent, and hence it cannot be the reason for the deviations in ε. The quantity that is mainly responsible for this difference in the profiles is du/dy. The agreement among these solutions in regions away from the near wall boundary is quite satisfactory.

One of the features of the statistical model is that it is possible to compute the turbulence intensity components that contribute to the kinetic energy of turbulence. The results for the components of turbulence intensity, $\langle v'^2 \rangle$ and $\langle u'^2 + w'^2 \rangle$ are illustrated in Figure 14. The solid lines represent the solutions for the three Reynolds numbers 9,810, 17,000 and 100,000, when the boundary conditions are applied at $\bar{y}/d = 0.09$. The broken lines give the solutions for Re = 100,000 when the boundary condition is applied at $\bar{y}/d = 0.0375$. It is seen that near the boundary point, all these curves give very nearly the same values for each component. This is a consequence of the constraints given in Equations (22b) and (23c), as these are obtained as moments of g and h. However, the differences in the values elsewhere are due to the inadequacy of the Chapman-Enskog distribution function.

Figure 15 shows the results for the skin-friction coefficient, c_f.

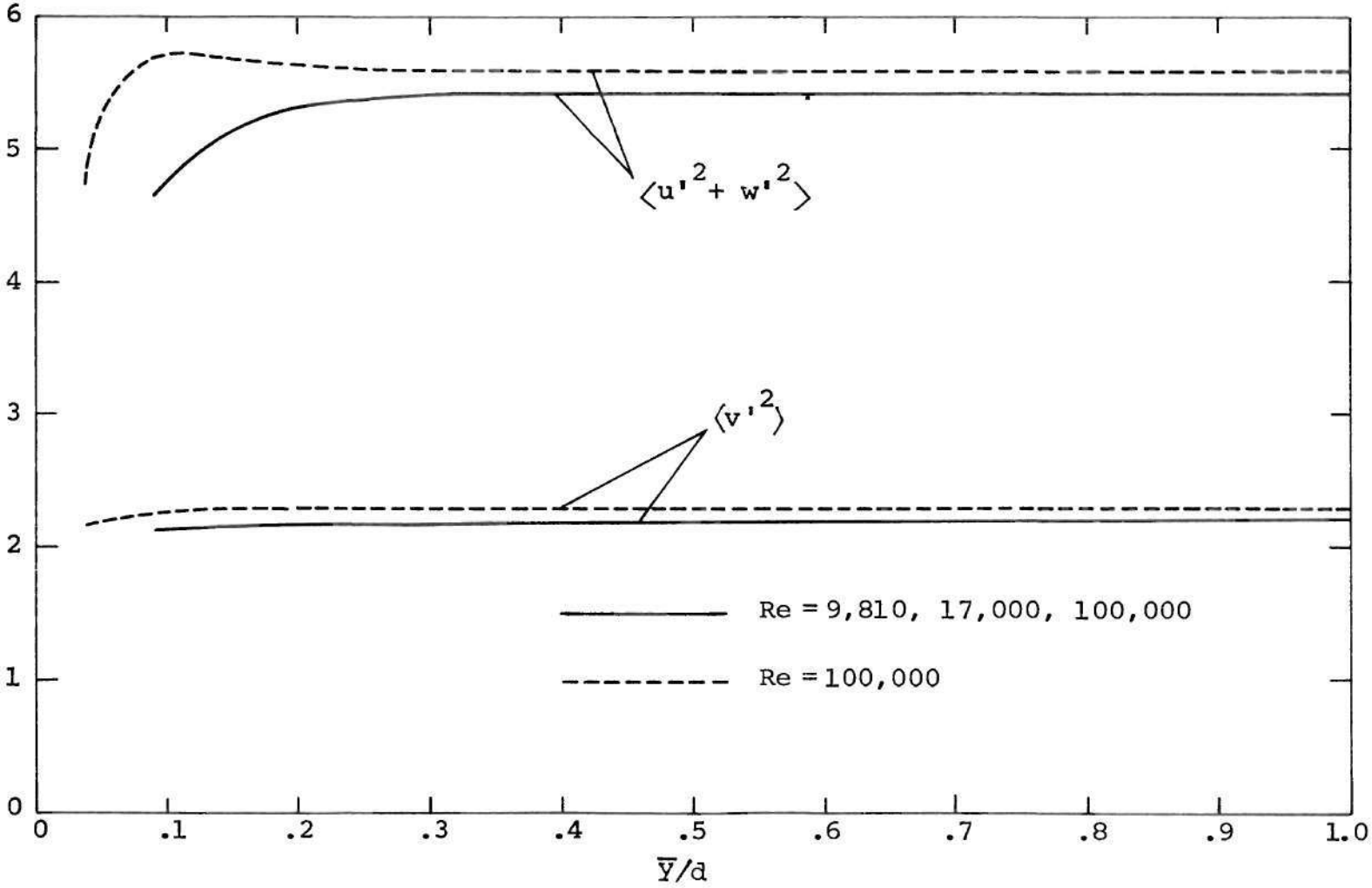

Figure 14. Components of Turbulence Kinetic Energy.

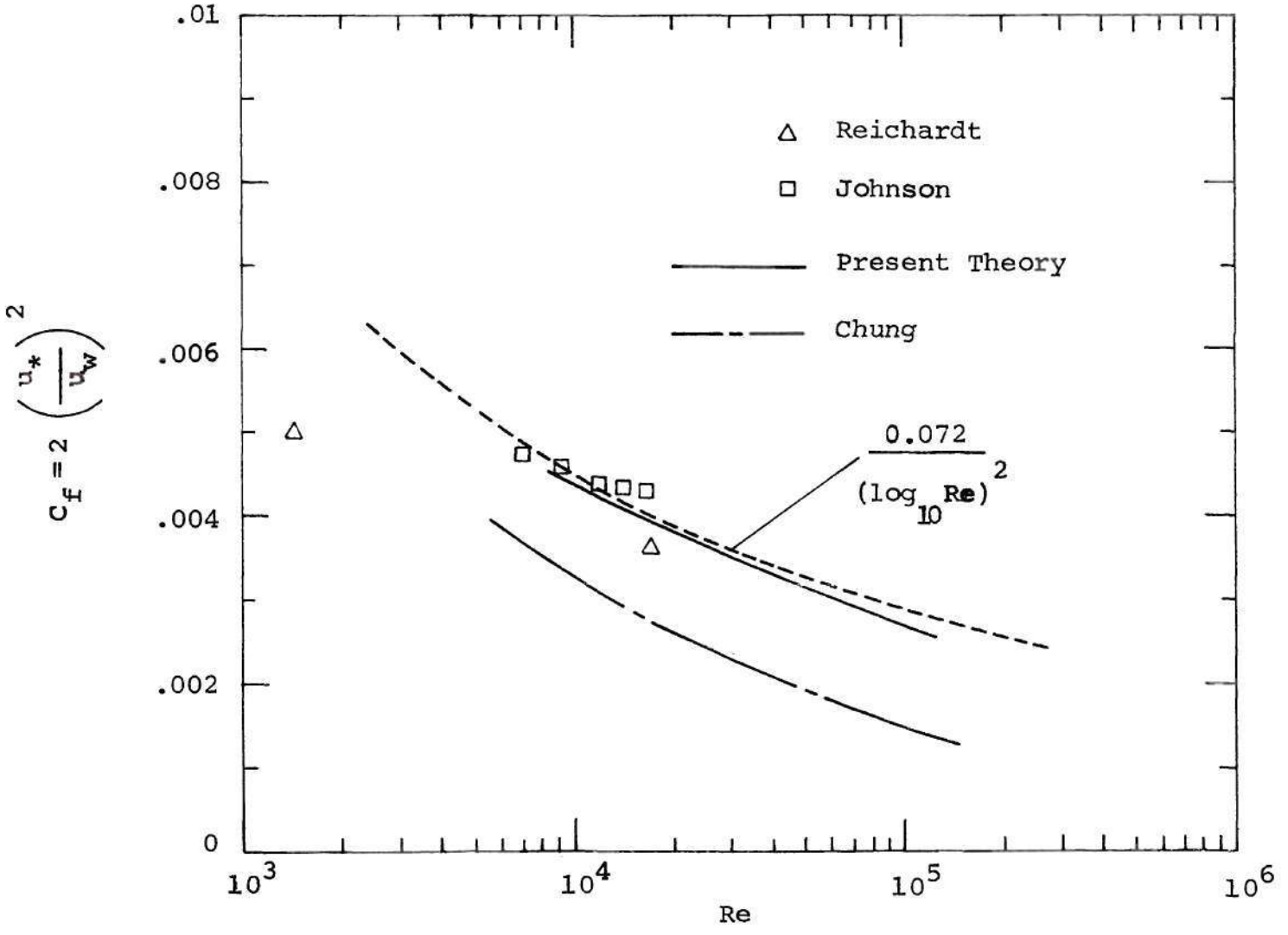

Figure 15. Skin-friction Coefficient.

The skin friction coefficient is obtained from the expression

$$c_f = 2\, u_*^2/u_w^2 \,.$$

The results obtained from the statistical model are compared in this figure with experimental data of Reichardt and Johnson. In addition, Chung's results and Robertson's empirical expression [18] for predicting skin friction coefficient are shown in the figure. The agreement between the present results and the empirical curve fit is quite good. Chung's reported solutions predict smaller values for the skin friction coefficient than the present solutions.

An interesting aspect of this statistical approach to turbulence is that the distribution functions are calculated without making any a priori assumption about the functional dependence on turbulence velocities. These distribution functions offer insight into the turbulence mechanisms and may aid in modelling turbulence.

Figure 16 illustrates the g distribution employed as a boundary condition for both zero-gradient and Chapman-Enskog cases. Figure 17 shows a similar graph for the j distribution function. It is emphasized that only the outgoing stream is modelled with these functions and the incoming stream is computed from the governing equations. If the incoming stream also yields the same result for the g distribution, the distribution functions for the two streams would by symmetric. For such a case, the zero-gradient distribution would have a flatness factor, K_u, of about 2.085 while the Chapman-Enskog function would give a flatness factor of 3 which is also the result for Gaussian distribution. The Chapman-Enskog distributions are somewhat broader than the zero-gradient

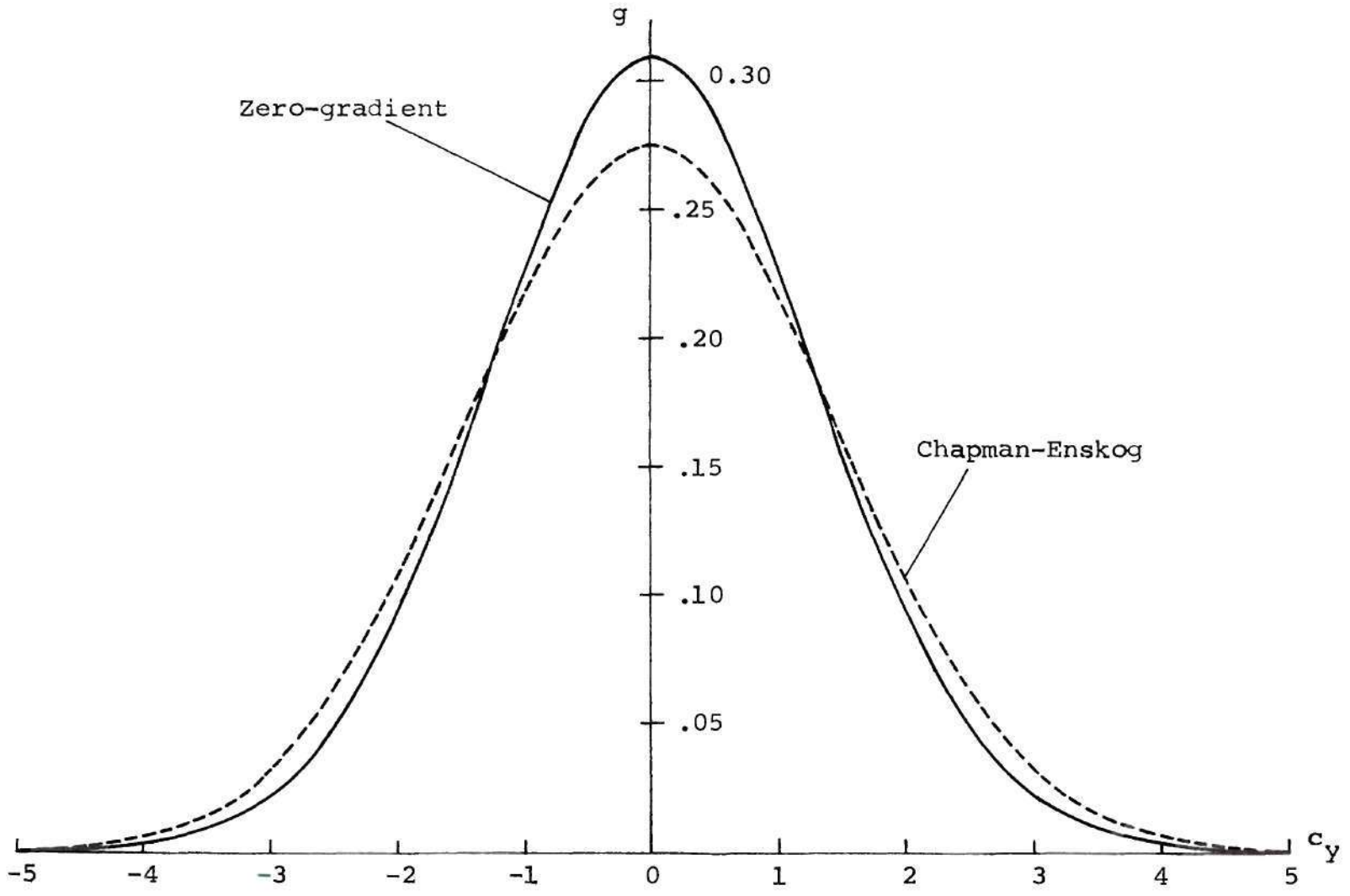

Figure 16. Distribution Function, g, at the Boundary Point.

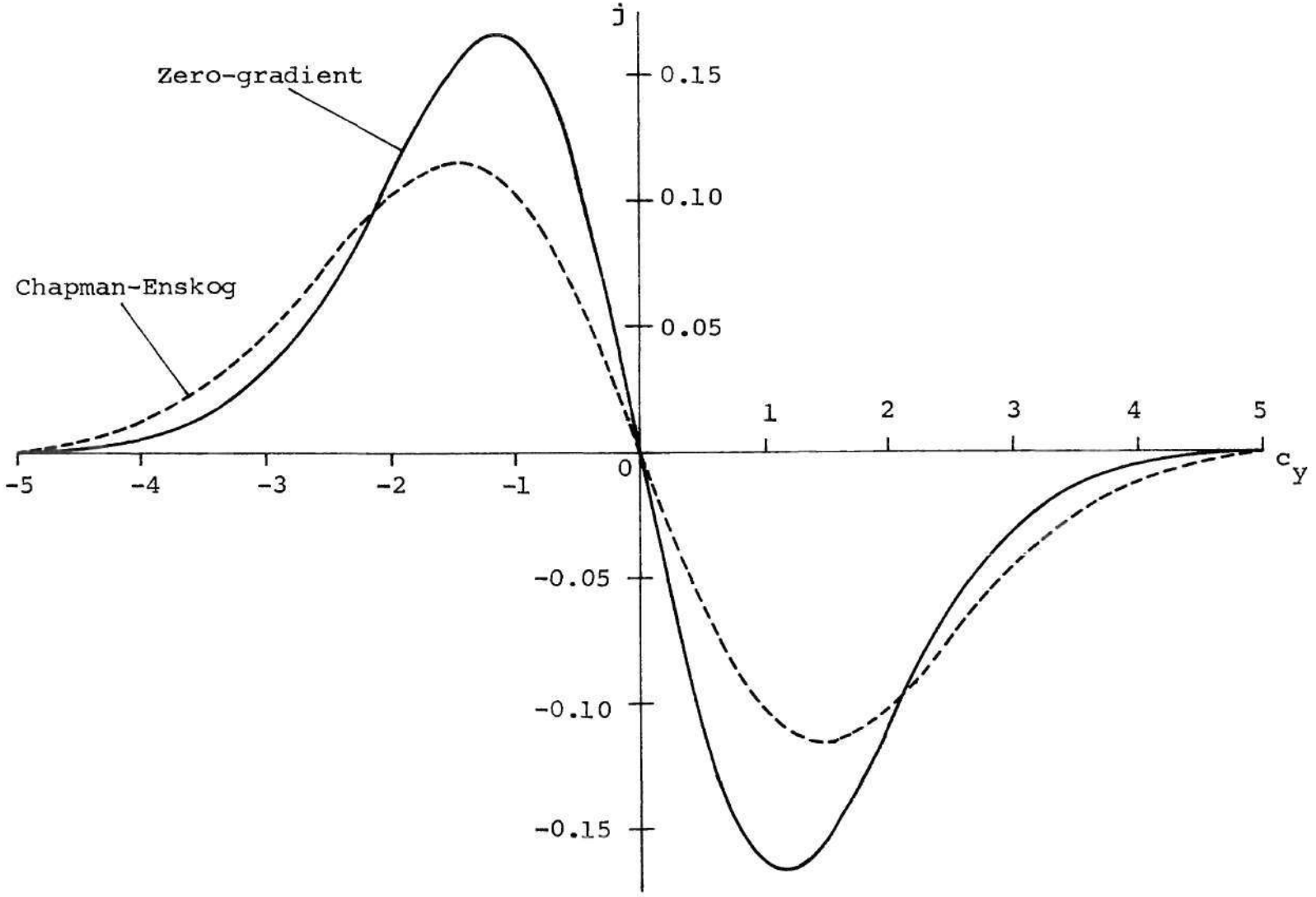

Figure 17. Distribution Function, j, at the Boundary Point.

distribution functions, even though both the distributions yield the same values for the first two moments. This is particularly noticeable in the j-function. It should be recalled that a Gaussian assumption would lead to $j = 0$ for all c_y and thus to a zero value for Reynolds stress.

Figures 18a, 18b, and 18c represent computed results for g at several y locations in the flow field corresponding to Reynolds numbers 9,810, 17,000 and 100,000 respectively, when the Chapman-Enskog boundary conditions are used. At the wall boundary ($y = 0.0375$ for $Re = 100,000$ and $y = 0.09$ for the lower Reynolds numbers), there is a discontinuity in g at $c_y = 0$. This is due to the integral constraints and the inadequacy of the Chapman-Enskog boundary conditions. These figures also show gradual variations in the distribution functions as y increases. This is a consequence of the relaxation term in the governing equation. Physically, the fluid elements are interacting to smooth out the distribution function. There are also small variations in the g distribution function for different Reynolds numbers. These variations are due to the inadequacy of the Chapman-Enskog boundary conditions and are likewise reflected in their moments.

Figures 19a, 19b and 19c illustrate the computed results for j distribution function for Reynolds numbers 9,810, 17,000 and 100,000 respectively. Similarly, Figures 20a, 20b and 20c show the results for h-function at these Reynolds numbers. These results are obtained by using Chapman-Enskog boundary conditions. The distribution functions, h, are very similar in shape to those of g and have noticeable discontinuities at the boundary point when $c_y = 0$. Similarly, discontinuities

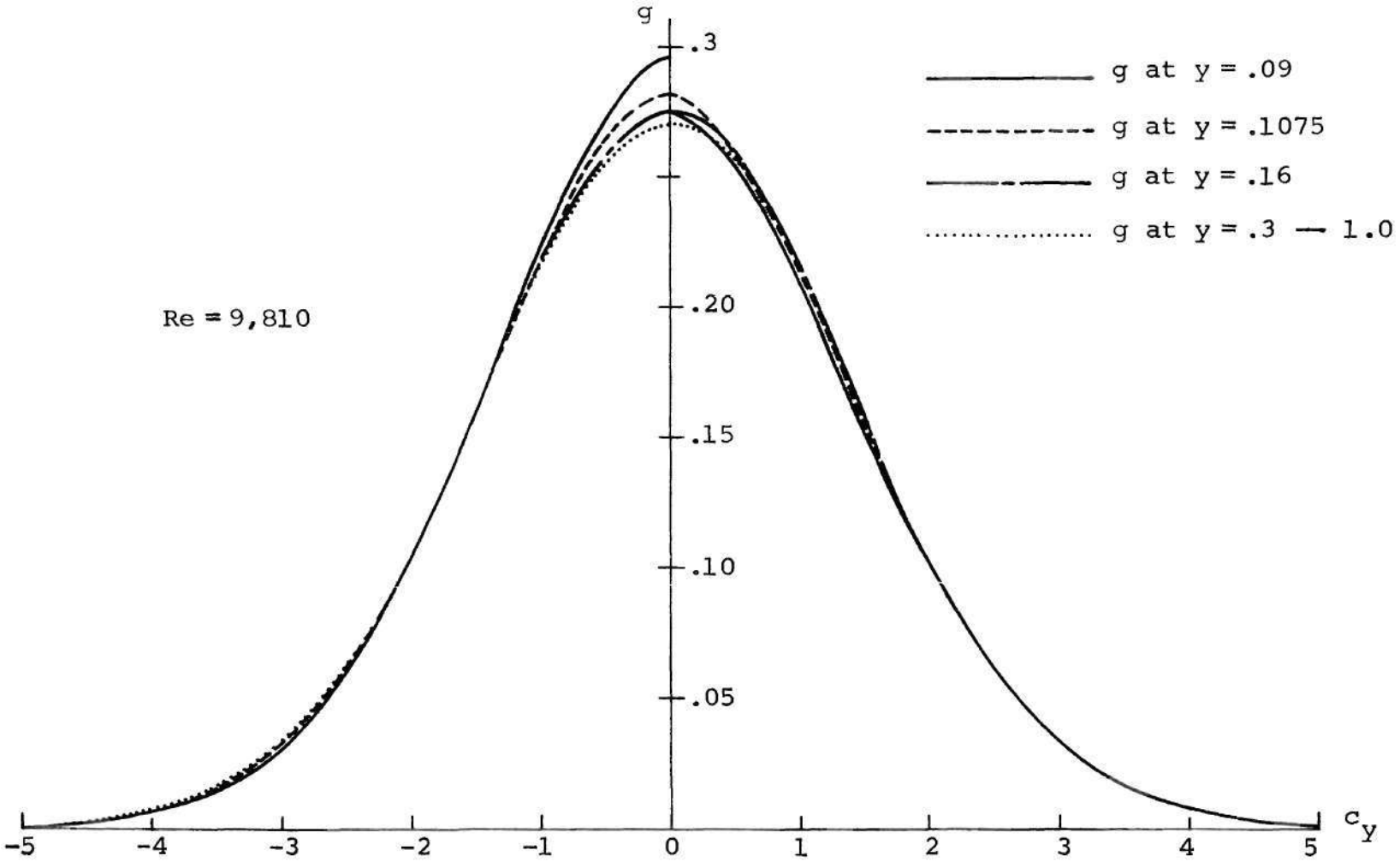

Figure 18a. Distribution Function, g, for Chapman-Enskog Boundary Condition ; Re = 9,810.

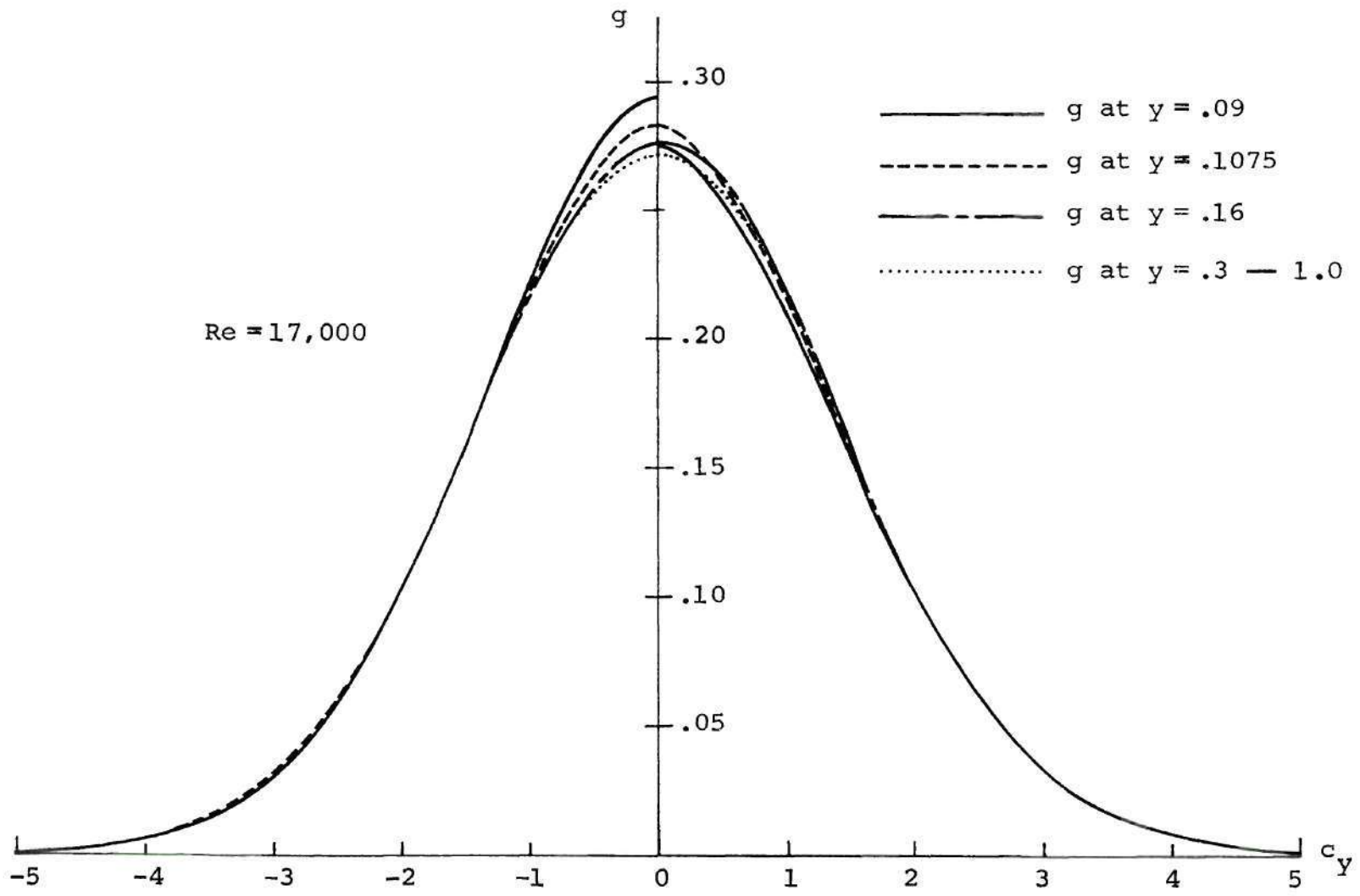

Figure 18b. Distribution Function, g, for Chapman-Enskog Boundary Condition ; Re = 17,000.

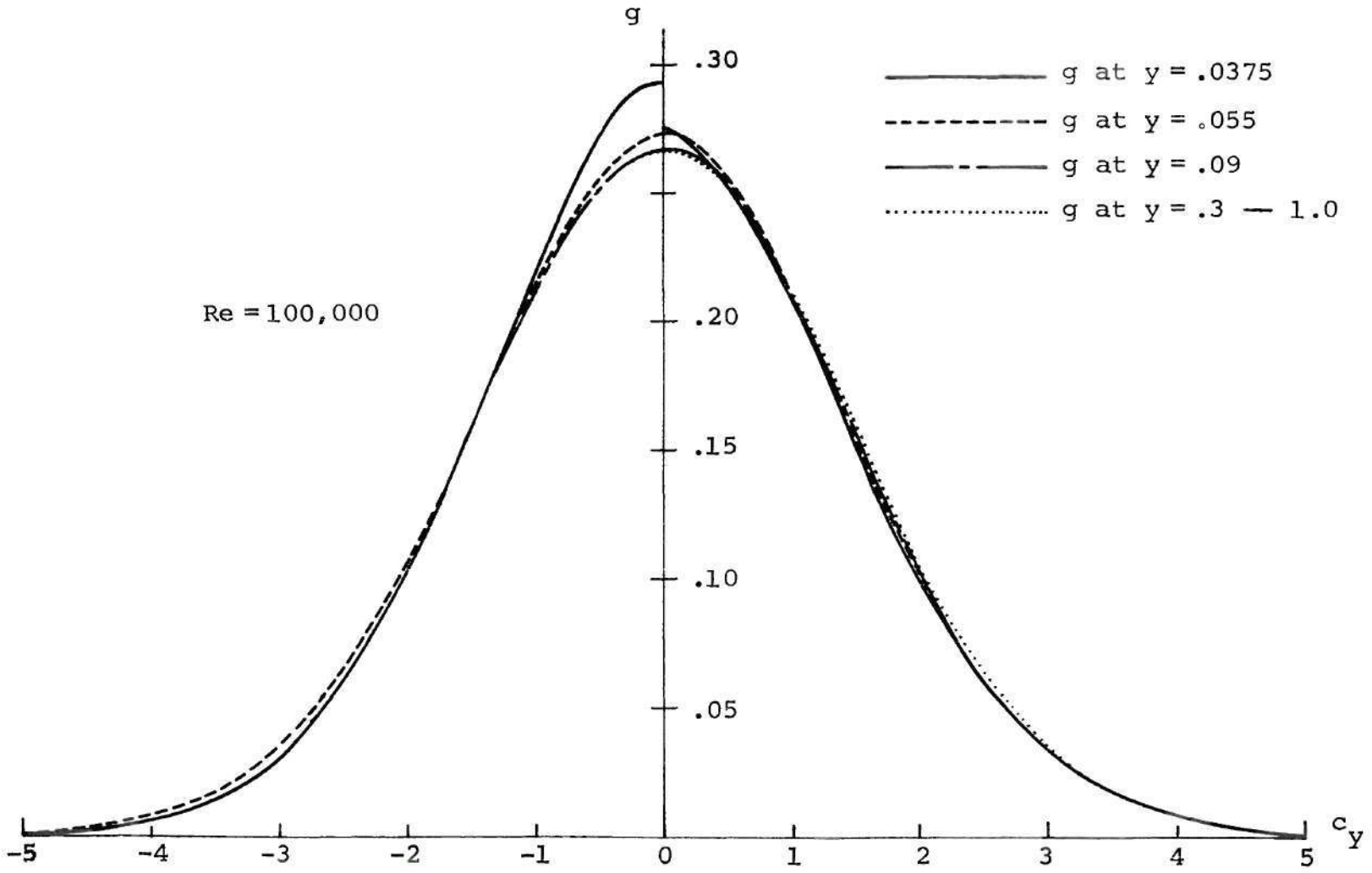

Figure 18c. Distribution Function,g, for Chapman-Enskog Boundary Condition ; Re = 100,000.

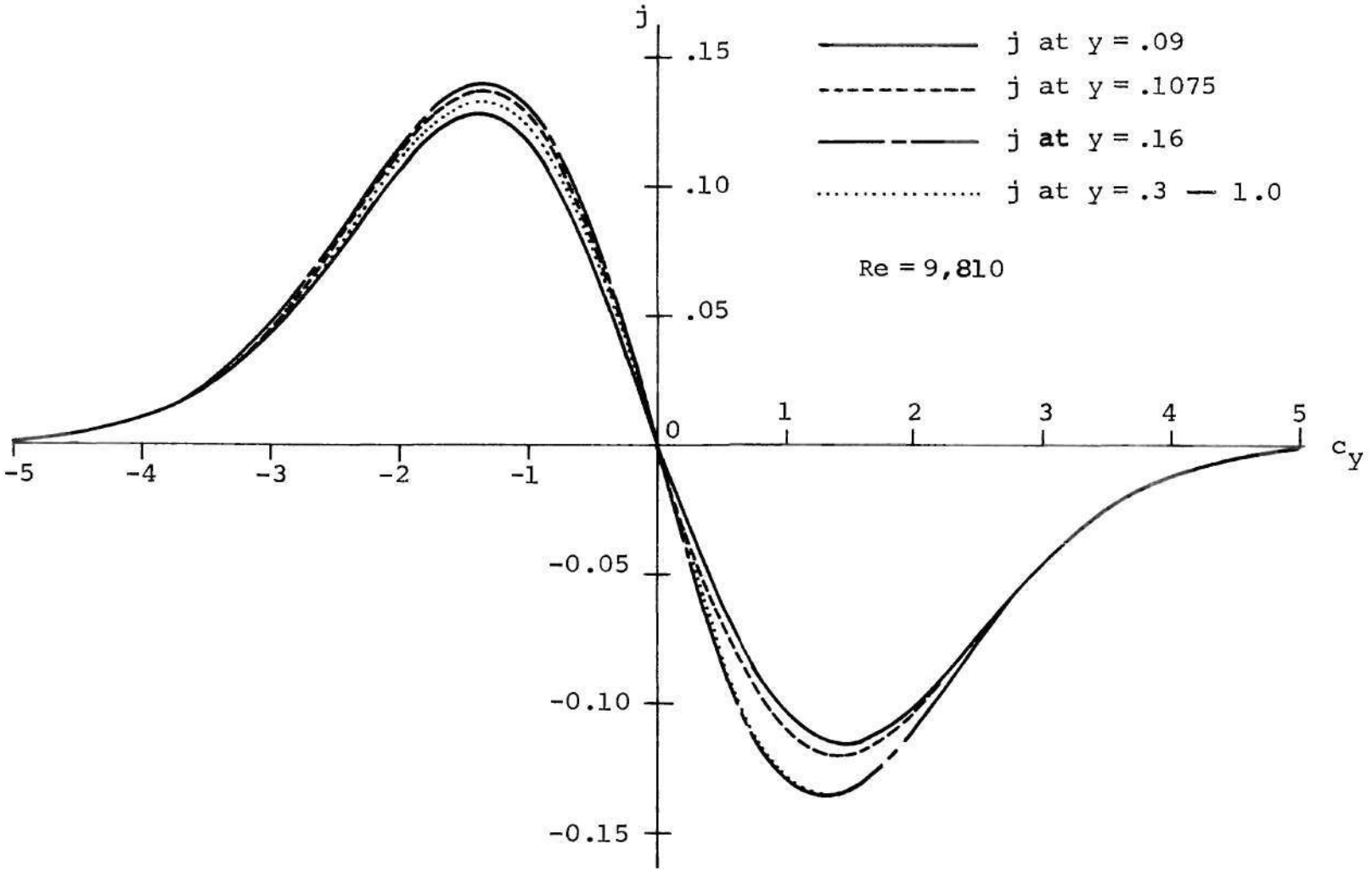

Figure 19a. Distribution Function, j, for Chapman-Enskog Boundary Condition ; Re = 9,810.

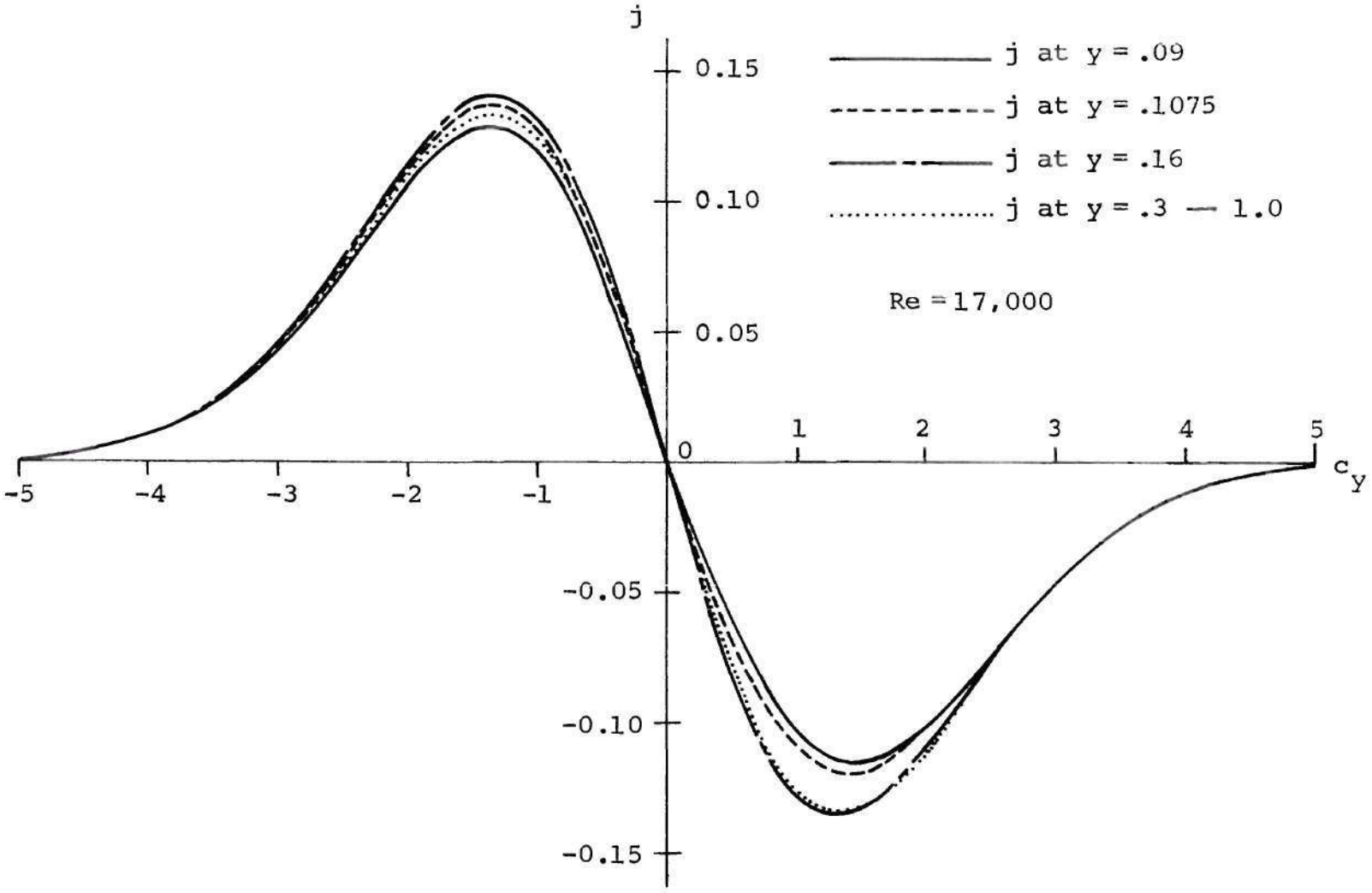

Figure 19b. Distribution Function, j, for Chapman-Enskog Boundary Condition ; Re = 17,000.

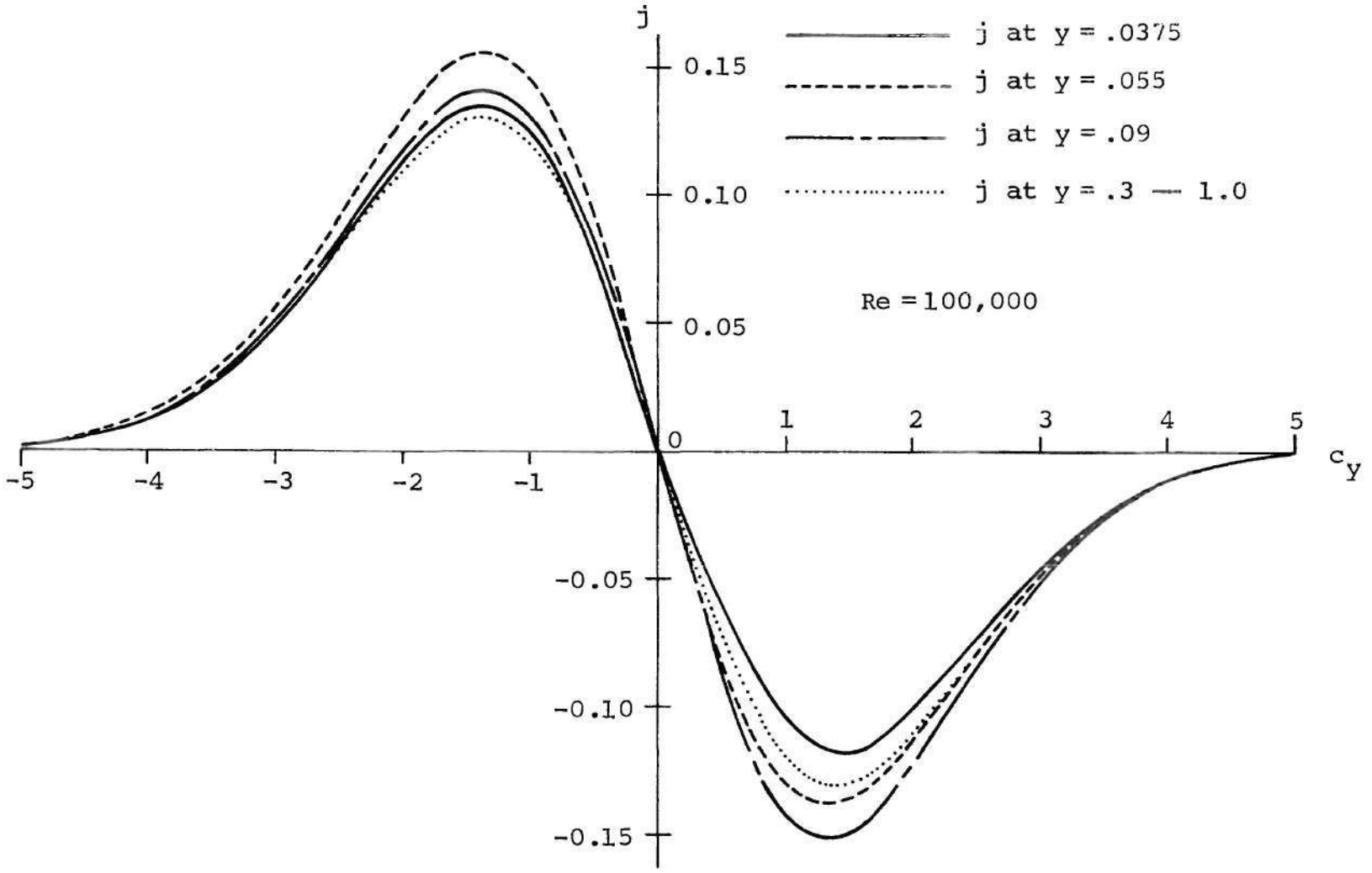

Figure 19c. Distribution Function, j, for Chapman-Enskog Boundary Condition ; Re = 100,000.

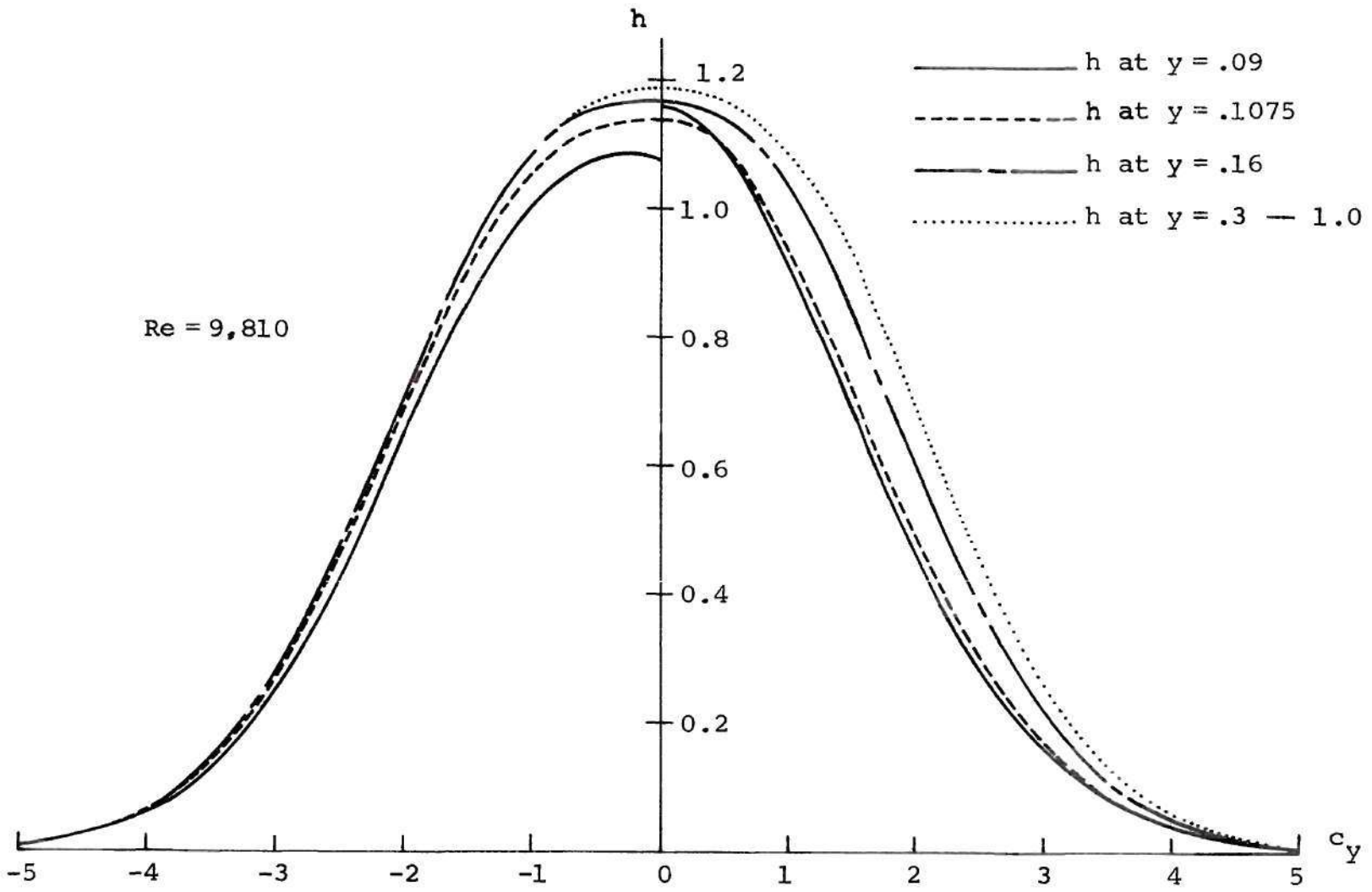

Figure 20a. Distribution Function, h, for Chapman-Enskog Boundary Condition ; Re = 9,810.

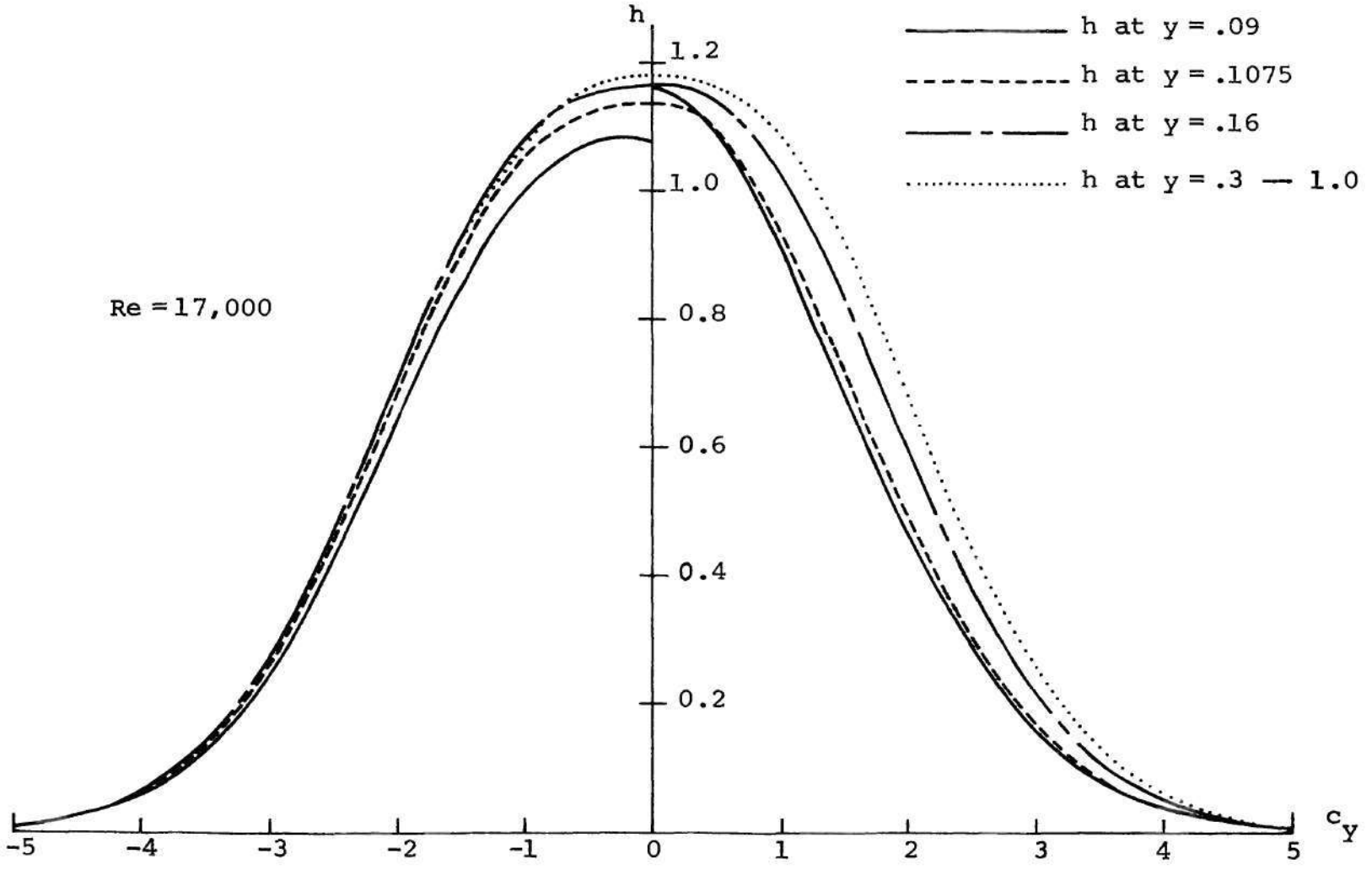

Figure 20b. Distribution Function, h, for Chapman-Enskog Boundary Condition ; Re = 17,000.

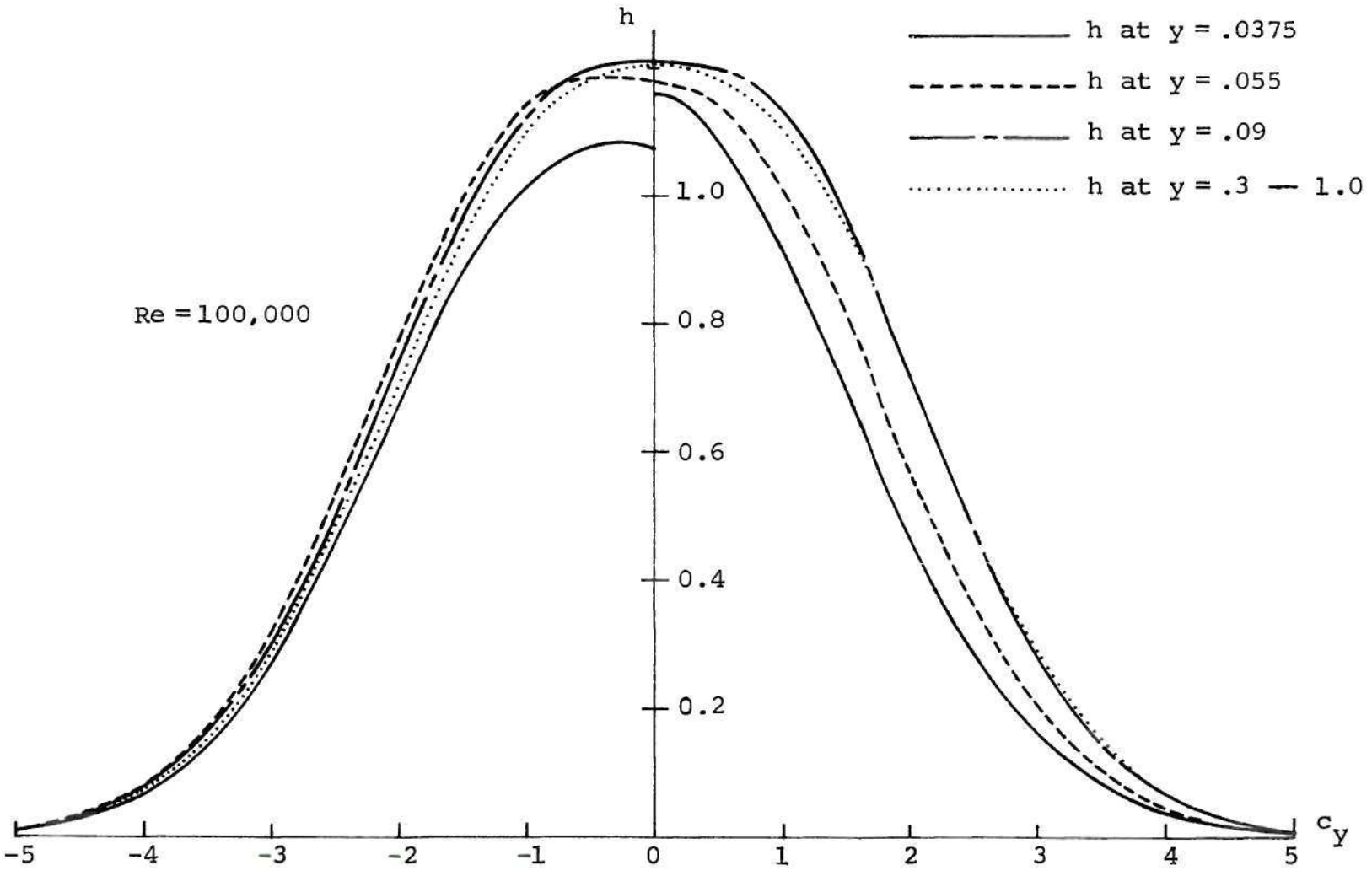

Figure 20c. Distribution Function, h, for Chapman-Enskog Boundary Condition ; Re = 100,000.

in the slope of j exist at $c_y = 0$ in Figures 19a, 19b and 19c. The variations in the distribution functions with Reynolds number is more clearly seen in the j functions than the g and h functions. This variation is due to the inadequacy of the Chapman-Enskog boundary conditions. It is interesting to note that the g, j and h functions have very little variations in the central core of the channel, indicating that the turbulent interactions have acted to adjust the boundary effects to the mean flow.

Even though the distribution functions g, j and h are nearly constant in the Couette flow (but for the small gradients near the boundary), the function j_v is not constant since it reflects the variation of mean velocity through the flow field. The computed results for j_v are represented in Figures 21a, 21b and 21c for Reynolds numbers 9,810, 17,000 and 100,000 respectively. These functions also exhibit discontinuities at the boundary point where $c_y = 0$. In addition, some differences in j_v values exist for different Reynolds numbers which are also exhibited in the velocity defect plot shown in Figure 9. Due to the configuration of the Couette flow problem, the mean velocity at the centerline is zero and at this location, j_v distribution is the same as the j distribution function.

Figure 22 shows the skewness factor, S, of the g distribution function for Reynolds numbers 9,810, 17,000 and 100,000. It is known from wall turbulence studies including visual methods [31, 32, 33, 34], that in the wall layer, the deviation from Gaussian distribution is mainly due to intermittent phases in which high momentum fluid is rushed into the sublayer and those in which low momentum fluid is ejected outward.

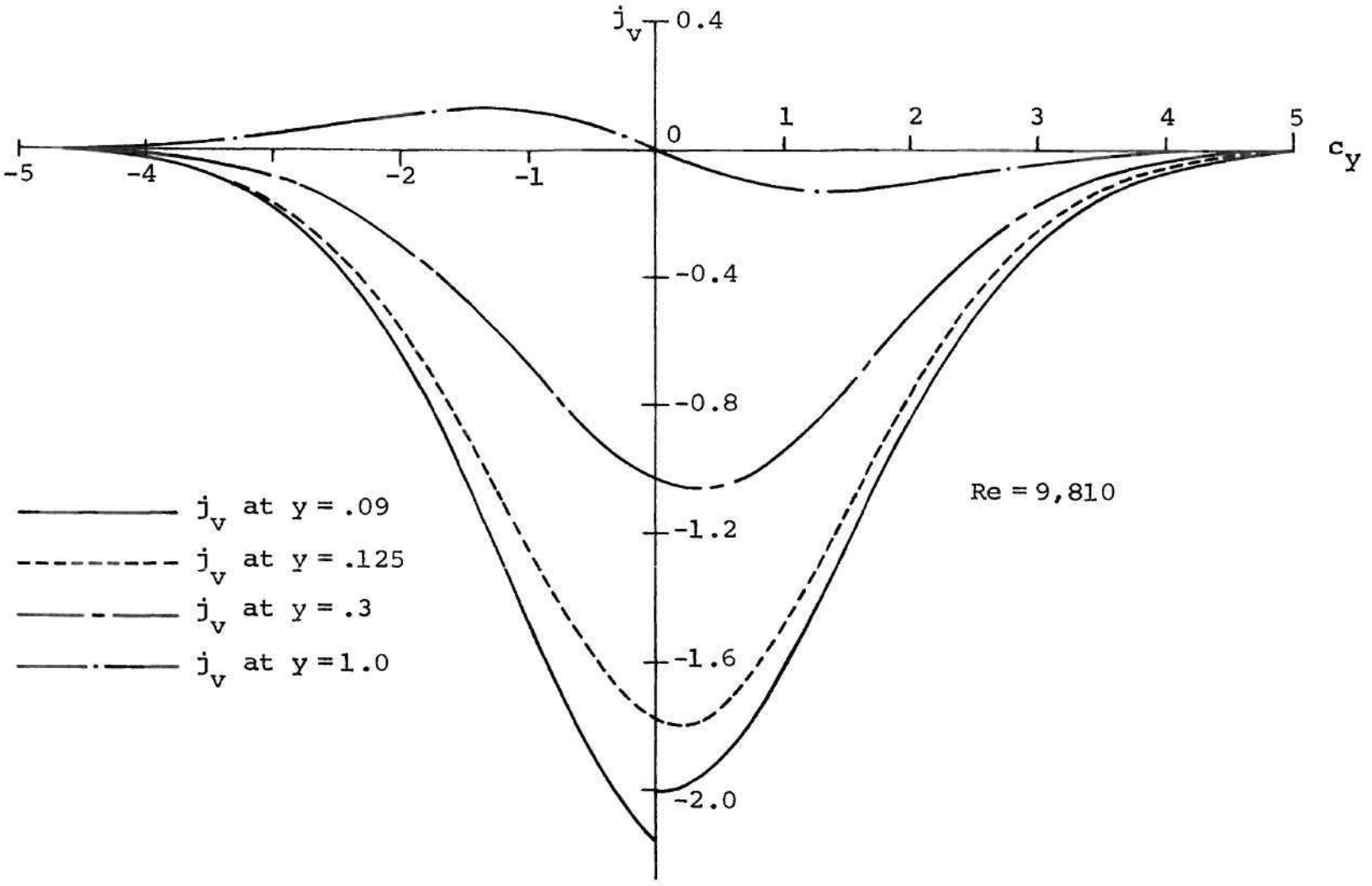

Figure 21a. Distribution Function, j_v, for Chapman-Enskog Boundary Condition ; Re = 9,810.

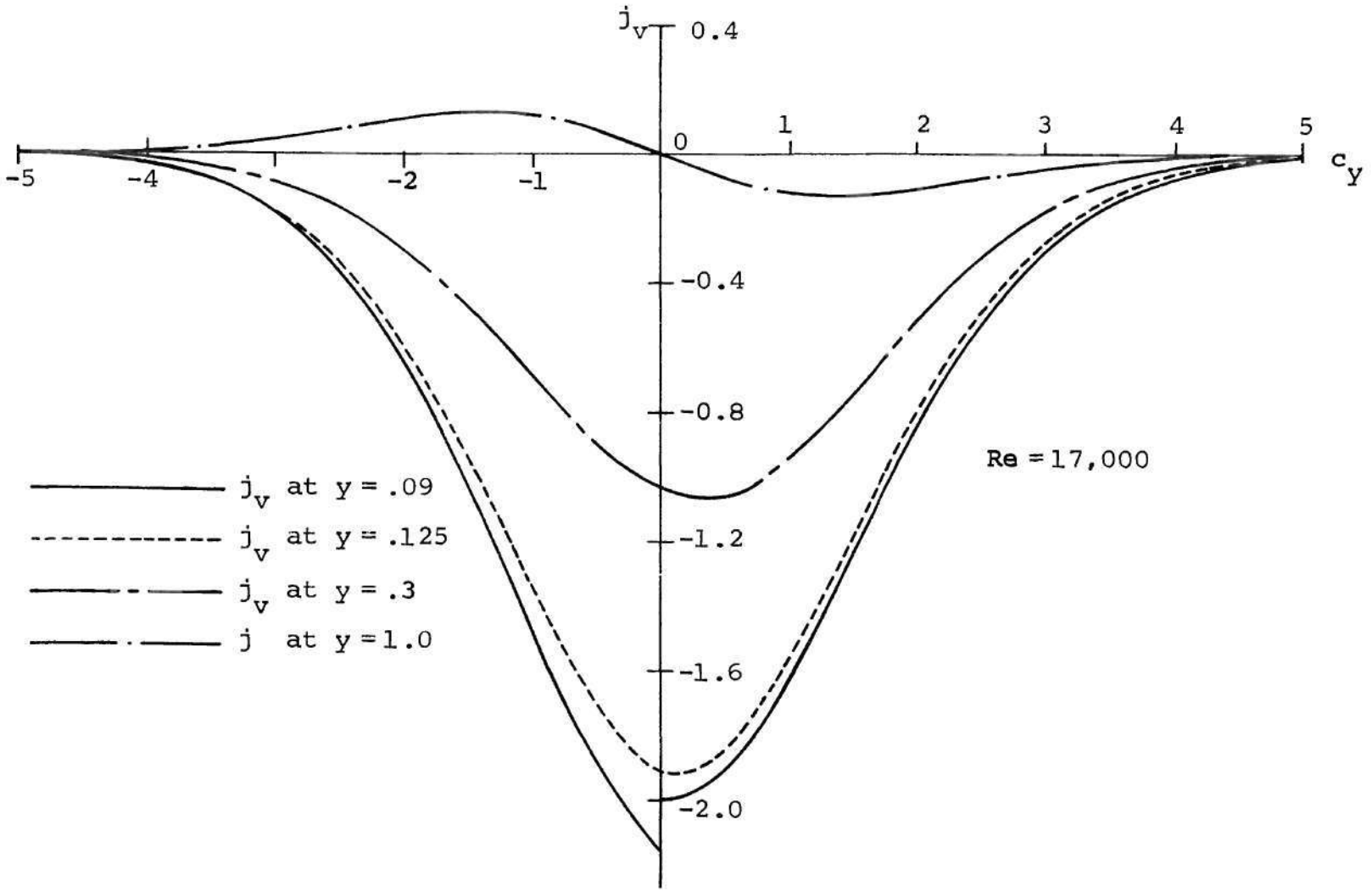

Figure 21b. Distribution Function, j_v, for Chapman-Enskog Boundary Condition ; Re = 17,000.

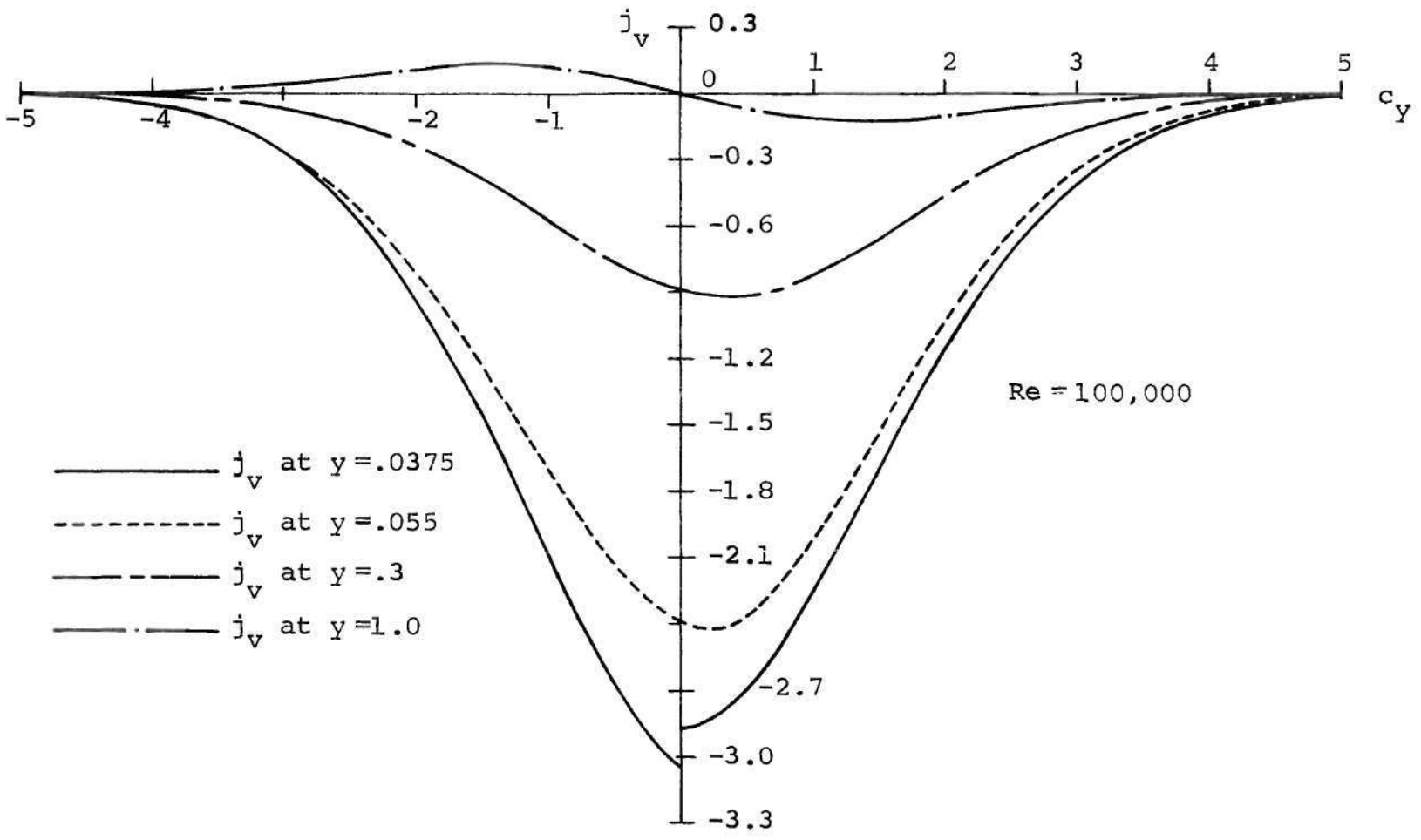

Figure 21c. Distribution Function, j_v, for Chapman-Enskog Boundary Condition ; Re = 100,000.

It is expected that the inrush phases would contribute to large negative c_y values and the ejection motions would be responsible for large positive c_y values. Thus, the inrush phases are likely to cause the skewness to be negative while the ejections phases would yield positive skewness factors. The skewness factors should become quite small in magnitude beyond $y_* \simeq 100$, and closer to the wall the ejection phases are observed to be dominant causing large positive skewness factors. In the present results, the large positive skewness near the wall is a consequence of the Chapman-Enskog boundary conditions. When zero-gradient boundary conditions are used, the skewness factors are nearly zero everywhere. The variation in the skewness factor with y indicates that the fluid elements are interacting to smooth out the boundary effects.

The Kurtosis or flatness factor, K_u, of the g distribution is shown in Figure 23. It is recalled that the Chapman-Enskog distribution gives a flatness factor of 3, which is also the value for the Gaussian distribution, and the zero-gradient has a smaller flatness factor of about 2.1. Thus, when the Chapman-Enskog distribution is used for the outgoing stream at the boundary point, the flatness factor tends to be closer to 3. In the central core of the flow field, the flatness factor is about 2.3 which is higher than that for zero-gradient distribution and yet quite different from Gaussian value. This is due to the interactions of the fluid elements adjusting the wall effects to the mean flow. This figure clearly shows that the distribution function near the centerline of the Couette flow is quite far from the Gaussian even though the turbulence is nearly isotropic and homologous.

In conclusion, the numerical scheme employing a combination of

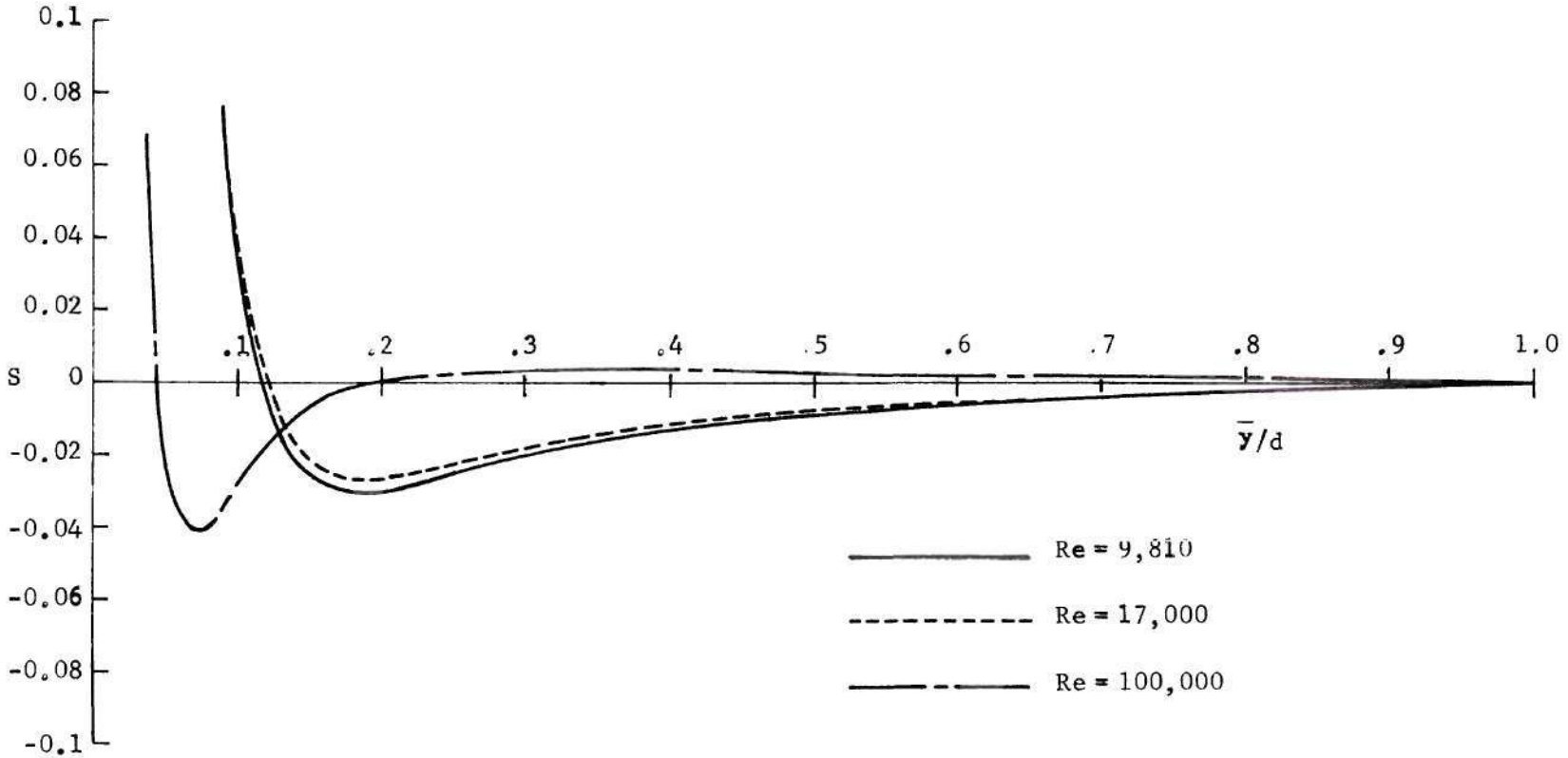

Figure 22. Skewness Factors of the g Distribution Functions.

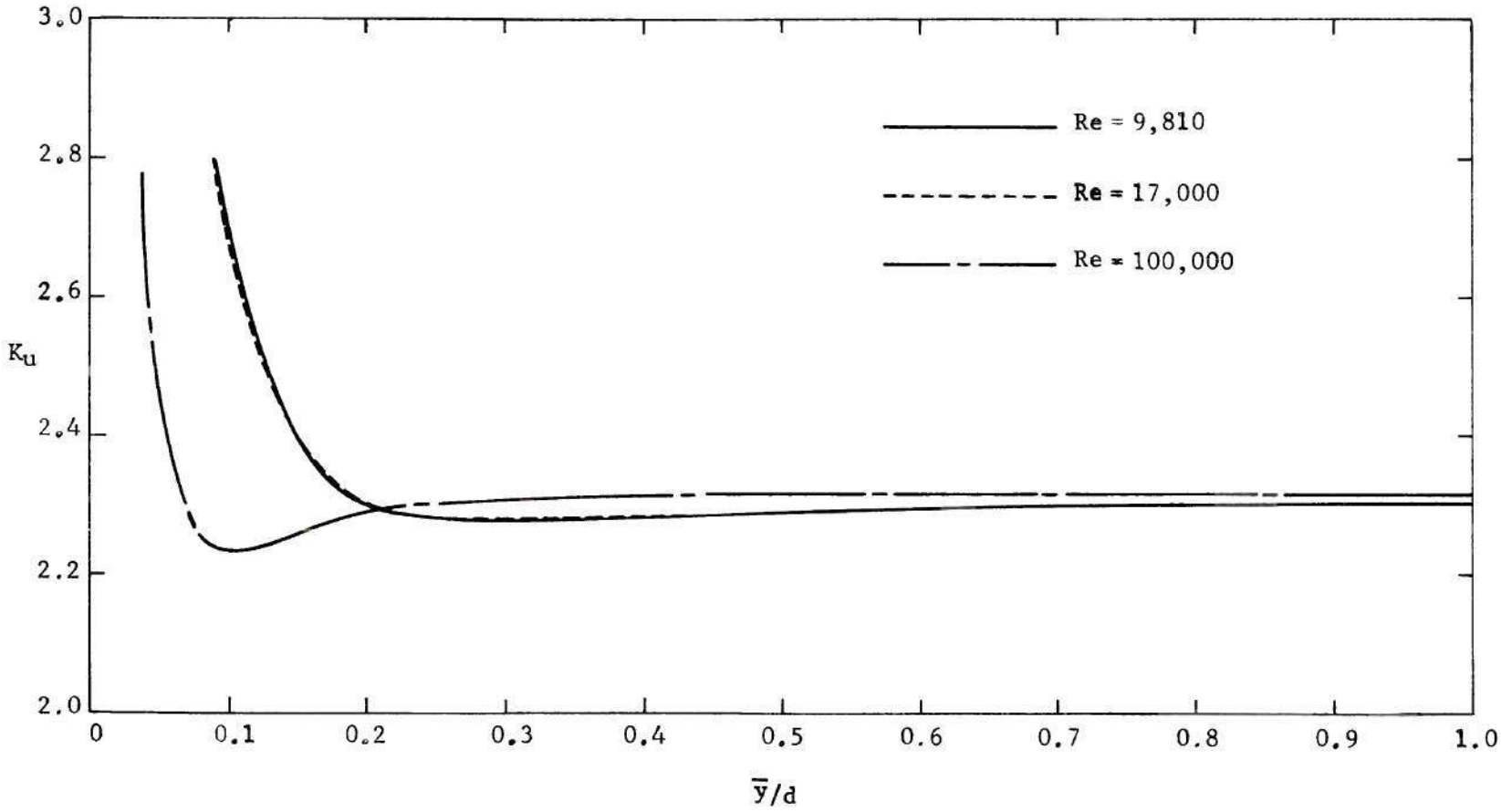

Figure 23. Flatness Factors of the g Distribution Functions.

discrete ordinate method and finite differences seems to be quite good for solving Lundgren's model equation. The statistical model equation yields results which compare very well with experimental data for mean velocity and skin friction. The present results show better agreement with experimental data than those of Chung. However, the inadequacy of the Chapman-Enskog boundary condition indicates the need for further studies in that area.

CHAPTER VI

TWO DIMENSIONAL CHANNEL FLOW

The results obtained for the Couette flow problem compare favorably with the available experimental data and thus indicate that Lundgren's model equation accurately describes that problem. The Couette flow problem with zero pressure gradient is perhaps the simplest case on which the model equation can be tested. In an effort to cover a more general class of problems, it is desirable to apply the model equation to fully developed turbulent flow problem in a two dimensional channel. The presence of pressure gradients in this problem gives rise to additional complications. Unlike the Couette flow problem, $\partial\bar{p}/\partial y$ is no longer zero. It can be seen from the y-momentum equation, that

$$\frac{d}{dy}\langle v'^2\rangle = -P_y. \tag{28}$$

However, this equation is automatically satisfied by the governing statistical equation, Equation (1), and so it can not be used to compute P_y. In the absence of any other independent scheme for computing P_y, in this study, this quantity is assumed to be zero everywhere. The streamwise pressure gradient, $\partial p/\partial x$, on the other hand, is more easily determined. If the forces occurring on a control volume in the channel flow, as shown in Figure 24, are balanced, there results

$$\frac{d}{\rho}\frac{\partial p}{\partial x} = -\frac{\left(P_{xy}\right)_w}{\rho} = -u_*^2$$

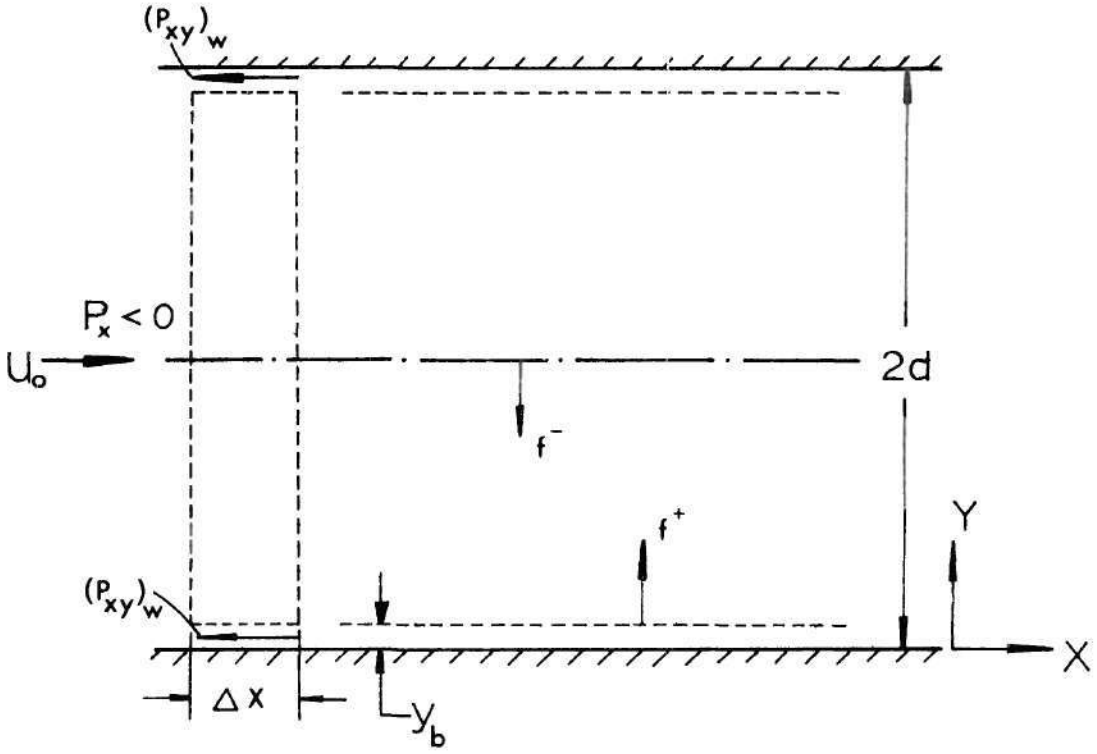

$P_x < 0$; $Re = u_0 d/\nu$

Figure 24. Channel Flow Configuration.

or,
$$P_x = \frac{d}{\rho u_*^2} \frac{\partial p}{\partial x} = -1. \tag{29}$$

Geometry and Boundary Conditions

The geometry of the channel flow problem is shown in Figure 24. The boundary conditions employed for this problem are the gradient and the Chapman-Enskog boundary conditions. The conditions at the centerline of this problem are different from those of the Couette flow, since the Reynolds stress in the Channel flow is not constant, but linear. However, due to the symmetry of the flow field, the changes in the distribution functions as the centerline is approached from either of the directions are the same. Since the directions of the positive and the negative streams are opposite to each other, the symmetry of the flow field requires

$$\frac{\partial f^-}{\partial y} = -\frac{\partial f^+}{\partial y} \tag{30a}$$

In terms of the reduced distribution functions, this equation becomes

$$\frac{\partial g^-}{\partial y} = -\frac{\partial g^+}{\partial y} \tag{30b}$$

$$\frac{\partial j^-}{\partial y} = -\frac{\partial j^+}{\partial y} \tag{30c}$$

$$\frac{\partial h^-}{\partial y} = -\frac{\partial h^+}{\partial y} \tag{30d}$$

Equation (13) gives

$$\frac{\partial j_v^-}{\partial y} = \frac{\partial j^-}{\partial y} + u \frac{\partial g^-}{\partial y} + g^- \frac{du}{dy}$$

At the centerline of the channel, $\frac{du}{dy} = 0$. Using Equations (30), this becomes,

$$\frac{\partial j_v^-}{\partial y} = - \frac{\partial j^+}{\partial y} - u \frac{\partial g^+}{\partial y} = - \frac{\partial j_v^+}{\partial y} \tag{30e}$$

Thus, Equations (30) can be used as boundary conditions for the negative stream. The constraints to be imposed at the near wall boundary are similar to those used in the Couette flow problem and are dependent on the form of the distribution function.

Gradient Boundary Condition

As pointed out in Chapter III, the zero-gradient condition is not appropriate for the channel flow problem. However, from the known trends of u, U and ϵ near the wall boundary, it should be possible to develop conditions on the derivatives of the distribution functions based on the governing differential equations, Equations (10). These conditions are shown in Appendix A, subject to the assumption $\partial p/\partial y = 0$ at the boundary point. To employ this condition, it is necessary to specify U and Re_* as inputs, analogous to the zero-gradient conditions in the Couette flow, and $Re = u_0 d/\nu$ can be obtained as a solution. But, there is not a specific value for u_* that should be used in this case, contrary to the situation in the Couette flow, since the mean velocity is not logarithmic in the entire flow field. Thus, the value of Re_* has to be specified arbitrarily or else should correspond to some experimental measurements. In this study, Re_* is obtained from Laufer's data [21] corresponding to $Re = \frac{u_0 d}{\nu} = 30{,}800$. Once Re_* is known, the boundary condition for mean velocity is obtained from the law of the wall,

$$u_b = \frac{1}{\kappa} \ln (Re_* y_b) + 5 \tag{31a}$$

The value of U at $y = y_b$ is specified from the formula [22]

$$U_b^2 = \frac{2}{3\sqrt{c_D}} \text{ , with } c_D = 0.1. \tag{31b}$$

Equations (A-11), (A-14) and (A-15) are then solved subject to these constraints to give boundary conditions on g, j, h, and j_v. These conditions are fixed for all iterations.

Chapman-Enskog Boundary Condition

As mentioned earlier for the Couette flow problem, when Chapman-Enskog form is used as a boundary condition for the positive stream, certain integral constraints are needed to adjust the parameters in the outgoing stream such that the moments of the distribution functions follow the known trends. In this study, the following constraints are used in the channel flow problem.

$$\int_{-\infty}^{\infty} c_y j dc_y = \int_{-\infty}^{0} c_y \bar{j} dc_y + \int_{0}^{\infty} c_y j^{(1)} dc_y = -1 + y_b + \frac{1}{Re_* \kappa y_b} \tag{32a}$$

$$U_b^2 = \frac{2}{3\sqrt{c_D}} \text{ with } c_D = 0.1. \tag{32b}$$

$$\int_{-\infty}^{\infty} g \, dc_y = \int_{-\infty}^{0} \bar{g} dc_y + \int_{0}^{\infty} g^{(1)} \, dc_y = 1.0 \tag{32c}$$

$$\int_{-\infty}^{\infty} j_v dv_y = \int_{-\infty}^{0} \bar{j}_v dv_y + \int_{0}^{\infty} j_v^{(1)} dv_y = u_b \tag{32d}$$

$$= \frac{1}{\kappa} \ln (Re \frac{u_*}{u_0} y_b) + 5.0$$

Equation (32a) implies that the total shear stress near the boundary point is linear. Equation (32b) is an empirical formula for kinetic energy of turbulence and Equation (32c) states that the probability of finding a fluid element somewhere in the velocity space is unity. Equation (32d) requires that the mean velocity at the boundary point conforms with the law of the wall. As pointed out earlier, it is more appropriate to require these constraints on the total moment and not restrict each stream to satisfy them. One way to achieve this is to treat the quantities u and $\frac{\nu_T}{Re_*}\frac{du}{dy}$ in Equations (15) as parameters to be evaluated from Equations (32). If Chapman-Enskog forms of Equations (15) are substituted into Equations (32), there results

$$-\frac{\nu_T}{Re_*}\frac{du}{dy} = P_{xy}^{+} = -2\left(1 - y_b - \frac{1}{Re_* \kappa y_b} + a_1\right) \tag{33a}$$

$$\frac{\nu_T}{Re_* U^2}\frac{dU}{dy} = \sqrt{2\pi}\,(0.5 - a_2) \tag{33b}$$

and

$$u = \left(u_b - a_3 - \frac{P_{xy}^{+}}{\sqrt{2\pi}U}\right) / (1.0 - a_2) \tag{33c}$$

where

$$a_1 = \int_{-\infty}^{0} c_y \, j^{-} \, dc_y$$

$$a_2 = \int_{-\infty}^{0} g^{-} \, d \, c_y$$

$$a_3 = \int_{-\infty}^{0} j_v^{-} \, dv_y$$

It is emphasized that u and P_{xy}^{+} in Equations (33) do not represent the

mean velocity and the Reynolds stress but rather the parameters employed in the outgoing stream. It is reiterated that this is the only point under the Chapman-Enskog scheme for boundary conditions, at which the law of the wall is assumed to hold.

With these constraints, the governing differential equations, Equations (10), are solved and the moments are evaluated at each iteration. Once the mean flow quantities are obtained, the dissipation rate, ε, can be computed from Equation (11a). This equation is a second order non-linear ordinary differential equation and consequently requires two boundary conditions. The requirement at the centerline of the channel is

$$\frac{d\varepsilon}{dy} = 0 \qquad \text{at } y = 1 \tag{34}$$

At the near wall boundary, the production and dissipation of turbulence kinetic energy are known to be equal. Using the law of the wall, this reduces to

$$\varepsilon_b = -(P_{xy})_b/\kappa y_b \qquad \text{at} \qquad y = y_b. \tag{35a}$$

For the channel flow, the shear stress is linear. If viscous stresses are included, the turbulence shear stress at the boundary point is given by

$$(P_{xy})_b = -(1 - y_b - \frac{1}{Re_* \kappa y_b})$$

Using this expression in Equation (35a), the near wall boundary condition for ε becomes

$$\varepsilon_b = (1 - y_b - \frac{1}{Re_* \kappa y_b})/(\kappa y_b) \quad \text{at } y = y_b \tag{35b}$$

With Equations (34) and (35b) as boundary conditions, Equation (11a) for ε can be solved. For the channel flow problem, the non-linear differential equation for ε is linearized by the Newton-Raphson-Kantorovich quasi-linearization technique [30]. The resulting linearized equation is solved by a finite difference scheme. The details of this procedure are given in Appendix D.

Results

As pointed out earlier, the pressure gradient, $\partial p/\partial y$, is required as an input for the problem. This gradient in pressure is due to the turbulence structure and hence should, in principle, be computed from the solutions. Since there are no independent equations available, in this study, $\partial p/\partial y$ is assumed to be equal to zero everywhere. This assumption imposes certain restrictions on the flow field which will be discussed along with the results. Two different boundary conditions are used to solve the channel flow problem. They are the Chapman-Enskog and the gradient boundary conditions given in Appendix A.

It is seen from the x-momentum equation for channel flow (which can be obtained as a moment of the governing differential equation, Equation (1)), that

$$\frac{d}{dy}(\overline{u'v'}) = \frac{1}{Re_*}\frac{d^2u}{dy^2} - P_x \tag{36}$$

where,

$$P_x = \frac{d}{\rho a_*^2}\frac{\partial p}{\partial x} = -1.$$

By integrating this equation, it is seen that the shear stress is linear. Or,

$$\overline{u'v'} = -1 + y + \frac{1}{Re_*} \frac{du}{dy} \tag{37}$$

It is recalled that even though the Chapman-Enskog distribution does not satisfy the governing differential equation exactly, it satisfies the moment equations, namely, continuity, momentum and turbulence kinetic energy equations. Consequently, if Chapman-Enskog distribution function for j,

$$j = \frac{\overline{u'v'}}{U^2} c_y G \tag{38}$$

is used, with $\overline{u'v'}$ from Equation (37), to replace the differential equation for j(Equation (10b)), it would yield the appropriate Reynolds stress profile. Besides, the Chapman-Enskog distribution automatically satisfies the condition $\bar{c}_x = 0$ at each iteration. In order to find out its implications, the Chapman-Enskog form for j, Equation (38), is used in a series of computations instead of the differential equation, Equation (10b). Thus, the results for channel flow are obtained for gradient boundary conditions and Chapman-Enskog boundary conditions and in the latter case, both Equations (10b) and (38) have been used separately. These results are compared with Laufer's experimental data [21]. All the computations are made at a Reynolds number, $Re = \frac{u_0 d}{\nu} = 30,000$.

Figure 25 illustrates the results for mean velocity at Re = 30,000. Laufer's experimental data [21] is shown for comparison. The agreement between the experimental data and the result obtained using Chapman-Enskog boundary conditions is quite good. The gradient boundary condition yields

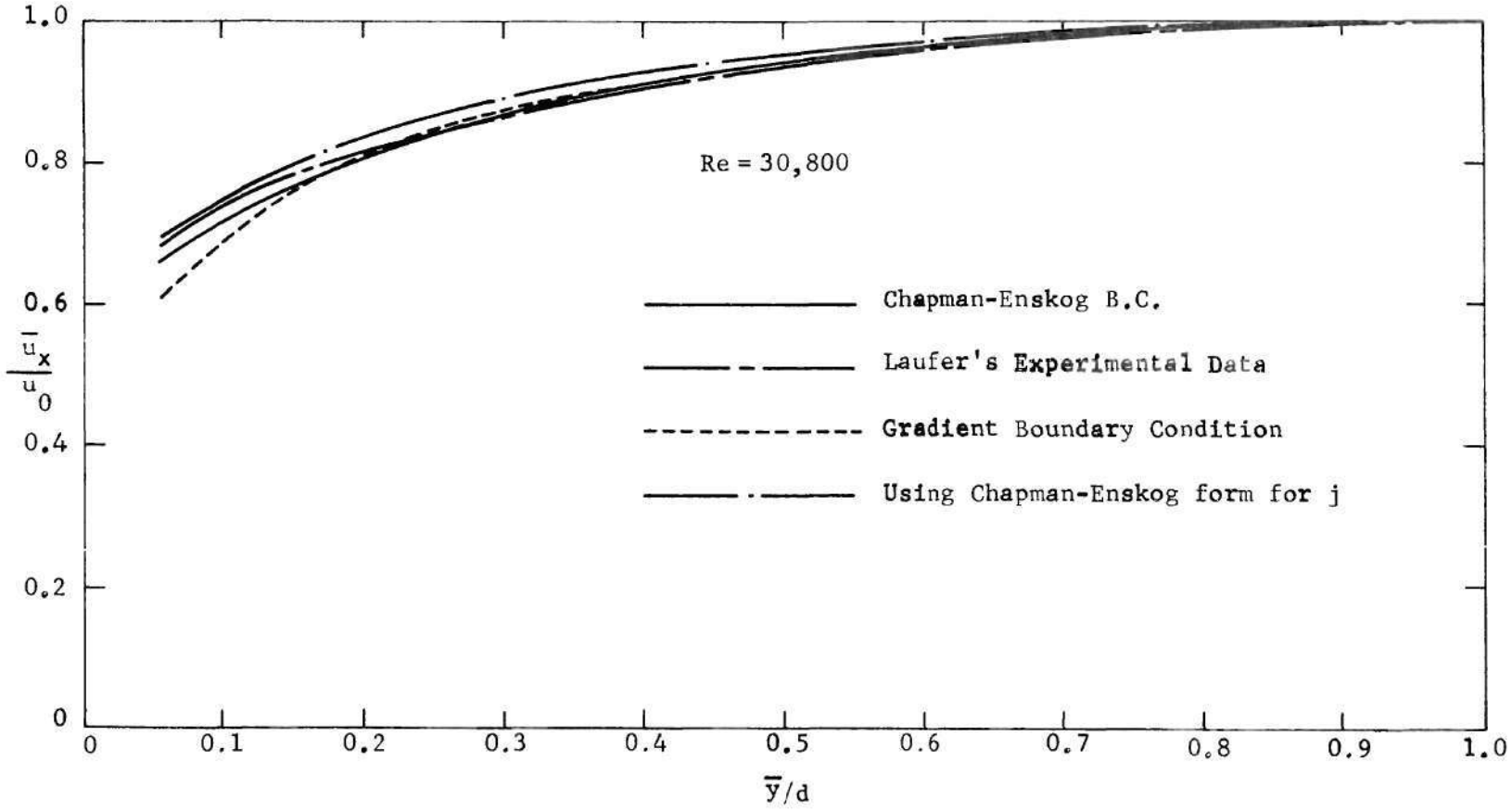

Figure 25. Mean Velocity Profiles in the Channel Flow.

somewhat larger slopes near the wall boundary and hence is in poorer agreement with Laufer's data in that region. When Equation (38) is used for j, the resulting mean velocity profile is somewhat fuller than the experimental data. In spite of all these small differences, the overall agreement of all these results with the experimental data is reasonably satisfactory.

The differences between these results in mean velocity are seen more clearly in the velocity defect coordinates shown in Figure 26. In the central core of the flow field, the agreement between the present results and the experimental data is quite satisfactory. The gradient boundary condition is not in good agreement with the measurements near the boundary point ($\bar{y}/d = 0.055$). These disagreements are partially due to the differences in u_*/u_0 values. It is interesting to note that the result obtained using Equation (38) for j has a very similar shape to that of the experimental data except for a lateral shift due to differences in u_0/u_* value, or the centerline velocity. The differences in the centerline velocities among these results is within 14 per cent of the experimental data and are likely due to the assumption $\partial\bar{p}/\partial\bar{y} = 0$. The value of u_*/u_0 for the case using gradient boundary condition is computed to be about 0.04 and the value obtained for Chapman-Enskog boundary condition is about 0.04276. When Equation (38) is used to replace Equation (10b), the resulting value for u_*/u_0 is 0.04395. The value obtained by Laufer for u_*/u_0 is reported to be 0.03873. It is emphasized again that all these results correspond to a Reynolds number of 30,000.

The Reynolds stress profiles are shown in Figure 27. As pointed out earlier, Equation (38) yields a linear profile for Reynolds stress.

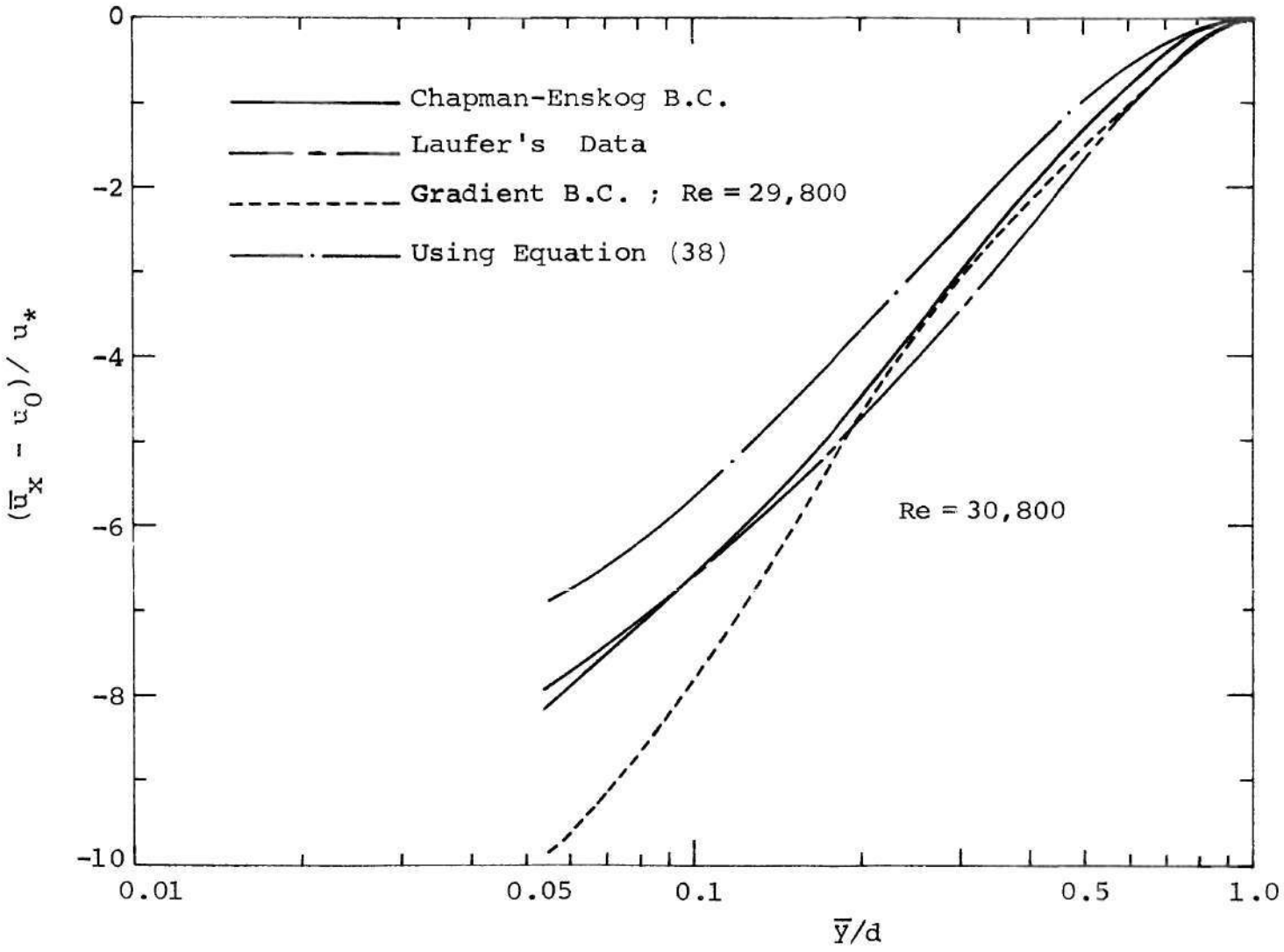

Figure 26. Velocity-defect Profiles in the Channel Flow.

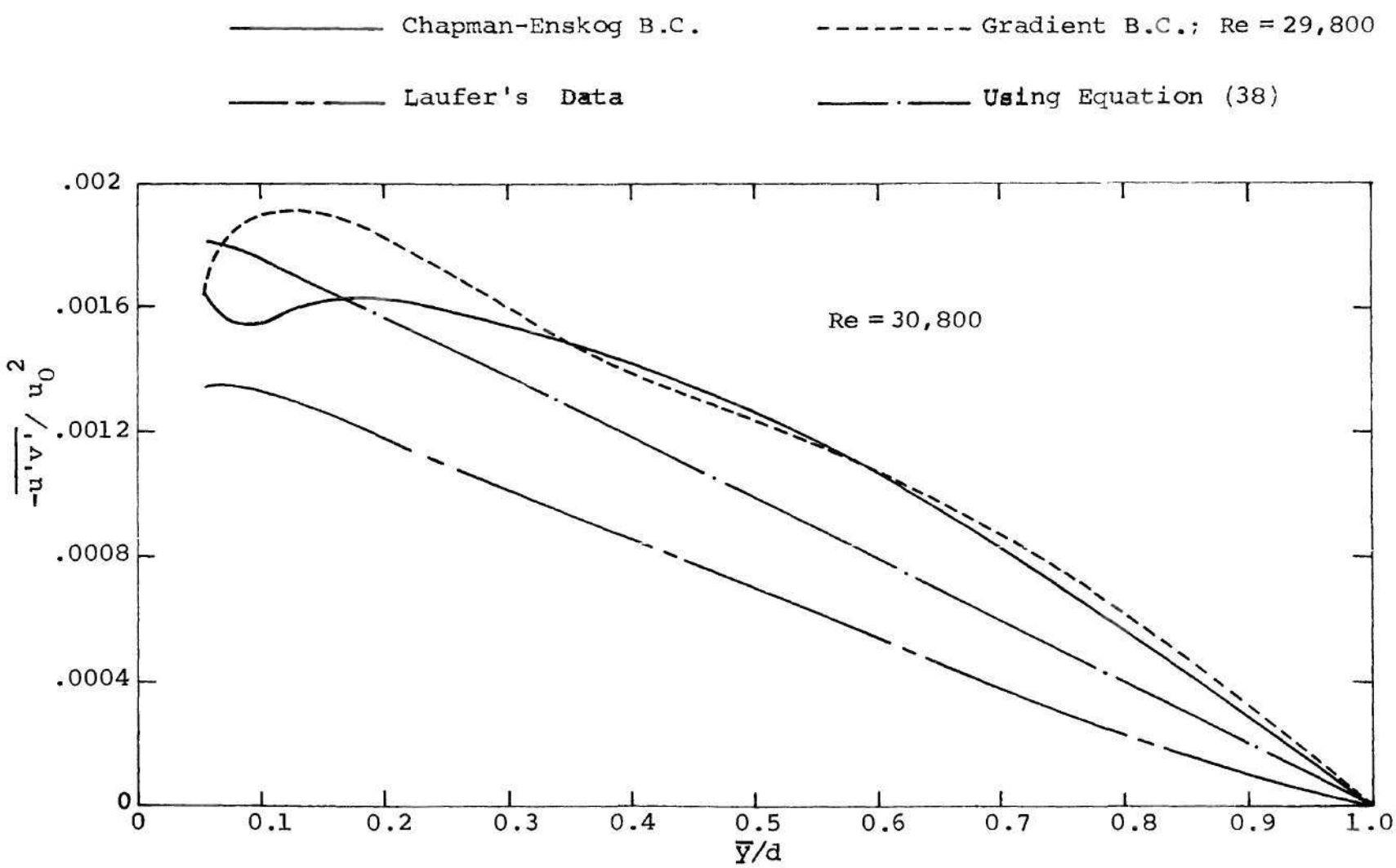

Figure 27. Variation of Reynolds Stress in the Channel Flow.

The disagreement with the experimental data in the slope of the line is due to the difference in the u_*/u_0 values. The Reynolds stress profile for gradient boundary conditions agrees well with that for Chapman-Enskog boundary condition, and is especially so in the central core of the flow field. The deviations near the boundary point is partially due to the gradients produced by the inadequacy of Chapman-Enskog boundary conditions. These Reynolds stress profiles are different from linear, and are not in very good agreement with the experimental data. This is also attributed to the assumption $P_y = 0$.

The variations of eddy viscosity for the three computations are shown in Figure 28. The differences in the profiles for eddy viscosity between results for the gradient boundary conditions and the Chapman-Enskog boundary conditions are essentially due to the differences in the Reynolds stress profiles. The equation used to compute eddy viscosity,

$$\nu_T = - Re_* \frac{P_{xy}}{(du/dy)} \tag{39a}$$

is not applicable at the centerline, since both P_{xy} and du/dy are zero there. Thus, if L'Hospital's rule is applied at the centerline, it yields

$$\nu_T = - Re_* \frac{d}{dy} (P_{xy}) / (\frac{d^2u}{dy^2}) \tag{39b}$$

In all these calculations, Equation (39b) gives a low value for eddy viscosity, and thus causes large gradients near the centerline. The gradient boundary condition gives the correct qualitative trend for the eddy viscosity.

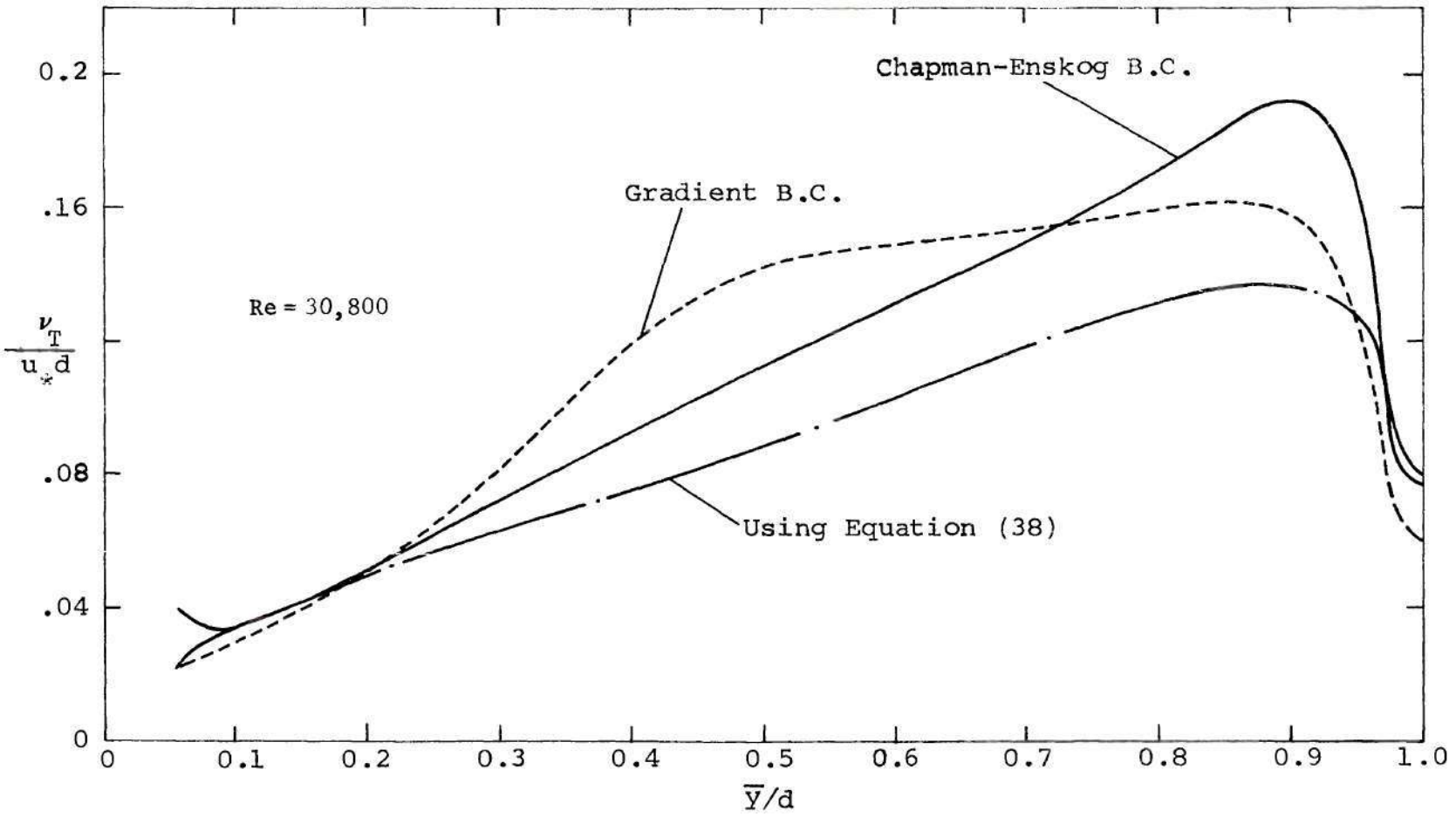

Figure 28. Eddy Viscosity Profiles in the Channel Flow.

The results for turbulence intensity, U, are shown in Figure 29. The present results yield somewhat higher intensities than those derived from Laufer's experimental data. In addition, these results also give nearly constant values for U. When Equation (38) is used to replace the differential equation for j (Equation (10b)), the resulting turbulence intensity is in better agreement with the experimental data, and has the same qualitative trend with the latter. Approximately constant values for U in these results are due to the absence of cross-stream pressure gradients, P_y, in the final equations.

This effect is also seen in the results for the components that contribute to turbulence kinetic energy, which are shown in Figure 30. If P_y is assumed to be zero everywhere,, it follows from the y-momentum equation, Equation (28), that $\langle v'^2 \rangle$ should be constant. But, the experimental data shows that $\langle v'^2 \rangle$ is not a constant, and hence P_y also is, in reality, non-zero. In moment approaches, where moment equations are solved instead of the equation for the distribution functions, each moment equation is independent of the other equations. Besides, in such a system, the pressure gradient, P_y, appears only in the y-momentum equation and thus the y-momentum equation is de-coupled from the rest. This decoupling enables one to model the equation for kinetic energy of turbulence without having to consider the effects of P_y. In the present approach, the P_y term appears in all of the differential equations for reduced distribution functions and thus affects the profiles of all the moments of the distribution functions. Thus, when P_y is set to be zero everywhere, the solutions for turbulence intensities tend towards a flat profile, similar to those obtained in the Couette flow.

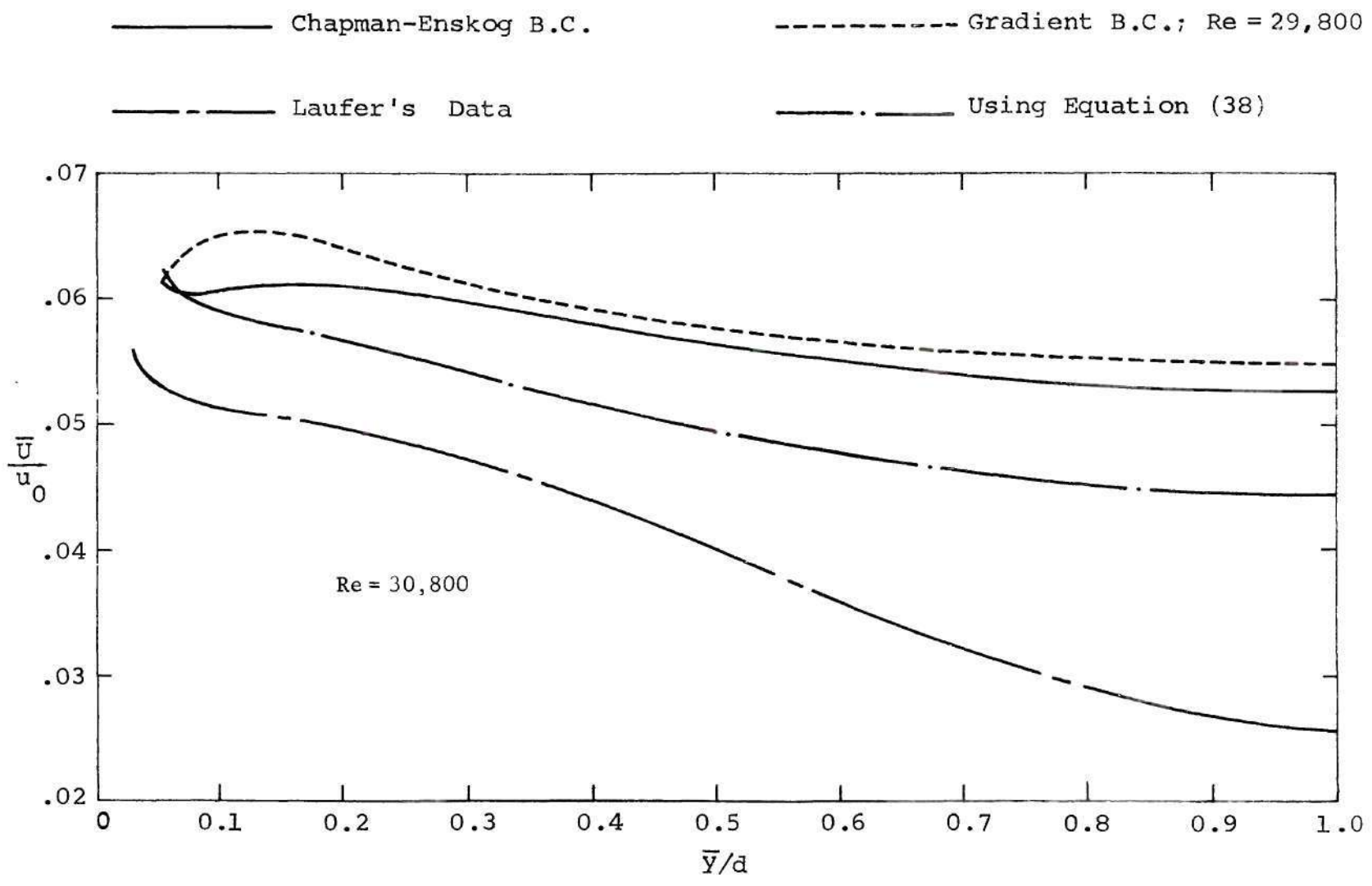

Figure 29. Turbulence Intensity in the Channel Flow.

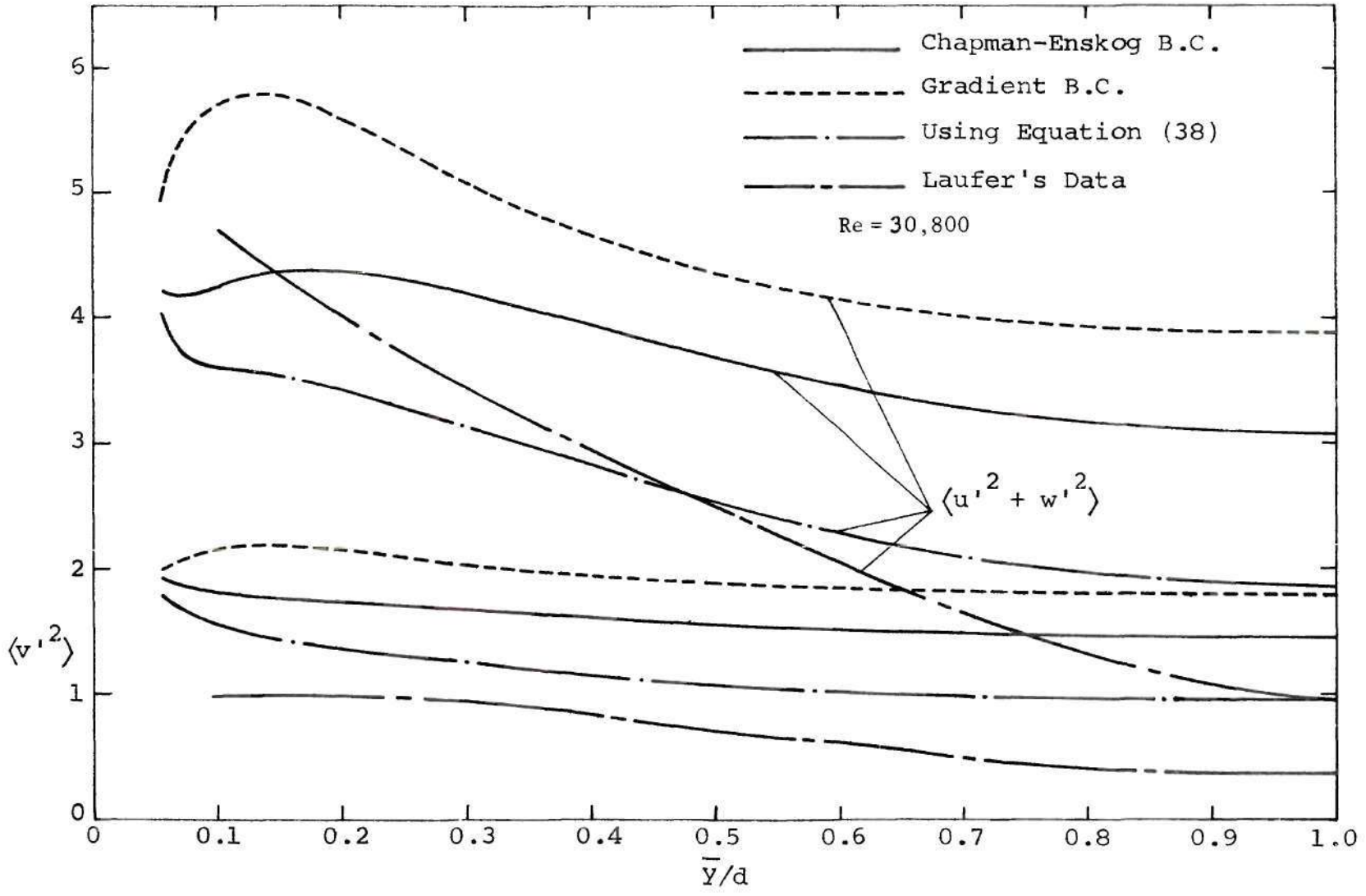

Figure 30. Components of Turbulence Kinetic Energy.

The computed results for the distribution function, g, are illustrated in Figures 31a, 31b and 31c. It is recalled that when the gradient boundary conditions are employed, $Re_* = \frac{u_* d}{\nu}$ is specified and $Re = \frac{u_0 d}{\nu}$ is computed from the solutions. This accounts for the difference in the Reynolds number values quoted in these figures. When the Chapman-Enskog boundary conditions are used, it gives rise to a discontinuity in g at the boundary point at $c_y = 0$. The solutions obtained using Chapman-Enskog boundary conditions give slightly more peaky distribution for g compared to those obtained using the gradient boundary conditions. The results for g using Equation (38) yields still higher values near $c_y = 0$. This is due to the relatively smaller values of turbulence intensities among the three cases. Gradual variations in the distribution functions are seen in the figures and in the central core of the flow, these variations are quite small. This indicates that fluid elements are gradually adjusting between the conditions at the two boundaries.

The results for the distribution function, j, are shown in Figures 32a, 32b and 32c. Figure 32c represents the Chapman-Enskog form for j and which is anti-symmetric with respect to c_y. Figures 32a and 32b illustrate the solutions of the differential equation for j using the gradient boundary conditions and the Chapman-Enskog boundary conditions respectively. These two solutions yield very similar profiles for j. These two figures show a gradual variation in the j distribution function with respect to y such that the c_y value at which $j = 0$ moves farther from zero as y increases. It is believed that this is due to neglecting the P_y term. From Equation (10b), it is seen that the term P_y appears in the form, $(\frac{\varepsilon}{3U^2} c_y + P_y) \frac{\partial j}{\partial c_y}$. From the experimental data, the largest

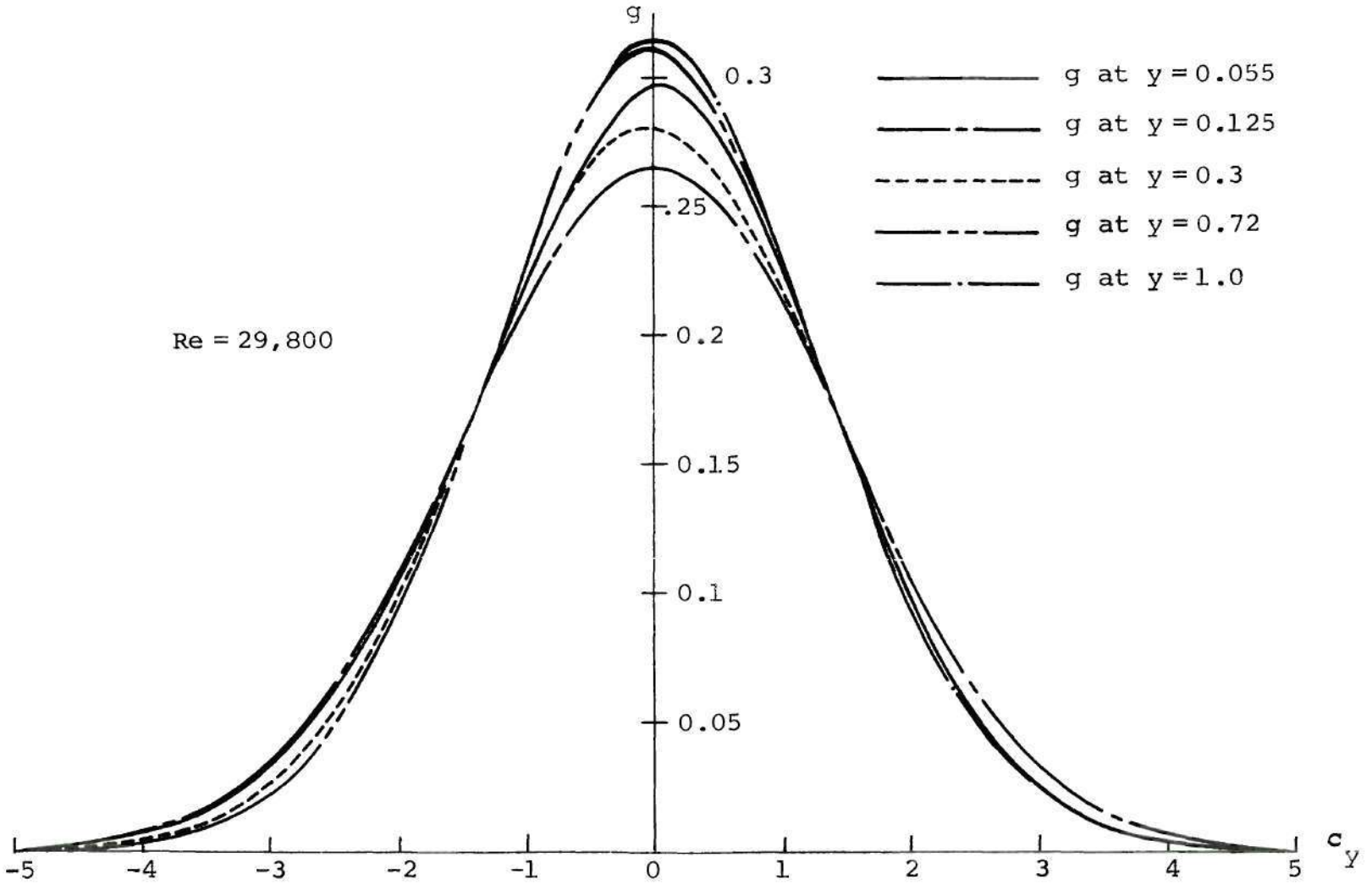

Figure 31a. Distribution Function, g, for Gradient Boundary Condition.

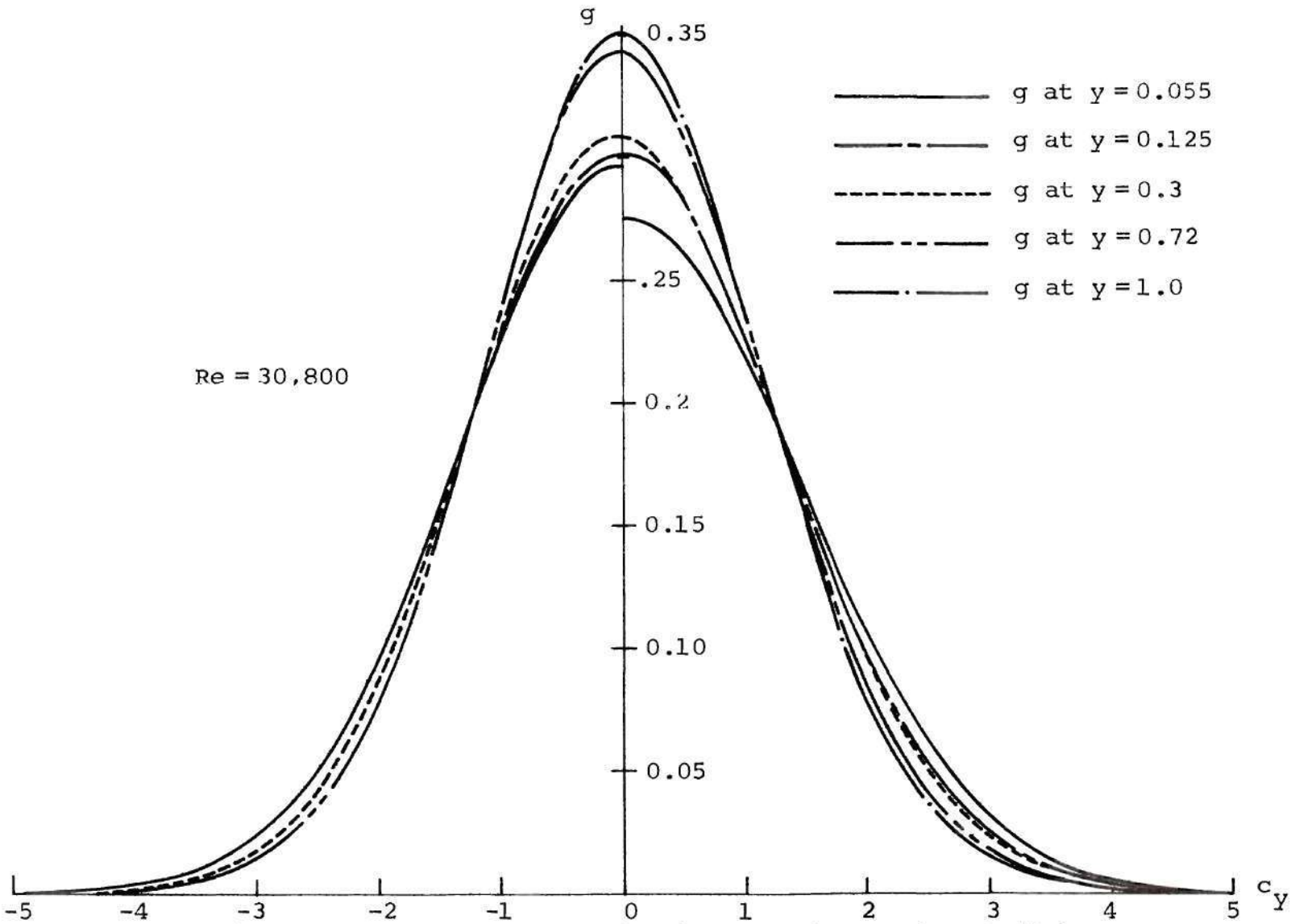

Figure 31b. Distribution Function,g, for Chapman-Enskog Boundary Condition.

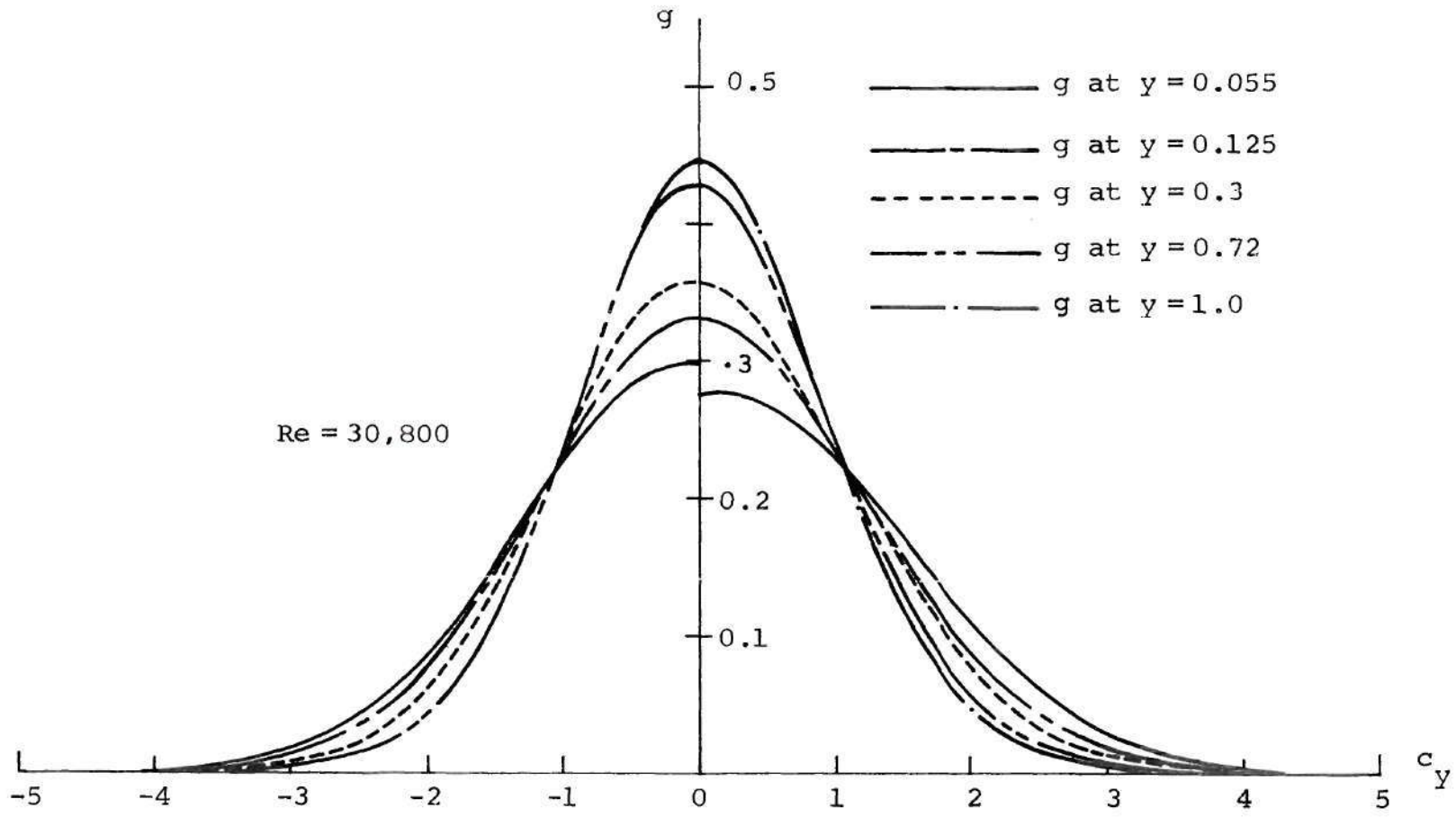

Figure 31c. Distribution Function,g, when Equation (38) is used.

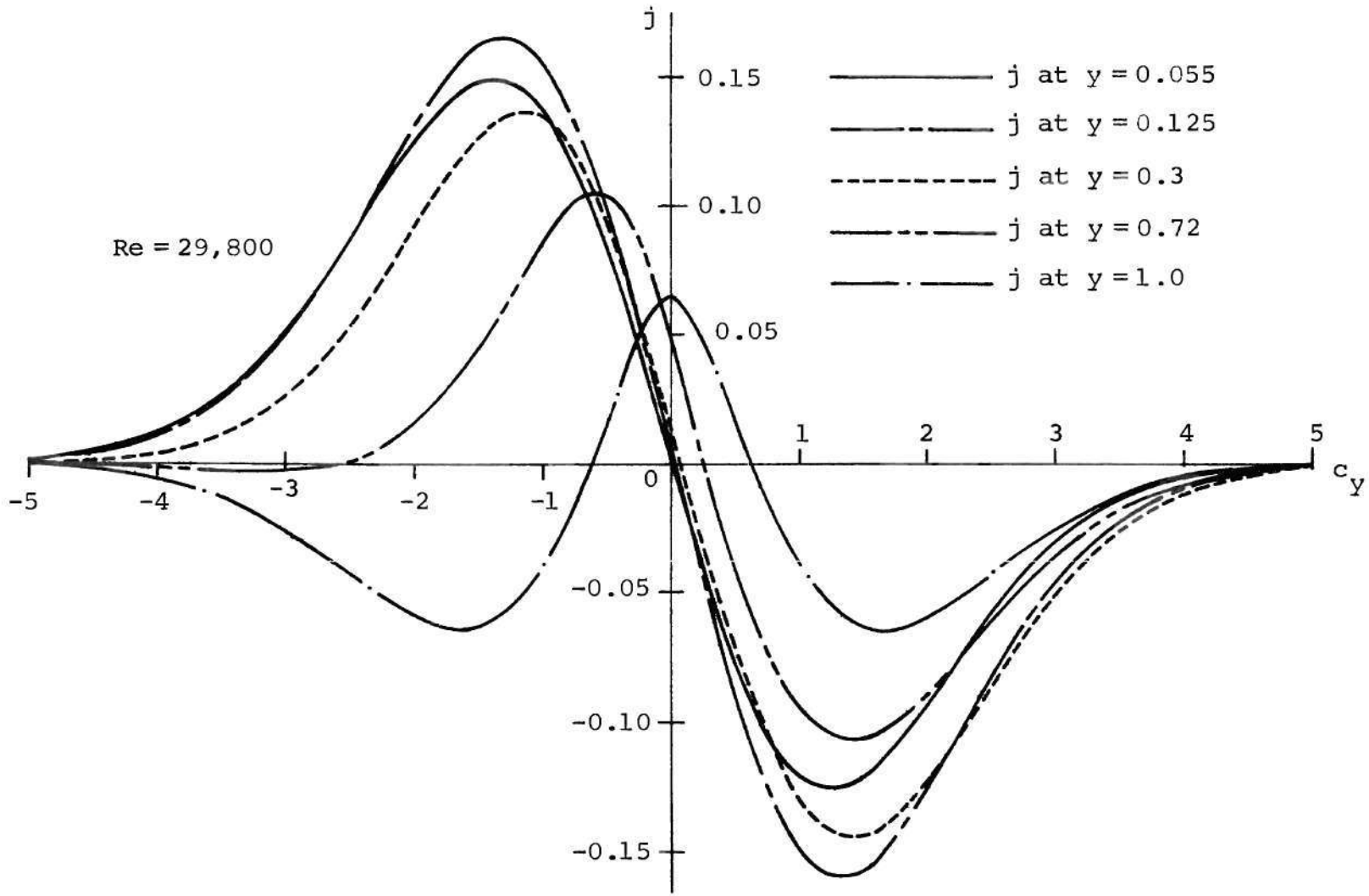

Figure 32a. Distribution Function, j, for Gradient Boundary Condition.

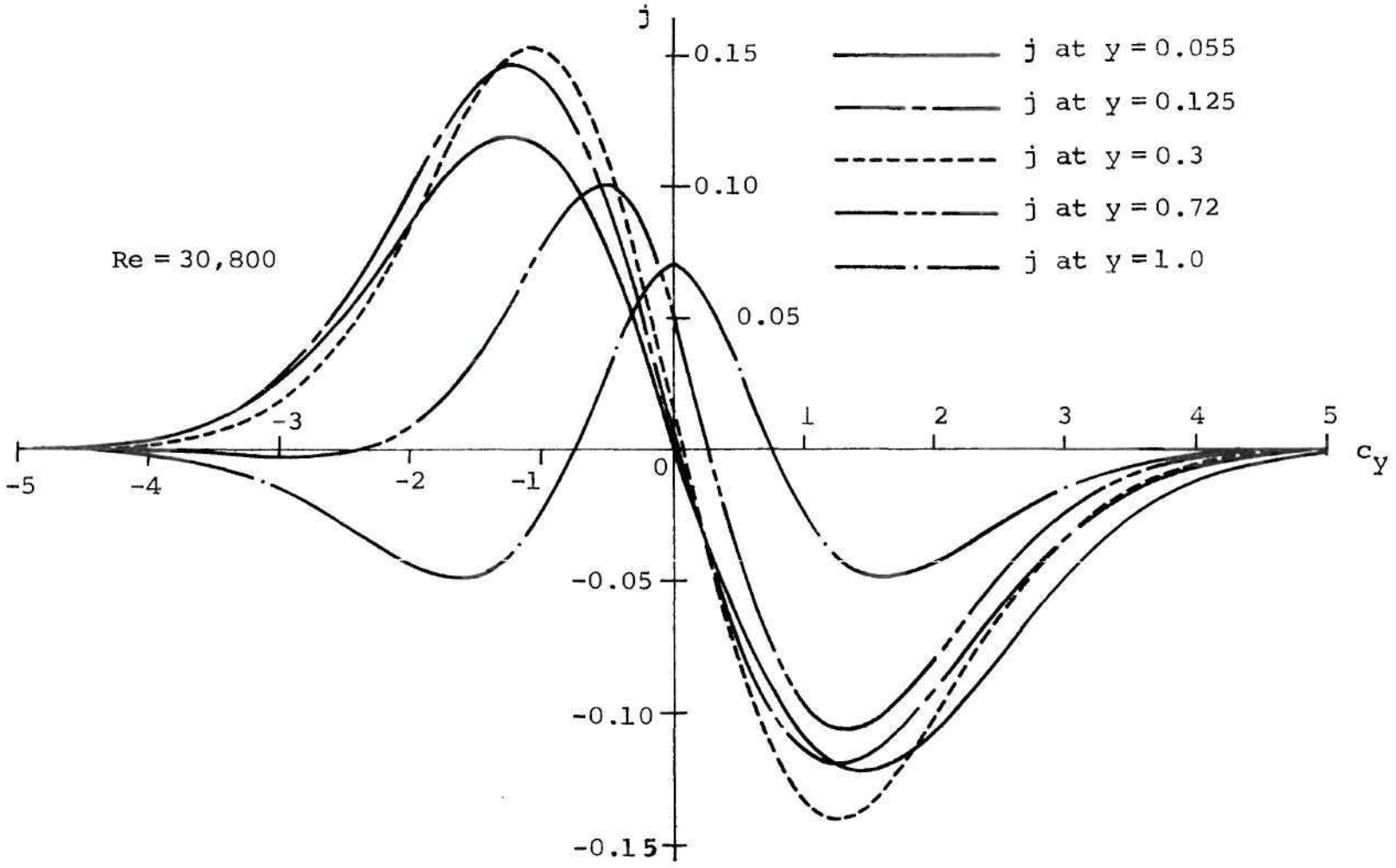

Figure 32b. Distribution Function, j, for Chapman-Enskog Boundary Condition.

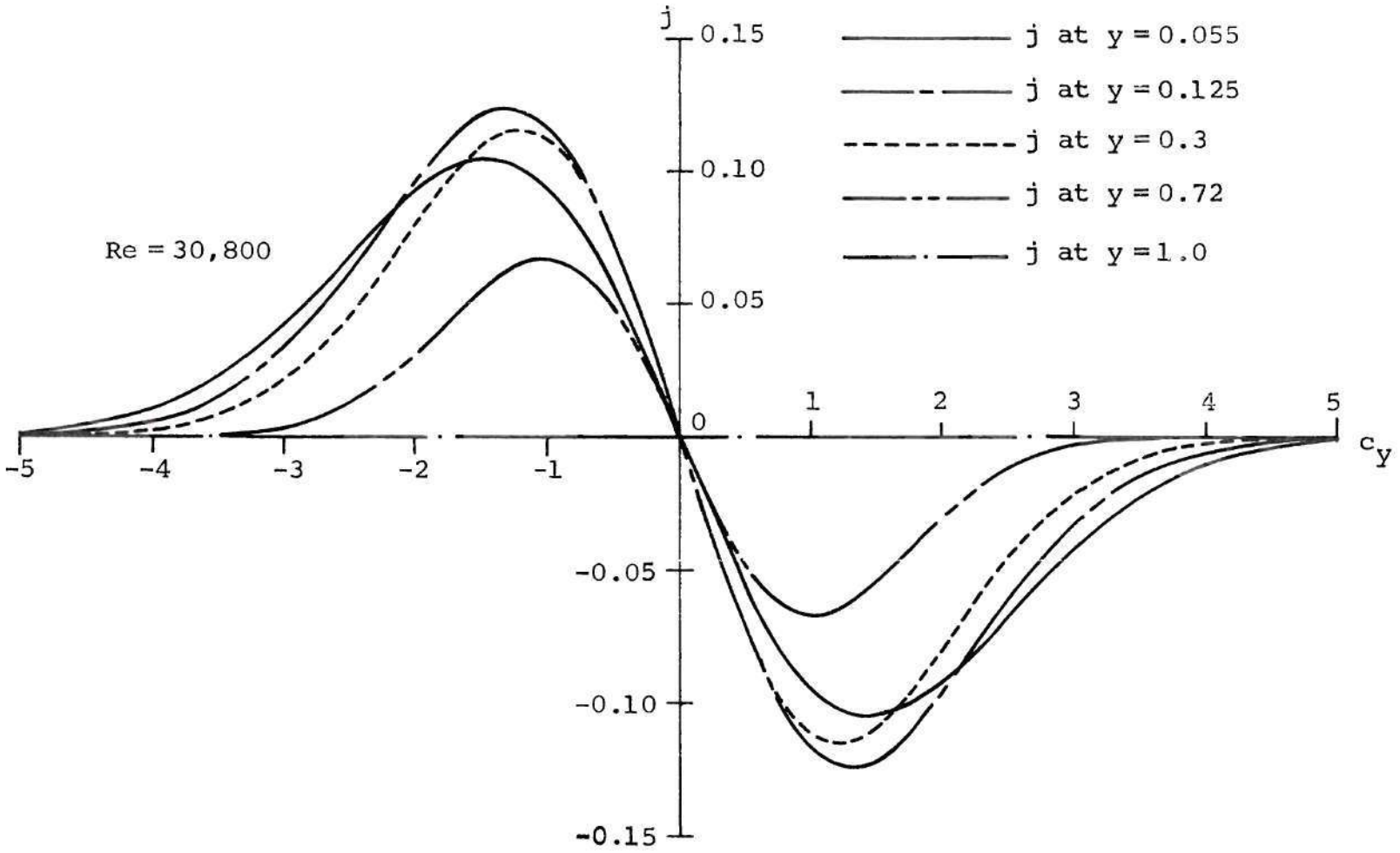

Figure 32c. Chapman-Enskog Form for the Distribution Function, j.

value of P_y is estimated to be about 1.5 near $\bar{y}/d = 0.3$. The smallest value of $\frac{\varepsilon}{3U^2}$ is about 1. Thus, it is seen that for large c_y values, it is reasonable to neglect P_y compared to the other term, while it becomes larger than or comparable to $\frac{\varepsilon}{3U^2} c_y$ for small values of c_y (for $|c_y|<1$). Consequently, when P_y is set to be zero, it gives rise to some error in the distribution function near $c_y = 0$ and this effect gradually propagates all the way to the centerline. It is recalled that the zeroth moment of j gives $\bar{c}_x$, which should be zero, and the first moment yields the Reynolds stress. Figures 32a and 32b show that the area under each curve is not zero exactly and this is more clearly observed at the centerline. However, due to the anti-symmetric nature, the Chapman-Enskog distribution functions for j give $\bar{c}_x = 0$ at all y locations, and the distribution function at the centerline is zero for all c_y.

The variations of the skewness factor, S, of the g distribution function for the three cases are shown in Figure 33. The effect of the Chapman-Enskog boundary condition, quite similar to that in the Couette flow, is to give a rather higher positive value for the skewness factor. The skewness factors for Chapman-Enskog boundary condition and those for gradient boundary condition agree fairly well with each other in regions away from the boundary. When Equation (38) is used to replace Equation (10b), it results in a higher skewness factor for the g distribution. At the centerline, because of the symmetry of the flow field, the skewness is zero.

The flatness factor, or kurtosis, K_u, of the g-function is illustrated in Figure 34. It is recalled that the Chapman-Enskog distribution, if employed for both the streams, would give a flatness factor of 3.

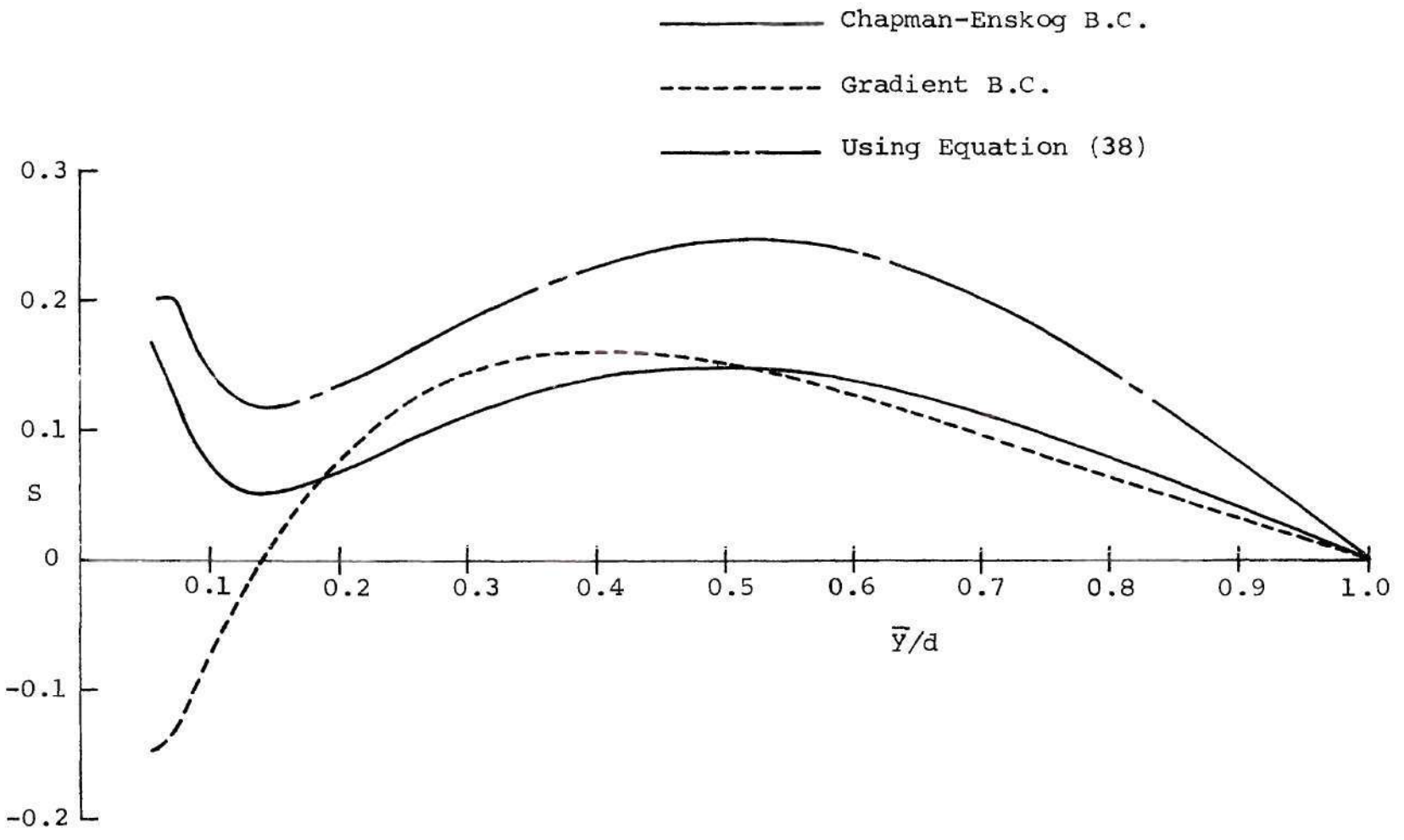

Figure 33. Skewness Factors of the g Distribution Function.

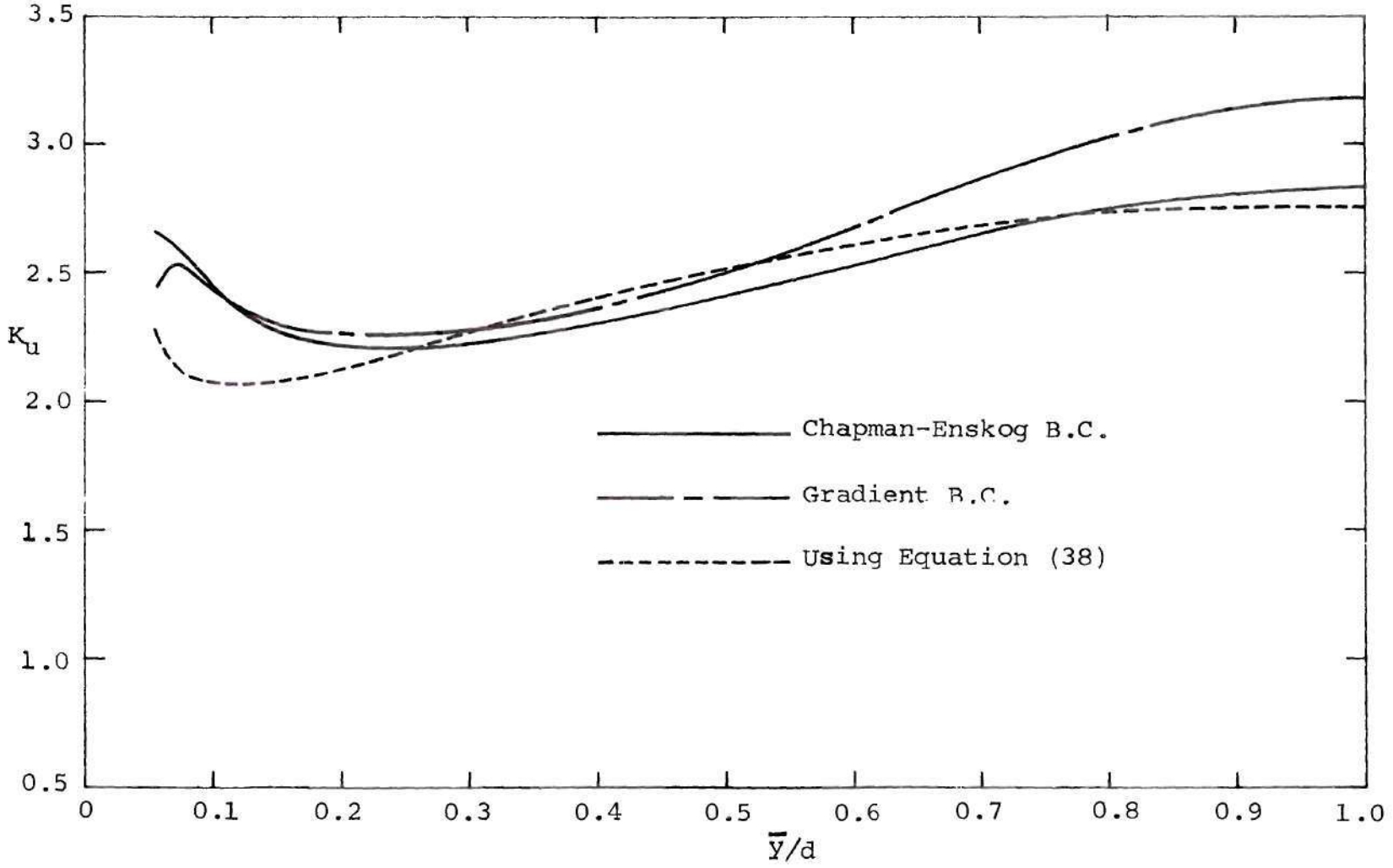

Figure 34. Flatness Factors of the g Distribution Functions.

Hence, when it is employed only for the outgoing stream, it tends to give a higher value for K_u compared to the gradient distribution function. However, in regions away from the boundary, these two results give nearly the same value for K_u, indicating that the boundary effects are smoothed out by the fluid elements. When Equation (38) is used, the resulting flatness factors are somewhat higher. At the centerline, where the turbulence intensities are nearly the same in all directions (or the turbulence is nearly isotropic), the flatness factor is about 2.8 which indicates that the distribution is nearly Guassian.

The distribution functions h and j in the channel flow are similar in shape to the results obtained for the Couette flow, but have larger variations in physical space, which are primarily due to the variation of the turbulence intensity, U.

Thus, it is seen that the results obtained using the gradient boundary conditions and those obtained using the Chapman-Enskog boundary conditions agree fairly well in regions away from the boundary. When Equation (38) is used to replace the differential equation for j, Equation 10b)), the resulting solutions are in better qualitative agreement with Laufer's experimental data, even though such an approach lacks in rigor. Some of the disagreement between the present results and the experimental data are attributed to the absence of pressure gradient, P_y, in the computations.

In the numerical study employed, the nodal points in the physical spacing were equally spaced at intervals of $\Delta\bar{y}/d = 0.0175$ while the discrete velocity points were located at unequal intervals. The number of discrete velocity points used in the computations is 440. The computing time required on CDC-6600 machine is about 6 seconds for each iteration.

CHAPTER VII

CONCLUSIONS AND RECOMMENDATIONS

The results of the present study and comparisons with available experimental data have established the following:

1. A numerical scheme employing a combination of the discrete ordinate method and finite differences has been developed for solving the one-dimensional form of Lundgren's model for turbulence. The method has proven to give convergent and stable results.

2. Physically realistic boundary conditions for the distribution function and model equation for the turbulence dissipation rate have been examined.

3. Lundgren's equation yields results for plane Couette flow which compare well with experimental data for mean velocity and skin friction coefficient. The results for Reynolds stress and turbulence kinetic energy are quite reasonable.

4. The zero-gradient boundary condition leads to the proper logarithmic mean velocity profile for Couette flow corresponding to a specific value of wall shear stress and a given set of constants used in the law of the wall.

5. The Chapman-Enskog boundary conditions, when applied within the near-wall region, provide very good agreement with the experimental data for the Couette flow problem.

6. The gradient boundary conditions have been developed so that

they may be applicable for more general situations involving pressure gradients.

7. Solutions obtained using the gradient boundary conditions and those corresponding to the Chapman-Enskog boundary conditions for two-dimensional channel flow are in good agreement with each other. The results for mean velocity compare well with Laufer's [21] experimental data.

8. The differences between the present results and the experimental data for channel flow in the profiles for Reynolds stress and turbulence kinetic energy are attributed to the fact that the cross-stream pressure gradient, P_y, has been neglected in the computations.

The results for the Couette flow problem show a slight sensitivity to the point of application of the Chapman-Enskog boundary conditions. This sensitivity indicates a need for further study of the boundary conditions. The present recommendation is that the boundary conditions be applied within the near-wall region, where the logarithmic law for the mean velocity is valid. One way to avoid this difficulty is to use experimentally determined distribution functions as boundary conditions. Another possibility is to apply the boundary conditions at the wall, where the distribution functions should be Gaussian. However, Lundgren's statistical model equation may not be applicable in that region unless further refinements of the relaxation model are incorporated. Such an effort would be an interesting area for future investigation since solutions for the distribution functions within the viscous sublayer could reveal details of turbulence production.

The results for channel flow problem in this study are limited by

the lack of an independent method of evaluating $\partial\bar{p}/\partial\bar{y}$. In the moment formulations, if all the components of Reynolds stresses are required, independent equations for each component must be available to close the system. In employing the statistical model equation, there is a similar closure problem. Hence, the development of an independent equation for computing $\partial\bar{p}/\partial\bar{y}$ can be computed from the moments of the distribution functions without using any of the moment equations, then the resulting solutions would be in more favorable agreement with the experimental data than the present results.

APPENDICES

APPENDIX A

GRADIENT BOUNDARY CONDITIONS

For flow fields with non-zero pressure gradient, $\partial\bar{p}/\partial\bar{x}$, it is desirable to obtain boundary conditions, similar to the zero-gradient boundary conditions used in the Couette flow problem, which are applicable in the near-wall region. In this region, it is known that the mean velocity profile is logarithmic and the turbulence kinetic energy is approximately constant. Besides the turbulence dissipation rate is nearly equal to the rate of production of turbulence kinetic energy. Thus, in this region, $\frac{du}{dy} = \frac{1}{\kappa y}$; $\varepsilon \sim \frac{1}{y}$ and $U \approx$ const. Let $\alpha(y) = \frac{\varepsilon}{3U^2} \sim \frac{1}{y}$ and $P_y = 0$. Under these conditions, the governing differential equations, Equations (10), reduce to

$$c_y \frac{\partial g}{\partial y} = 3K\alpha(G - g) + \alpha\left(c_y \frac{\partial g}{\partial c_y} + g\right) \tag{A-1}$$

$$c_y \frac{\partial j}{\partial y} = -3K\alpha j - \left(\frac{1}{Re_* \kappa y^2} + P_x + \frac{c_y}{\kappa y}\right) g + \alpha\, c_y \frac{\partial j}{\partial c_y} \tag{A-2}$$

$$c_y \frac{\partial h}{\partial y} = 3K\alpha(H - h) - 2\left(\frac{1}{Re_* \kappa y^2} + P_x + \frac{c_y}{\kappa y}\right) j + \alpha\left(-h + c_y \frac{\partial h}{\partial c_y}\right) . \tag{A-3}$$

From a theorem in Sneddon [35], the general solution of the partial

differential equation

$$P(x,y,z)\,\frac{\partial z}{\partial x} + Q(x,y,z)\,\frac{\partial z}{\partial y} = R(x,y,z) \tag{A-4}$$

is $F(u,v) = 0$, where F is an arbitrary function and $u(x,y,z) = c_1$ and $v(x,y,z) = c_2$ form a solution of the equations

$$\frac{dx}{P} = \frac{dy}{Q} = \frac{dz}{R} \tag{A-5}$$

If this theorem is applied to Equation (A-1), the general solution is obtained from solutions of the equations

$$\frac{dy}{c_y} = \frac{-dc_y}{\alpha c_y} = \frac{dg}{\alpha[3KG-(3K-1)g]} \tag{A-6}$$

Integration of the equation

$$-\frac{dc_y}{\alpha c_y} = \frac{dg}{\alpha[3KG-(3K-1)g]}$$

Yields, for $c_y \neq 0$,

$$\ell n(c_1 c_y) = \left(\frac{1}{3K-1}\right) \ell n[3KG - (3K-1)g]$$

or,
$$3KG - (3K - 1)g - c_2\, c_y^{(3K-1)} = 0 \tag{A-7}$$

Likewise, the equation

$$\frac{dy}{c_y} = \frac{dg}{\alpha[3KG-(3K-1)g]}$$

yields, upon integration and assuming $\alpha(y) = \frac{a}{y}$, with a being a constant of proportionality,

$$\ell n(c_3 y^{a/c_y}) = -\left(\frac{1}{3K-1}\right) \ell n[3KG - (3K - 1)g].$$

This equation is further simplified to the form

$$3KG - (3K - 1)g - c_4 y^{-(3K-1)a/c_y} = 0. \qquad \text{(A-8)}$$

The general solution of (A-1) is given by $f_1(u,v) = 0$ where f_1 is an arbitrary function,

$$u(y,c_y,g) = 3KG - (3K - 1)g - c_2 c_y^{(3K-1)} = 0$$

and

$$v(y,c_y,g) = 3KG - (3K - 1)g - c_4 y^{-(3K-1)a/c_y} = 0.$$

Since f_1 is an arbitrary function, let $f_1(u,v) = b_1 u + b_2 v$ where b_1 and b_2 are arbitrary constants. Regrouping terms, the general solution of Equation (A-1) becomes

$$3KG - (3K - 1)g = c_5 c_y^{(3K-1)} + c_6 y^{-(3K-1)a/c_y}. \qquad \text{(A-9)}$$

In the near wall region, it is known that the zeroth and the second velocity moments of g are approximately constants. To satisfy these requirements, the constant of integration, c_6, must be zero. Equation (A-9) further yields

$$\frac{\partial g}{\partial y} = \left(\frac{3K}{3K-1}\right) \frac{\partial G}{\partial y}. \qquad \text{(A-10)}$$

Since Equation (A-10) is obtained from a general solution of the governing equation, it gives a necessary condition that the distribution function, g, must satisfy to be consistent with Equation (A-1). If U is a

constant in the region where Equation (A-1) is applicable, then $\frac{\partial G}{\partial y} = 0$ and hence $\frac{\partial g}{\partial y} = 0$. This condition is not valid for $c_y = 0$. However, at $c_y = 0$, the governing equation requires that $g(y,0) = \left(\frac{3K}{3K-1}\right) G(0)$. For non-zero c_y values, if $\frac{\partial g}{\partial y}$ is set equal to zero in Equation (A-1), one gets the required boundary condition for g from the equation

$$c_y \frac{dg_b}{dc_y} - (3K-1)g_b = -3KG \qquad \text{(A-11)}$$

The subscript b is used to indicate that the distribution function obtained by solving this equation is to be used as a boundary condition.

Using a similar approach, it can be shown that near the wall boundary,

$$\frac{\partial j}{\partial y} = -\frac{g}{3Ka}\left(P_x - \frac{1}{Re_* \kappa y^2}\right) = w_1(y,c_y) \qquad \text{(A-12)}$$

and

$$\frac{\partial h}{\partial y} = \frac{2(P_x - \frac{1}{Re_* \kappa y^2})}{(3K+1)a}\left\{\frac{g}{3Ka}\left(\frac{1}{Re_* \kappa y} + P_{xy} + \frac{c_y}{\kappa}\right) - j\right\} = w_2(y,c_y). \qquad \text{(A-13)}$$

After substituting these forms for $\frac{\partial j}{\partial y}$ and $\frac{\partial h}{\partial y}$ into Equations (A-2) and (A-3), the boundary conditions for j and h are obtained from the equations

$$c_y w_1(y,c_y) = -3K j_b - \left(\frac{1}{Re_* \kappa y^2} + P_x + \frac{c_y}{\kappa y}\right) g_b + \alpha c_y \frac{dj_b}{dc_y} \qquad \text{(A-14)}$$

and

$$c_y w_2(y,c_y) = 3K\alpha(H-h_b) - 2\left(\frac{1}{Re_* \kappa y^2} + P_x + \frac{c_y}{\kappa y}\right) j_b$$

$$+ \alpha\left(-h_b + c_y \frac{dh_b}{dc_y}\right). \qquad \text{(A-15)}$$

Equations (A-11), (A-14) and (A-15) are solved numerically using finite differences. Since distribution functions and their velocity gradients must approach zero as $c_y \to \infty$, this is used as a boundary condition in velocity space. The result of the numerical integration is a set of numerical values for the reduced distribution functions which are then employed as boundary conditions in the solution of the model equation.

The boundary condition for j_v is obtained from the relation

$$j_{v_b} = j_b + u_b g_b \qquad \text{(A-16)}$$

where $u_b = \frac{1}{\kappa} \ell n(Re_* y_b) + 5$.

It is seen from Equations (A-10), (A-12) and (A-13) that for the case of Couette flow with zero pressure gradient ($P_x = 0$), if the viscous terms are neglected, the zero-gradient boundary conditions discussed in Chapter III are appropriate.

APPENDIX B

FINITE DIFFERENCE EQUATIONS

The non-dimensionalized governing equations for the reduced distribution functions with $P_y = 0$ are

$$c_y \frac{\partial g}{\partial y} = \frac{1}{\tau}(G - g) + \frac{\varepsilon}{3U^2}\left(g + c_y \frac{\partial g}{\partial c_y}\right) \tag{B-1}$$

$$c_y \frac{\partial j}{\partial y} = -\frac{j}{\tau} + \left(\frac{1}{Re_*}\frac{d^2u}{dy^2} - P_x - c_y \frac{du}{dy}\right)g + \frac{\varepsilon}{3U^2} c_y \frac{\partial j}{\partial c_y} \tag{B-2}$$

$$c_y \frac{\partial h}{\partial y} = \frac{1}{\tau}(H-h) + 2\left(\frac{1}{Re_*}\frac{d^2u}{dy^2} - P_x - c_y \frac{du}{dy}\right)j + \frac{\varepsilon}{3U^2}\left(-h + c_y \frac{\partial h}{\partial c_y}\right) \tag{B-3}$$

and

$$v_y \frac{\partial j_v}{\partial y} = \frac{1}{\tau}(J_v - j_v) + \left(\frac{1}{Re_*}\frac{d^2u}{dy^2} + \frac{\varepsilon}{3U^2} u - P_x\right)g - \frac{\varepsilon}{3U^2} v_y \frac{\partial j_v}{\partial v_y} \tag{B-4}$$

Using the second-order finite difference schemes outlined in Chapter IV, the Equations (B-1) - (B-4) can be approximated for each

node (i, σ) as shown in the following. The subscript "i" denotes the i^{th} point in the physical space, y_i, and the subscript "σ" represents the discrete velocity point, c_σ.

Finite-difference equations for $c_\sigma > 0$ can be obtained by using backward difference in physical space and forward difference in velocity space. The reduced distribution functions for the positive stream are denoted by a superscript "+." Thus, Equation (B-1) can be written, for $c_\sigma > 0$, as

$$\frac{c_\sigma}{2(\Delta y)}(3g^+_{i,\sigma} - 4g^+_{i-1,\sigma} + g^+_{i-2,\sigma}) = \frac{1}{\tau_i}(G^+_{i,\sigma} - g^+_{i,\sigma})$$

$$+ \frac{\varepsilon_i}{3U_i^2} g^+_{i,\sigma} + \frac{\varepsilon_i c_\sigma}{3U_i^2}(D_1^+ g^+_{i,\sigma} + D_2^+ g^+_{i,\sigma+1} + D_3^+ g^+_{i,\sigma+2}) \qquad \text{(B-5)}$$

where,

$$D_1^+ = \frac{2c_\sigma - c_{\sigma+1} - c_{\sigma+2}}{(c_\sigma - c_{\sigma+1})(c_\sigma - c_{\sigma+2})}$$

$$D_2^+ = \frac{c_\sigma - c_{\sigma+2}}{(c_{\sigma+1} - c_\sigma)(c_{\sigma+1} - c_{\sigma+2})}$$

and

$$D_3^+ = \frac{c_\sigma - c_{\sigma-1}}{(c_{\sigma+2} - c_\sigma)(c_{\sigma+2} - c_{\sigma+1})}$$

solving for $g^+_{i,\sigma}$ from Equation (B-5), there results

$$g^{+}_{i,\sigma} = [\frac{G^{+}_{i,\sigma}}{\tau_i} + (\frac{c_\sigma}{\Delta y})(2g^{+}_{i-1,\sigma} - \frac{1}{2} g^{+}_{i-2,\sigma}) + \frac{\varepsilon_i c_\sigma}{3U_i^2}(D_2^{+} g^{+}_{i,\sigma+1} + D_3^{+} g^{+}_{i,\sigma+2})]$$

$$/(\frac{3}{2}\frac{c_\sigma}{\Delta y} + \frac{1}{\tau_i} - \frac{\varepsilon_i}{3U_i^2} - \frac{\varepsilon_i}{3U_i^2} c_\sigma D_1^{+}) \qquad \text{(B-6)}$$

Similar expressions for positive stream can be derived for the other reduced distribution functions.

Finite difference equations for $c_\sigma < 0$ can be derived by using forward differences in physical space and backward difference in velocity space. Equation (B-1) can be written for negative stream, indicated by a superscript "-", as

$$\frac{c_\sigma}{2(\Delta y)}(4g^{-}_{i+1,\sigma} - g^{-}_{i+2,\sigma} - 3g^{-}_{i,\sigma}) = \frac{1}{\tau_i}(G^{-}_{i,\sigma} - g^{-}_{i,\sigma})$$

$$+ \frac{\varepsilon_i}{3U_i^2} g^{-}_{i,\sigma} + \frac{\varepsilon_i}{3U_i^2} c_\sigma (D_1^{-} g^{-}_{i,\sigma-2} + D_2^{-} g^{-}_{i,\sigma-1} + D_3^{-} g^{-}_{i,\sigma}) \qquad \text{(B-7)}$$

where

$$D_1^{-} = \frac{c_\sigma - c_{\sigma-1}}{(c_{\sigma-2} - c_{\sigma-1})(c_{\sigma-2} - c_\sigma)}$$

$$D_2^{-} = \frac{c_\sigma - c_{\sigma-2}}{(c_{\sigma-1} - c_{\sigma-2})(c_{\sigma-1} - c_\sigma)}$$

and

$$D_3^{-} = \frac{2c_\sigma - c_{\sigma-1} - c_{\sigma-2}}{(c_\sigma - c_{\sigma-2})(c_\sigma - c_{\sigma-1})}$$

Solving for $g^{-}_{i,}$, there results

$$g^{-}_{i,\sigma} = [\frac{G^{-}_{i,\sigma}}{\tau_i} + \frac{c_\sigma}{\Delta y}(\frac{1}{2} g^{-}_{i+2,\sigma} - 2g^{+}_{i+1,\sigma}) + \frac{\varepsilon_i}{3U_i^2} c_\sigma(D_1^{-} g^{-}_{i,\sigma-2} + D_2^{-} g^{-}_{i,\sigma-1})]$$

$$/(\frac{1}{\tau_i} - \frac{3}{2} \frac{c_\sigma}{\Delta y} - \frac{\varepsilon_i}{3U_i^2} - \frac{\varepsilon_i}{3U_i^2} c_\sigma D_3^{-}) \qquad \text{(B-8)}$$

Similar expressions for negative stream can be derived for the other reduced distribution functions.

APPENDIX C

COMPUTATION OF DISSIPATION RATE FOR THE COUETTE FLOW PROBLEM

The non-dimensionalized governing differential equation for the dissipation rate, ε, for the plane Couette flow is

$$\frac{\nu_T}{\sigma_\varepsilon}\frac{d^2\varepsilon}{dy^2} + \frac{1}{\sigma_\varepsilon}\frac{d\nu_T}{dy}\left(\frac{d\varepsilon}{dy}\right) + \frac{2}{3}c_1\frac{\nu_T}{U^2}\left(\frac{du}{dy}\right)^2\varepsilon$$

$$-\frac{2}{3}c_2\,Re_*\frac{\varepsilon^2}{U^2} = 0 \qquad \text{(C-1)}$$

where, σ_ε, c_1 and c_2 are constants and ν_T, U and u are known functions of y. Equation (C-1) is a second-order non-linear ordinary differential equation and requires two boundary conditions. This equation is applicable in the region $y_b \leq y \leq 1$. The boundary conditions for ε in the Couette flow are

$$\varepsilon_b = (du/dy)_b = \frac{1}{\kappa y_b}, \qquad \text{at } y=y_b \qquad \text{(C-2)}$$

and

$$\text{and } \left(\frac{d\varepsilon}{dy}\right) = 0 \qquad \text{at } y=1. \qquad \text{(C-3)}$$

It is known that, for the Couette flow problem, $\varepsilon \sim \frac{1}{y}$ in an approximate sense. It can be seen that if this form is used in Equation (C-1), even a small error in the computation of the term containing $\frac{d^2\varepsilon}{dy^2}$ gets magnified as $y \to 0$. One way to reduce this effect is to use the method of

differential variations [28].

In this method, solutions for ε are sought as a correction about approximate or guess values. In other words, one sets

$$\varepsilon(y) = \alpha(y) + \theta(y) \tag{C-4}$$

where $\alpha(y)$ is the guessed profile and $\theta(y)$ is the correction required to produce the correct solution for ε. Substitution of Equation (C-4) in (C-1) gives

$$\frac{\nu_T}{\sigma_\varepsilon}\frac{d^2\theta}{dy^2} + \frac{1}{\sigma_\varepsilon}\left(\frac{d\nu_T}{dy}\right)\frac{d\theta}{dy} + \frac{2}{3}c_1\frac{\nu_T}{U^2}\left(\frac{du}{dy}\right)^2\theta$$

$$+ \frac{2}{3}c_2\frac{Re_*}{U^2}(2\alpha\theta + \theta^2) + h(y) = 0 \tag{C-5}$$

where

$$h(y) = \frac{\nu_T}{\sigma_\varepsilon}\frac{d^2\alpha}{dy^2} + \frac{1}{\sigma_\varepsilon}\frac{d\nu_T}{dy}\frac{d\alpha}{dy} + \frac{2}{3}c_1\frac{\nu_T}{U^2}\left(\frac{du}{dy}\right)^2\alpha - \frac{2}{3}c_2 Re_*\frac{\alpha^2}{U^2}\,.$$

Equation (C-5) is a second-order, non-linear ordinary differential equation for θ and requires two boundary conditions. The appropriate boundary conditions for θ are obtained from (C-2) and (C-3) as

$$\theta_b = \frac{1}{\kappa y_b} - \alpha_b \qquad \text{at } y=y_b \tag{C-6}$$

and

$$\frac{d\theta}{dy} = -\frac{d\alpha}{dy} \qquad \text{at } y=1 \tag{C-7}$$

This is a two-point boundary value problem and since the differential equation is non-linear, a shooting technique [29] is appropriate. The

potential convergence problems associated with the shooting techniques render them less desirable. However, if Equation (C-5) can be linearized by a suitable numerical approximation, the principle of superposition can be used to eliminate the iterative procedure involved in shooting techniques. One way of linearizing the equation is to set $\theta^2 = \theta \cdot \theta_0$ where θ_0 are the known values of θ from the previous iteration. This procedure is partly justified for the Couette flow problem because, an estimate of the relative magnitudes of the four terms in the equation show that the linear term is always larger than the non-linear term. Equation (C-5) can be written as a system of two first-order differential equations. Further, the linearized equations can be written in the form

$$\frac{dz_1(y)}{dy} = a_1(y)\, z_1 + a_2(y)\, z_2 + a_3(y) \tag{C-8}$$

and

$$\frac{dz_2(y)}{dy} = b_1(y)\, z_1 + b_2(y)\, z_2 + b_3(y) \tag{C-9}$$

Since these equations are linear, one can seek solutions of the form $z_1(y) = w_1(y) + \lambda w_2(y)$ and $z_2(y) = w_3(y) + \lambda w_4(y)$, where λ is an arbitrary constant. Using these with Equations (C-8) and (C-9) one gets

$$\frac{d}{dy}(w_1 + \lambda w_2) = a_1(w_1 + \lambda w_2) + a_2(w_3 + \lambda w_4) + a_3 \tag{C-10}$$

$$\frac{d}{dy}(w_3 + \lambda w_4) = b_1(w_1 + \lambda w_2) + b_2(w_3 + \lambda w_4) + b_3. \tag{C-11}$$

Since λ is arbitrary, it is necessary that

$$\frac{dw_1}{dy} = a_1\, w_1 + a_2\, w_3 + a_3 \tag{C-12}$$

$$\frac{dw_2}{dy} = a_1 w_2 + a_2 w_4 \tag{C-13}$$

$$\frac{dw_3}{dy} = b_1 w_1 + b_2 w_3 + b_3 \tag{C-14}$$

and

$$\frac{dw_4}{dy} = b_1 w_2 + b_2 w_4 \tag{C-15}$$

This system of coupled first order equations need four conditions. They are obtained from Equations (C-6) and (C-7), which are of the form

$$z_1(y=y_b) = \theta_b = w_1(y=y_b) + \lambda w_2(y = y_b) \tag{C-16}$$

and, $$z_2(y=1) = \left(\frac{d\theta}{dy}\right)_{y=1} = w_3(y = 1) + \lambda w_4(y = 1) \tag{C-17}$$

To satisfy these conditions, it is convenient to set

$$w_1(y = y_b) = \theta_b \text{ and } w_2(y = y_b) = 0. \tag{C-18}$$

Also let $$w_3(y - y_b) = d_1, \text{and } w_4(y = y_b) = d_2 \tag{C-19}$$

where d_1 and d_2 are arbitrary constants.

With Equations (C-18) and (C-19) as boundary conditions, the system of Equations (C-12) to (C-15) are integrated using the Runge-Kutta method [36]. At $y = 1$, Equation (C-17) can be used to evaluate λ, with the computed values of w_3 and w_4. Once λ is evaluated, the solutions z_1, and z_2 are obtained from the expressions, $z_1 = w_1 + \lambda w_2$ and $z_2 = w_3 + \lambda w_4$.

In the present study, the values of the constants in Equation (C-1) are taken to be $\sigma_\varepsilon = 1.3$, $c_1 = 1.45$ and $c_2 = 1.92$.

APPENDIX D

COMPUTATION OF DISSIPATION RATE FOR THE CHANNEL FLOW PROBLEM

The differential equation governing the dissipation rate, ε, for the channel flow is

$$\frac{\nu_T}{\sigma_\varepsilon}\frac{d^2\varepsilon}{dy^2} + \frac{1}{\sigma_\varepsilon}\frac{d\nu_T}{dy}\frac{d\varepsilon}{dy} + \frac{2}{3}\frac{c_1\nu_T}{U^2}\left(\frac{du}{dy}\right)^2\varepsilon - \frac{2}{3}c_2 Re_* \frac{\varepsilon^2}{U^2} = 0 \qquad \text{(D-1)}$$

with

$$\varepsilon(y = y_b) = \varepsilon_b = \frac{1}{\kappa y_b} \qquad \text{(D-2)}$$

and

$$\left(\frac{d\varepsilon}{dy}\right)_{y=1} = 0 \qquad \text{(D-3)}$$

as boundary conditions.

For the channel flow, the method described in Appendix C fails. One of the reasons for this is due to the fact that the non-linear team (fourth team) in Equation (D-1) is larger in magnitude than the linear term (third term) for the channel flow problem. The integration of the non-linear differential equation using shooting techniques have not been successful. If finite difference schemes are to be employed, the equation should be linearized. In this study, the quasilinearization technique of Newton-Raphson-Kantorovich [30] is used for this purpose. An outline of this method is described in the following paragraphs.

The governing equation for ε, Equation (D-1) can be rewritten in the form

$$\varepsilon''(y) = f(\varepsilon(y), \varepsilon'(y), y) \tag{D-2}$$

where $(\,)'$ indicates derivative with respect to y. Let an initial approximation of the function $\varepsilon(y)$ be given and be represented by $\varepsilon_0(y)$, and from this, let $\varepsilon_0'(y)$ also be known. The function f can be expanded around the functions $\varepsilon_0(y)$ and $\varepsilon_0'(y)$ by the use of the Taylor series

$$\begin{aligned} f(\varepsilon(y), \varepsilon'(y), y) &= f(\varepsilon_0(y), \varepsilon_0'(y), y) \\ &+ (\varepsilon(y) - \varepsilon_0(y))\, f_{\varepsilon}(\varepsilon_0(y), \varepsilon_0'(y), y) \\ &+ (\varepsilon'(y) - \varepsilon_0'(y))\, f_{\varepsilon'}(\varepsilon_0(y), \varepsilon_0'(y), y) \end{aligned} \tag{D-3}$$

with second and higher order terms omitted. The expressions f_{ε} and $f_{\varepsilon'}$ are the partial derivatives of f with respect to ε and ε' respectively. Combining Equations (D-2) and (D-3), results

$$\begin{aligned} \varepsilon''(y) = f(\varepsilon_0(y), \varepsilon_0'(y), y) &+ (\varepsilon(y) - \varepsilon_0(y))\, f_{\varepsilon}(\varepsilon_0(y), \varepsilon_0'(y), y) \\ &+ (\varepsilon'(y) - \varepsilon_0'(y))\, f_{\varepsilon'}(\varepsilon_0(y), \varepsilon_0'(y), y) \end{aligned} \tag{D-4}$$

where $\varepsilon_0(y)$ are known functions of y. Equation (D-4) is a linear differential equation. Substituting for f from Equation (D-1), Equation (D-4) becomes

$$\begin{aligned} \varepsilon'' = h(y) + \left[\frac{4}{3}\frac{c_2\sigma_\varepsilon Re_*}{\nu_T U^2}\varepsilon_0 - \frac{2}{3}\frac{c_1\sigma_\varepsilon}{U^2}\left(\frac{du}{dy}\right)^2\right](\varepsilon - \varepsilon_0) \\ - \frac{1}{\nu_T}\frac{d\nu_T}{dy}(\varepsilon' - \varepsilon_0') \end{aligned} \tag{D-5}$$

where $h(y) = \frac{2}{3} \frac{c_2 \sigma_\varepsilon Re_*}{\nu_T U^2} \varepsilon_0^2 - \frac{2}{3} \frac{c_1 \sigma_\varepsilon}{U^2} \left(\frac{du}{dy}\right)^2 \varepsilon_0 - \frac{1}{\nu_T} \left(\frac{d\nu_T}{dy}\right)\left(\frac{d\varepsilon_0}{dy}\right)$.

The boundary conditions for Equation (D-5) are

$$\varepsilon = \varepsilon_b \text{ at } y = y_b \tag{D-6}$$

and

$$\frac{d\varepsilon}{dy} = 0 \text{ at } y = 1 \tag{D-7}$$

Equation (D-5) is solved using finite difference approximation. Let this be denoted by $\varepsilon_1(y)$. With $\varepsilon_1(y)$ known, Equation (D-2) can be expanded about $\varepsilon_1(y)$ and $\varepsilon_1'(y)$. This procedure can be continued until the desired accuracy is obtained. In this study, central differences are used to approximate the derivatives. The resulting tri-diagonal system of equations is solved using standard recursion relations [37]. The number of iterations of the Newton-Raphson-Kantorovich technique required to converge to within 0.0001 per cent is between 2 and 4 depending on the convergence of the moments of the distribution functions.

BIBLIOGRAPHY

1. G. K. Batchelor, Theory of Homogeneous Turbulence, Cambridge University Press, Cambridge, 1970, Chapter 8.

2. E. Hopf, "Statistical Hydromechanics and Functional Calculus," Journal of Rational Mechanics and Analysis, Volume 1, p. 87 (1952).

3. A. S. Monin, "Equations of Turbulent Motion," Prik. Mat. Mekh., Volume 31, p. 1057, (1967) [Journal of Applied Mathematics and Mechanics, Volume 31, p. 1057, 1967].

4. E. G. D. Cohen, Fundamental Problems in Statistical Mechanics, North-Holland Publishing Company, Amsterdam, 1962, p. 110.

5. T. S. Lundgren, "Distribution Functions in the Statistical Theory of Turbulence," Physics of Fluids, Volume 10, p. 969 (1967).

6. R. L. Fox, "Solution for Turbulent Correlations Using Multipoint Distribution Functions," Physics of Fluids, volume 14, p. 1806 (1971).

7. R. L. Fox, "Multipoint Distribution Calculation of the Isotropic Turbulent Energy Spectrum," Physics of Fluids, Volume 16, p. 977 (1973).

8. T. S. Lundgren, Statistical Models and Turbulence, edited by M. Rosenblatt and C. Van Atta, Springer-Verlag, Berlin, 1972, p. 70.

9. T. S. Lundgren, "Model Equation for Nonhomogeneous Turbulence," Physics of Fluids, Volume 12, p. 485 (1969).

10. P. L. Bhatnagar, E. P. Gross and M. Krook, Physics Review, Volume 94, p. 511 (1954).

11. P. M. Chung, "A Simplified Statistical Model of Turbulent, Chemically Reacting Shear Flows," AIAA Journal, Volume 7, p. 1982 (1969).

12. P. M. Chung, "Turbulence Description of Couette Flow," Physics of Fluids, Volume 16, p. 980 (1973).

13. H. M. Mott-Smith, Physics Review, Volume 82, p. 885 (1951).

14. P. M. Chung, "Chemical Reaction in a Turbulent Flow Field with Uniform Velocity Gradients," Physics of Fluids, Volume 13, p. 1153 (1970).

15. D. P. Giddens, "Study of Rarefied Gas Flows by the Discrete Ordinate Method," Georgia Institute of Technology, Ph.D. Thesis (1966).

16. A. B. Huang, P. F. Hwang, D. P. Giddens and R. Srinivasan, "High-speed Leading Edge Problem," Physics of Fluids, Volume 16, p. 814 (1973).

17. W. P. Jones and B. E. Launder, "The Prediction of Laminarization with a Two-equation Model of Turbulence," International Journal of Heat and Mass Transfer, Volume 15, p. 301 (1972).

18. J. M. Robertson, "On Turbulent Plane Couette Flow," Proceedings of the Sixth Midwestern Conference on Fluid Mechanics, Austin University Press, Austin, Texas, 1959, p. 169.

19. H. Reichardt, "Gesetzmässigkeiten der geradlinigen turbulenten Couetteströmung," Report No. 22 of the Max-Planck-Institut für Strömungsforschung und Aerodynamische versuchsanstalt, Gottingen, 1959.

20. H. F. Johnson, "An Experimental Study of Plane Turbulent Couette Flow," University of Illinois, M. S. Thesis, (1965).

21. J. Laufer, "Investigation of Turbulent Flow in a Two-dimensional Channel," NACA Report 1053, (1951).

22. B. E. Launder and D. B. Spalding, Mathematical Models of Turbulence, Academic Press, New York, 1972, Chapter 4.

23. S. Chapman and T. G. Cowling, The Mathematical Theory of Non-Uniform Gases, Cambridge University Press, New York, 1960 , Chapter 7.

24. S. Chandrasekhar, Radiative Transfer, Oxford at Clarendon Press, 1950, Chapter 2.

25. A. B. Huang and D. P. Giddens, "A New Table for a Modified (Half range) Gauss-Hermite Quadrature with an Evaluation of the Integral $\int_0^\infty e^{-u^2-x/u} du$, Journal of Mathematics and Physics, Volume 47, p. 213 (1968).

26. M. Abromovitz and I. A. Stegun, Handbook of Mathematical Functions, Dover Publications, Inc., New York, 1964, Chapter 25.

27. P. Bradshaw, An Introduction to Turbulence and its Measurements, Pergamon Press, New York, 1971, Chapter 3.

28. W. E. Milne, Numerical Solution of Differential Equations, Dover Publications, Inc., New York, 1970, Chapter 7.

29. B. Carnahan, H. A. Luther and J. O. Wilkes, Applied Numerical Methods, John Wiley and Sons, New York, 1969, Chapter 6.

30. E. Stanley Lee, Quasilinearization and Invariant Imbedding, Academic Press, New York, 1968, Chapter 2.

31. H. T. Kim, S. J. Kline and W. C. Reynolds, "The Production of Turbulence near a Smooth Wall in a Turbulent Boundary Layer," Journal of Fluid Mechanics, Volume 50, Part 1, p. 133 (1971).

32. S. S. Lu and W. W. Wilmarth, "Measurements of the Structure of the Reynolds Stress in a Turbulent Boundary Layer," Journal of Fluid Mechanics, Volume 60, Part 3, p. 481 (1973).

33. R. S. Brodkey, J. M. Wallace and H. Eckelmann, "Some Properties of Truncated Turbulence Signals in Bounded Shear Flows," Journal of Fluid Mechanics, Volume 63, p. 209, (1974).

34. Z. Zaric, "Statistical Analysis of Wall Turbulence Phenomena," Paper presented at the Second IUTAM-IUGG Symposium on Turbulent Diffusion in Environmental Pollution, April 1973, Charlottesville, Virginia.

35. I. N. Sneddon, Elements of Partial Differential Equations, McGraw Hill, New York, 1957, Chapter 2, p. 50.

36. A. Ralston and H. S. Wilfe, Mathematical Methods for Digital Computers, Volume 1, John Wiley and Sons, New York, 1967, Chapter 9.

37. P. J. Roache, Computational Fluid Dynamics, Hermosa Publishers, Albuquerque, New Mexico, 1972, Appendix A.

VITA

Ramanujam Srinivasan was born in Chidambaram, Tamil Nadu, India on July 19, 1947. He had his early education at P. S. High School, Madras, India. He completed his Pre-University course at Madras University in 1963. He entered the Indian Institute of Technology, Madras in 1964. He obtained the degree of Bachelor of Technology in Aeronautical Engineering in 1969.

In September 1969, Mr. Srinivasan entered the Georgia Institute of Technology and received the degree of Master of Science in Aerospace Engineering in March 1971. He continued his education as a Ph.D. student in the school of Aerospace Engineering at Georgia Institute of Technology.

Mr. Srinivasan is an associate member of Sigma Xi and a student member of the AIAA.